ADDIS ABABA UNIVERSITY

ADDIS ABABA INSTITUTE OF TECHNOLOGY

AFRICAN RAILWAY CENTER OF EXCELLENCE

Performance of Vulnerable Railway Bridge Piers Subjected to Vehicular Impact Loads
Case Study: Addis Ababa Light Rail Transit

A Thesis in MSc. Railway Engineering (Civil Infrastructure)

By

MWESIGE BAKOLE DEOGRACIUS

31st MAY- 2019

Addis Ababa

A Thesis Submitted to the School of Graduate Studies of Addis Ababa University in Partial Fulfillment of the Requirement for the Award of Degree of Master of Science in Railway Engineering (Civil Infrastructure)

EXAMINING COMMITTEE MEMBERSHIP AND CERTIFICATION

The undersigned have examined the thesis entitled **"**Performance of Vulnerable Railway Bridge Piers Subjected to Vehicular Impact Loads" Case Study: Addis Ababa Light Rail Transit" presented by **Mwesige Bakole Deogracius (GSR/3414/10)**, a candidate for the degree of **Master of Science in Railway Engineering (Civil Infrastructure)** and hereby certify that it is worthy of acceptance since it complies with the regulations of the University and meets the accepted standard with respect to originality and quality.

Dr. Bedilu Habte		July 8/2019
Advisor	Signature	Date
Dr Abrham Gebre		July 08/2019
Internal Examiner	Signature	Date
Dr Asnake Adamu		July 09/2019
External Examiner	Signature	Date
Mr. Ntakiyemungu Mathieu		09.07.2019
Chairperson	Signature	Date

DECLARATION

I certify that research work titled “Performance of Vulnerable Railway Bridge Piers Subjected to Vehicular Impact Loads Case Study: Addis Ababa Light Rail Transit” is my own work. The work has not been presented elsewhere for assessment. Where material has been used from other sources it has been properly acknowledged/referred.

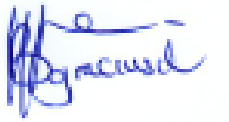

Mwesige Bakole Deogracius

GSR/3414/10

ABSTRACT

Addis Ababa Light Rail Transit (AALRT) contains 39 stations, nine (9) of which are elevated with help of bridges. A situation that could involve a truck accidentally or intentionally hitting a railway bridge pier in a metropolitan setting like Addis Ababa Light Rail Transit in Addis Ababa City leading to the collapse of the bridge structure would have serious consequences to not only the human lives, transportation in the city but also onto the entire Ethiopian economy. Bridges being overland structures that are designed to overcome an obstacle for the purpose of connecting communities are critical components of any rail road infrastructure therefore, the collapse of a bridge due to any cause would be extremely costly in terms of direct and indirect costs. Vehicle-bridge pier collisions are mostly extreme loading cases with a very low probability of occurrence during the lifetime of a structure that is usually associated with high disruption to traffic flow, especially in a metropolitan setting.

A total of 276 piers were investigated to ascertain the extent of their vulnerability to vehicular impact load and it was found out that 6 piers corresponding to 2.174 % are highly susceptible to vehicle impact, while 269 piers (97.464%) are moderately exposed and 1 pier (0.362%) was of low exposure to vehicle collision. Further analysis of the highly and moderately exposed piers shows that by location, 35.273% are located along curved sections while 56.727% are located along the tangent section, 4.727% are located along roundabouts and 3.273% are at intersections.

The average damage ratio obtained from the piers along AALRT gave a damage ratio of 0.066 which is a very insignificant damage only capable of causing micro cracks at the impact location which is a clear indicator that the piers can be repairable (minor) without replacement of the concrete component or any major effect on the operation of the train. Basing on deformation as a serviceability requirement for structural performance, a deformation of up to a maximum of 6.4 mm is equally too small to lower the confidence of the train users as obtained from numerical simulations using ANSYS.

Regression-based sensitivity conducted on combinations generated by Latin Hypercube used as input parameters to ANSYS which generated deformation, clearly indicated that vehicle speed is the lead cause of deformation while stirrup spacing is the most significant parameter in resisting deformation of the pier during a pier-vehicle collision.

Key Words: Railway Bridge Piers, Bridge Pier Vulnerability, Vehicular Impact Loads, ANSYS, LHS Sampling, Sensitivity analysis, and Simulation.

ACKNOWLEDGMENTS

I wish to express my sincere acknowledgment, appreciation, and gratitude to my advisor Dr. Bedilu Habte who offered timely and selfless professional support. It is because of his guidance, constant involvement that I boast of the success of this work and personal enrichment of my technical knowledge and improved confidence for the successful completion of this research. I wholeheartedly believe that this work would not have come to fruition without the trust and the encouragement of my supervisor.

The following people deserve mention and appreciation for their different roles in making this research a success story; Dr. Abrham G (Lecturer Bridges and Director ARCE); Eng. Tegegne Eshetu T (Bridge Expert -Best Consulting Engineers) Eng. Tsegaab. D and Ms. Nakyanja Phillomera. The help offered was invaluable to this research and helped me a lot in the completion of my thesis.

The following organizations that were so helpful during different stages of my research also deserve thanks for their contribution;

1) Addis Ababa Light Rail Transit
2) Ethiopian Railway Corporation
3) Addis Ababa City Transport Bureau
4) Addis Ababa city Roads Authority

I would also like to convey my thanks to the Department of Railway Engineering (Civil infrastructure) and the entire management of African Railway Center of Excellence (ARCE) at Addis Ababa Institute of Technology of Addis Ababa University for their academic and financial support. Your involvement and humility made the whole MSc program a challenging and yet interesting adventure with great exposure during my stay in Ethiopia-THANK YOU SO MUCH.

Finally, my deepest gratitude and appreciation go to my wife and sons, my parents (Edson and Lillian) and my brothers (Joseph, Jimmy, and Ronald) for their unconditional love and encouragement throughout these years. Your presence in my life has been nothing short of continuous inspiration to push forward and achieve my ultimate goals. I truly hope that I will always live up to your expectations, and pay back some of my debt to you for your limitless kindness and compassion. Thank you very much for believing in me and giving me all the support, I need to pursue my dreams.

DEDICATION

I dedicate this thesis to the following people who are so dear to me: -

- Stella Asingo- Wife,
- Seth Ngonzi Bakole and Asa Kagaba Bakole- Sons

TABLE OF CONTENTS

LIST OF TABLES

LIST OF FIGURES

LIST OF EQUATIONS

LIST OF ACRONYMS AND ABBREVIATIONS

AALRT-	Addis Ababa Light Rail Transit
AASHTO	American Association of State Highway and Transportation officials
ArcGIS	Arc- Geographic Information System
AREMA	American Railway Engineering and Maintenance-of-way Association
ASTS	Automatic_Surface_To_Surface
CBE	Commercial Bank of Ethiopia
COMESA	Common Market for Eastern and Southern Africa
CSCM	Continuous Surface Cap Model.
ERA	Ethiopian Roads Authority
ERC	Ethiopian Railways Corporation
ESF	Equivalent static forces
FEM	Finite Element Modelling
ft	Feet
FWHA	Federal Highway Administration
GPS	Global Position System
in	Inch(es)
km/hr	Kilometres Per Hour
KN	Kilo Newton
LHS	Latin Hypercube Sampling
LRFD	Load and Resistance Factor Design
MCS	Monte Carlo simulation

mph	Miles Per Hour
ms	Microseconds
NYSDT	New York State Department of Transportation
PDF	Probability Density Function
PRA	Probabilistic Risk Assessment
RC	Reinforced Concrete
UNECA	United Nations Economic Commission for Africa
WHO	World Health Organization

Chapter 1 : INTRODUCTION

1.1 Background

Addis Ababa Light Rail Transit (AALRT) is an electrified double track standard gauge (1.435 meters) light rail transport system with two operational lines North-South (N-S) and East-West (E-W) (Figure1-1) in Addis Ababa City since May 2015. It is currently 31.025 Km and contains 39 stations nine (9) of which are elevated with help of Bridges. According to China Railway Group limited [1], [2], E-W route has the total length of 17,400 m, 2,730 m of which are elevated section excluding the stations. All the elevated stations have a total length of about 340 m and the total elevated structure has the length of 3,070 m, which takes 17.644% of the whole route.

Bridges are overland structures that are designed to overcome an obstacle for the purpose of connecting communities are critical components of any rail road infrastructure. Therefore, bridge collapse due to any cause would be extremely costly in terms of direct and indirect costs, Kamaitis [3]. In investigating bridge-pier collision C. Eugene Buth [4] reported that, in nearly every accident case, the damage to the impacted bridge pier was catastrophic, resulting in reconstruction of the pier. Bridge piers as structural components of a bridge are designed to hold out enormous compressive axial loads and as well as resist lateral loads such as vehicle impacts applied to them and that they are often vulnerable to fail under eccentric out-of-plane loads, such as those created by an impact or explosion according to WisDOT [5]. Similarly, Agrawal and Xu [6] concluded that external events were responsible for triggering bridge failures despite other principal factors affecting bridge failures.

Impact load due to vehicle-bridge pier collision is considered as an extreme loading event which can result into significant damage to the structural supports including piers, bent cap, foundation, and superstructure but also with the possibility of leading to full structural failure or collapse. Eric [7],[8] identified the use of vehicles as the most likely approach by terrorists to attack a bridge. This, therefore, calls for newly designed bridges and existing structures crossing highway or railroad to be capable of resisting over height impacts or lateral impacts vehicular collision loads.

Harik et al. [9] conducted a study that showed that collisions involving ships, trucks, and trains are among the leading causes of bridge failures. A similar study by Wardhana and Hadipriono

[10], outlined the major causes of bridge failures as; - hydraulic damage, vehicle collision, material deterioration, and overloading of the structure.

According to World Health Organization (WHO) [11], the prevalence of road traffic fatality in Ethiopia for the year 2013 was 25.3 per 100,000 people a rate that is among the highest in the world. The United Nations Economic Commission for Africa (UNECA) [12] report also showed that Ethiopia had one of the world's worst crash records with 170 fatalities per 10,000 vehicles as of 2009 despite having a very low road network density and vehicle ownership, the country (Ethiopia) has been cited as the worst example in road crash. According to Tariku et al. [13], road crashes are on an increasing trend in Addis Ababa and that road crashes reported and registered by Police in 2017 showed that most of the crashes were associated with drivers' errors and demographic characteristics. Tariku [13] further points out that Ethiopia's capital city – shares 60% of the total number of vehicles in the country and sadly these contribute to about 60% of all road crashes occurring in the country.

According to Fesseha and Sileshi [14], vehicle road structure type of interaction as shown in Table 1-1 accounted for 35.5% of the road traffic crashes in 2014 from the three main categories of vehicles that were considered are small vehicles, freight vehicles, and passenger vehicles. Similarly, Getu S et al.[15], [16] concluded that the speed differentials (5 km/hr. to 80 km/hr.) in urban centres were recognized as risk factors for road traffic crashes and therefore, recommended that the road crash problem in Ethiopia be investigated because of its linkages with other development objectives.

Table 1-1 Types of Road accident Crashes [14]

Type of interaction	**Number**	***Percentage%***
Vehicle-Pedestrian	5030	54.5
Vehicle-Road Structure	3318	35.5%
Vehicle-Vehicle	907	10%
Total	9255	100%

Figure 1-1 Addis Ababa Light Rail Transit Network (2018)

Vehicle-bridge pier collisions are mostly extreme loading cases with a very low probability of occurrence during the lifetime of a structure according to Laurent and Yann [17] usually associated with high disruption to traffic flow and this is worse if it is in a metropolitan setting as shown in Figure *1-2*. However, Haimes [18] points out that, "a low probability of occurrence does not justify minimizing our efforts to manage the potential adverse effects of a catastrophic event".

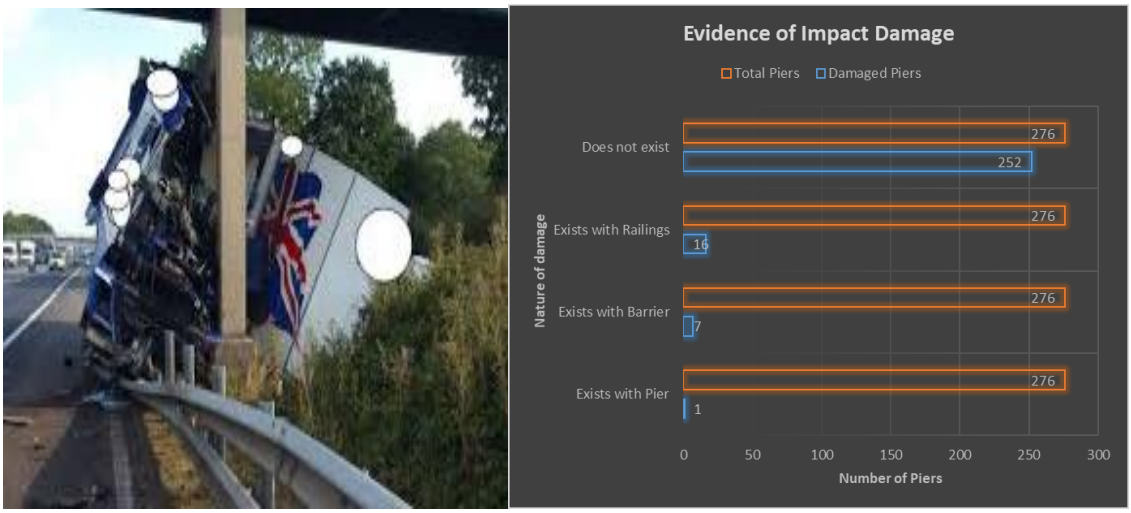

Figure 1-2 L-R Lorry Crashes into a Bridge [19], AALRT Impact Summary

The overall long-term objective of this research was to investigate the performance of the Railway bridge pier due to unavoidable threats from vehicular impact loads. Therefore,

simulating the performance of railway bridge piers subjected to vehicular impact load for Addis Ababa Light Rail Transit system was conducted.

1.2 Problem Statement

Addis Ababa City contributes 60% of the vehicular accidents in Ethiopia. 35.5% of all accidents that occur in Ethiopia involve vehicle road structure collision [11] [13]. Addis Ababa Light Rail Transit being a city-based transport system, combined with lack of crash walls and barriers on some of its bridge piers as required by AREMA 2010(C-2.1.5) and AASHTO-LRFD 2010(11.7.2) specifications greatly exposes the bridge piers to the extreme event of vehicular impact loads in case of a collision. Such bridge pier structures found susceptible to vehicle collisions must be designed to either redirect or absorb the impact force or provide structural resistance.

A situation that could involve a vehicle-truck accidentally or intentionally due to terror attack there by hitting any of AALRT's railway bridge pier leading to the collapse of the bridge structure would have serious consequences not only to the human lives, transportation in the city but also onto the entire Ethiopian economy. Considering that civil infrastructure is the backbone most economies, it has a large impact on personal and economic well-being if destroyed. Every nation's infrastructure is the foundation for its workforce and provides safety for the public. Therefore, it is crucial to create structures that are more resilient under extreme load cases. Despite the rare occurrence of bridge-pier collision accidents, questions that seem of great importance and need to be answered are; What percentage of AALRT's bridge piers are highly vulnerable to vehicular impact loads? To what extent will the AALRT most vulnerable bridge piers be damaged and deformed when subjected to vehicular impact load(s)? Which parameters are critical when designing to overcome damage of a bridge pier?

Therefore, this study seeks to use ANSYS software to numerically model and simulate the vehicle-bridge pier collision so as to evaluate the performance of such vulnerable piers along AALRT and further provide reliable information that will be a basis for future structural design consideration of such vulnerable piers and other possible risk mitigation measures.

1.3 Research Objectives

1.3.1 General Objective

To evaluate the performance of vulnerable railway bridge piers subjected to vehicular impact load case for Addis Ababa Light rail Transit system (AALRT).

1.3.2 Specific Objectives

- To identify the most vulnerable bridge piers at risk of being subjected to vehicular impact load along AALRT.
- To analyze the vehicle - pier collisions for the most vulnerable bridge piers along AALRT
- To conduct a parametric study and sensitivity analysis related to bridge pier-vehicle collision.

1.4 Research Questions

1) Which and how many railway bridge piers along AALRT are at risk to vehicular impact loads?
2) What will be the structural response of the vulnerable railway Bridge piers along AALRT when subjected to vehicular impact loads?
3) Which parameters are critical in the performance of vulnerable railway bridge piers subjected to vehicular impact loads?

1.5 Significance of the Study

The data obtained from this study, can be used by the road and rail safety authorities and stakeholders for planning and evaluating road accidents and safety measures. The study will also be very helpful for engineers and policymakers with an emphasis to AALRT, ERC and ERA to take preventive and intervention measures to reduce the effect of vehicle-pier collision based on up-to-date scientific evidence on the magnitude and contributing parameters to catastrophic outcomes of vehicle-pier collisions in Addis Ababa and Ethiopia at large.

1.6 Scope and Limitations of the Study:

During this study, only vehicular collisions were considered as impact loads with the AALRT vulnerable bridge piers being investigated within the period November 2018 to May 2019. Therefore, all simulations that were conducted during this study were restricted to head on (lateral) impacts of vehicles striking the bridge piers in a direction at an appropriate angle in the range of 0-15 degrees to the span of the bridge and the study was considered as a Hard Impact collision. Finite element bridge models were developed for bridges along the AALRT.

The bridge model used for safety analysis study was not based on up-to-date as-built drawings but rather a combination of design reports and field investigations only. No experiments were done for model verification therefore, this means that model validation was based on published data. The study was conducted on the assumption that an accident occured and therefore, the performance of the bridge pier when subjected to vehicular impact was evaluated.

1.7 Structure of the Thesis Report

Chapter 1 and 2: Chapter 1gives a thorough background as to why the study of vehicle- bridge pier collision has to be conducted with a study case of AARLT as an appropriate one. While Chapter 2: Introduces the general impact loading, simulation, modeling, sampling, and sensitivity analysis procedure through a comprehensive literature review on the topic of vehicle collisions with bridge piers, as well as general knowledge and basic considerations to take while modeling using finite element software such as ANSYS.

Chapter 3: aims at analytically quantifying piers that are susceptible to vehicle collision along the AALRT route and to be able to generate a bridge Pier Vulnerability Map with an intention of identifying the most critical piers with their corresponding characteristics for simulation of vehicle pier-collision.

Chapter 4: aims at validating finite element materials and controls that can be used to conduct vehicle impact simulations. Due to the lack of experimental data involving vehicle collisions with bridge piers, a similar impact phenomenon was modelled for a drop hammer experiment. Rectangular reinforced concrete (RC) beams with varying longitudinal reinforcement ratios were subjected to impact loads. The numerical results have to be compared in terms of crack patterns and maxiumum mid span defelection for the beam impact test and the validated finite element controls and material models were adopted for use with impact load simulations.

Validation of vehicle-Pier collision was based on comparison for shear and deformations of numerical simulations and published data.

Chapter 5: Details the procedure followed to determine the structural response of AALRT's bridge Piers when subject to vehicular impact load at speeds of 70 km/hr up to a maximum of 120km/hr. This Chapter also describes the findings from the vehicle-bridge pier collision.

Chapter 6: Discusses how the identified different parameters affect the failure of bridge piers subjected to vehicle collisions for the different generated models. Systematic sampling using Latin Hypercube sampling technique was used to generate different probabilistic combinations for the following parameters of interest: vehicle velocity, vehicle mass, cylinder compressive strength, Stirrup spacing and area of longitudinal reinforcement. A sensitivity analysis was conducted to evaluate the impact of the above-mentioned parameters for two performance-based analysis consideration and that is deformation and damage ratio.

Chapter 7: Summarizes the findings of the study and provides recommendations and also suggests possible areas for future research.

Appendix A: This appendix provides details about the photographic evidence of field survey to identify piers susceptible to overhead and lateral impact, posted speeds along the AALRT route (these speeds were adopted for ranking of pier vulnerability), evidence of damage to the piers and extent of protection to the piers.

Appendix B: This section seeks to illustrate the different parameters that were used in assessing the performance of AALRT identified vulnerable piers when subjected to vehicular impact loads.

Appendix C: This shows the data that was adopted for the calculation of mean and standard deviation values for speed and axle loads. It also gives the table from which the coefficient of variation was adopted for the calculation of standard deviation when given the mean value.

Appendix D: This appendix provides the detailed summary outputs for regression statistics and ANOVA of the different stages of multiple regression analyses that were conducted based on ANSYS simulations for the generation of deformation as an output.

Chapter 2 LITERATURE REVIEW

2.1 Introduction

In order to satisfy the serviceability limit states, a concrete structure must be serviceable and perform its intended function throughout its working life. Excessive deflection should not impair the function of the structure or be aesthetically unacceptable. Cracks should not be unsightly or wide enough to lead to durability problems, Gilbert [20]. Design for the serviceability limit states involves making reliable predictions of the instantaneous and time-dependent deformation of the structure. This is complicated by the non-linear behavior of concrete caused mainly by cracking, tension stiffening, creep and shrinkage. Due to the brittleness of concrete, impact damage is a major cause of the reduction in a life span of any concrete construction. Generally, when an impact load is applied to a concrete structure, various forms of damages will occur during the loading process. The most common damages are the different types of global or localized damage, including flexural cracking, shear cracking, crushing of concrete beneath the projectile and spalling at the bottom of a concrete element. According to Gilbert [20], the broad design objective for a concrete structure is that it should satisfy the needs for which it was contrived. In doing so, the structural designer must ensure that it is both safe and serviceable so that the chances of it failing during its design lifetime are sufficiently small. The two primary structural design objectives are therefore strength and serviceability.

It is evident that the performance of reinforced concrete member, both the ultimate state (strength) and the serviceability state (crack and deflection), relies on the transfer capacity of the interfacial regions between the concrete and the reinforcement. The transfer forces, in turn, depend on the bond quality between the two materials (steel and concrete)

Laurent and Yann [17] suggested that reliable prediction of the structural response of concrete under impact requires the knowledge of the strain rate dependency of concrete constitutive behavior. The strain rate at some point within the material measures the rate at which the distances of adjacent parcels of the material change with time in the neighborhood of that point. It comprises both the rate at which the material is expanding or shrinking (expansion rate) and also the rate at which it is being deformed by progressive shearing without changing its volume (shear rate). It is zero if these distances do not change, as happens when all particles in some region are moving with the same velocity (same speed and direction) and/or rotating with the same angular velocity, as if that part of the medium were a rigid body.

According to Agrawal et al. [21], the understanding of the damage modes of bridges after the collision is crucial for the safety assessment and the consequential impact on the local transportation network. Despite all that, the current understanding of impact resistance for reinforced concrete (RC) bridge piers is still limited. Irrespective of being reliable, the high-cost levels and complexity associated with vehicle-bridge full-scale collision experimental tests for structural bridge assessment and analysis explain why most research scholars prefer numerical simulation of structural impact response since it is a more efficient way of testing the behavior of members with different characteristics. Most researchers have used the finite element analysis in order to predict impact response of reinforced concrete elements with reasonable accuracy.

According to SB-LRA [22], bridge assessment is categorized into three main types depending on the reasons for performing a load capacity assessment and the required level of detail varies with the type of assessment as shown in Figure 2-1

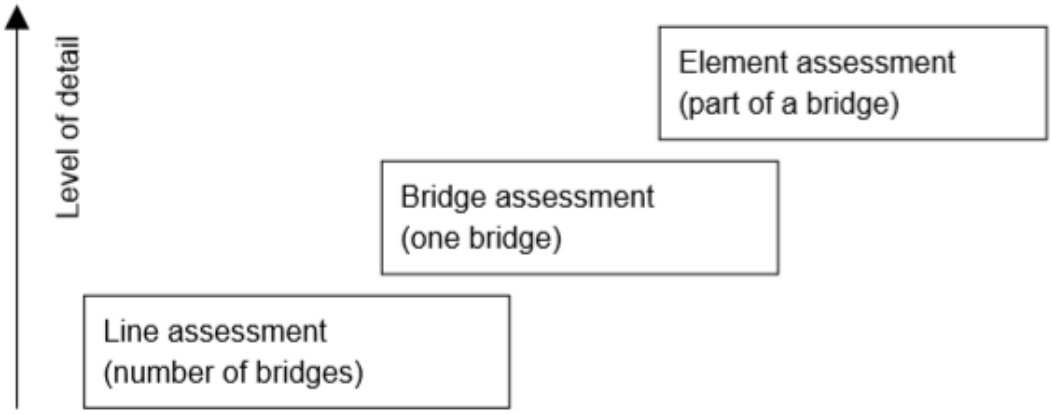

Figure 2-1 Types of Assessment (SB-LRA, [22])

A study by Tawil [23] demonstrated that numerical modeling could serve as a powerful tool to investigate the vulnerability of bridges or to improve general design criteria. One of the noticeable gaps is that most of the research carried out to date mainly considers the validation of already affected bridge piers and little attention is paid to assessing the maximum possible impact the piers can sustain during their operational stage.

2.2 Impact Loading

2.2.1 Impact Loading Terminology and design standards

According to Engin et al [24], any given structure is generally under the effect of two main loads as static and dynamic loads. While static loads are permanent ones, dynamic loads occur

suddenly and affect structures for a length of time. Since destructive damages may happen due to dynamic loads, the response of the structure against these loads shall be estimated correctly. Impact effects are the changes in mechanical properties of members due to stresses occurring at the striking moment between objects. Car, helicopter, plane strikes, ship strikes to abutments, water structures, and petrol platforms, explosions in military establishments, projectile and missile strikes, crane accidents while carrying members and stone and rock falls to structures located in roadsides are the examples of impact incidents. Performing studies about impact effect are helpful in determining the mechanical properties of members under high-stress values Engin et al. [24].

RC structural member subjected to impact loading scenarios deform over a relatively short period of time, the effect of strain rate, lateral confinement, and inertia force become more significant. As a result, the structural response and failure mode may be different from those under static loads Li et. al. [25]; Chen and May [26].

In general, materials subjected to dynamic effects, such as impact loading, respond over a relatively short period of time. As a result of such high loading rate, the strain rates reach magnitudes considerably higher than that of static conditions CEB-FIP, [27]. Numerous experimental studies have demonstrated that high strain rates result in enhancing mechanical properties in most materials and these properties include compressive strength; ductile tensile strength; flexural strength; elastic modulus; Poison's ratio, fracture toughness, and density. This includes the constituents of RC structures, namely: concrete and steel reinforcement. Dynamic increase factor (DIF) is the most popular method for taking account of strain rate effects on both deformation and failure Li et al. [25]. DIF which is defined as the ratio of the dynamic to static strength is generally reported as a function of strain rate. Most reported relations of DIF and strain rate are linear-logarithmic or double logarithmic. It is important to mention that DIF is of direct use in FE analysis of structures subjected to dynamic loading conditions Li et al., [25]; Othman and Marzouk [28].

Impact loading may be classified as hard or soft impact, depending on the deformation of the impactor (projectile) with respect to the deformation of the target. In hard impact, the deformation of the impactor is considered negligible compared with the target's deformation. In such an impact type, the impactor is considered rigid. In contrast, in soft impact, the impactor itself undergoes significant deformation and must be considered in the analysis of impact

problem (Li et al. [25]). In either of two impact types, the response, as well as the failure mode of the concrete target, may be classified as follows:

Global response: the RC member responds globally with deformation of the entire member. There are two failure modes of global response for RC members: flexural failure and punching shear failure. Both failure modes are caused by the elastic-plastic response. Figure 2-2 shows the two modes of global response. The majority of global response investigations were carried out on RC beams.

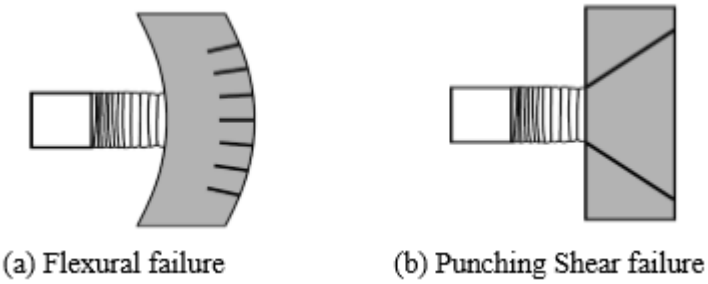

Figure 2-2 Global Response of RC Target [29]

Local response: the RC member responds locally and the impact energy is dissipated around the impact zones. Most of the local impact investigations were carried out on RC plates. Local impact effect is briefly sub-divided into seven phenomena as classified in (Li et al. [25]): a) penetration, b) cone cracking and plugging, c) spalling, d) radial cracking associated to (i) impact face and (ii) back face, e) scabbing ejection of fragments from the back face of the target, f) perforation. Local impact damage mechanisms are illustrated in Figure 2-3.

Combined response: the impact energy is dissipated through a combination of local and overall structure deformations.

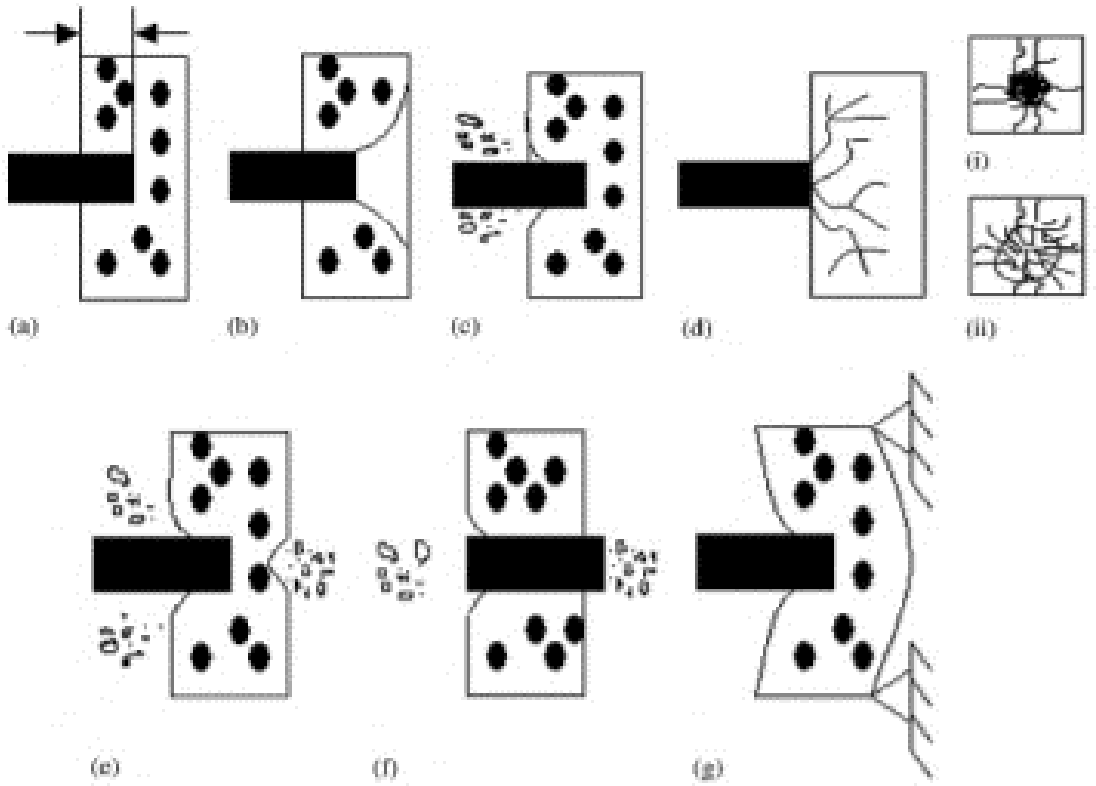

Figure 2-3 Impact effects on concrete Target [25]

A brief review of design standards

The American Association of State Highway and Transportation Officials (AASHTO) *Load and Resistance Factor Design (LRFD) Bridge Design Specifications* (2010) requires that abutments and piers within 9.144 m of the roadway to be considered for the extreme event of a vehicle collision. The required equivalent static force (ESF) that the structure must be designed for is a 2,669 KN single point load applied to the pier at a height of 1.524 m above the ground and at an angle of incidence from 0 to 15 degrees with the edge of pavement in a horizontal plane. This recommendation, however, is based on experimental testing involving a single semi-tractor-trailer(36.2 ton truck) colliding into a rigid pier at 50 mph. This leaves a large room for uncertainty when designing a bridge pier with different design specifications that could possibly undergo different loading conditions such as varying vehicle mass and velocity. Past research has shown that AASHTO's design specifications underestimate the demand expected on the bridge pier from collision loadings according to Agrawal et al. [21]. This raises a concern of safety in regards to the current bridges in service today.

2.2.2 Review of Previous Low-velocity Impact Studies

According to Othman [28] and Safri et al [30], There are several categories of impact loading, and specifically these are: low velocity (large mass), intermediate velocity, high/ballistic velocity (small mass), and hyper velocity impact. These categories of impact loading are important because there are extreme changes in energy transfer between the projectile and target, energy dissipation and damage propagation mechanisms as the velocity of the projectile varies (4). Low velocity impacts occur at a velocity below 10 m/s, intermediate impacts occur between 10 m/s and 50 m/s, high velocity (ballistic) impacts have a range of velocity from 50 m/s to 1000 m/s, and hyper velocity impacts have the range of 2 km/s to 5 km/s (5). Low and intermediate velocity impact studies are the common impact scenarios for civil engineering. In High-velocity impact studies, the loading impulse acts over a very short time, much shorter than the natural period of structural member vibration by perhaps one or two orders of magnitude. As a result, the entire structural member has no time to respond globally and the failure of beams or plates is localized in the form of punching ejection cone.

According to Othman [28], generally, the low-velocity and intermediate impact is relevant to most common dynamic accidental loading cases in civil engineering structures. Low and intermediate-velocity impact tests are commonly based on large mass low-velocity technique using the potential energy method to generate the impact energy. Examples of such setups include falling drop-weight and pendulum-type.

Several types of impact tests exist but due to the difficulty while being performed and the sophisticated equipment required [32]. ACI Committee 544 [33] has proposed a drop-weight impact test to evaluate the impact resistance of concrete due to its simplicity and economy.

Experimental and numerical work studying the behavior of RC beams subjected to impact loads by steel drop hammers and vehicles has been published ([6], [21], [23],[31],[34], [35],[36],[37]). Experimental work performed by Zhou et al.[31] Fujikake et al.[34] and Saatchi and Vecchio[35] consisted of analyzing a beam behavior under impact which has been used in simulating the vehicle-pier collisions.

Agrawal et al. [21], conducted a comprehensive investigation of the behavior of three-span reinforced concrete highway bridge piers (as shown in Fig 2-5) subjected to impacts by medium weight trucks moving at 30, 50 and 70 mph which were modelled in LS-DYNA. The behavior of concrete during high strain rate impact loading was modelled nonlinearly using the

Continuous Surface Cap Model (CSCM) concrete model in LS-DYNA so as to capture dynamic failure modes of the bridge pier. Various failure modes of the bridge pier have been identified by impacting the bridge pier by the truck as shown in Table 2-1.

In a similar study conducted in New York El-Tawil et al. [23], used inelastic transient finite element simulations to investigate the structural demands generated during three accidental collisions between heavy vehicles and bridge piers that occurred with catastrophic consequences and related loss of life. In this study, the 14-kN Chevy truck and 66-kN Ford truck models developed by FHWA for safety/crashworthiness were used. The two truck models were crashed at various approach speeds into finite element models of two bridge piers (rectangular and circular) with different structural characteristics. ESF were computed as a more appropriate measure of the design structural demand and used to critique the AASHTO-LRFD vehicle collision provisions. From their study, the provisions of AASHTO-LRFD were found not to be sufficient against some crashing situations.

Table 2-1 Damage Classification Based on Failure Mechanism [6]

Failure mechanisms	*Damage Classification*
Spalling of concrete surface; breakage of the pier;	Repairable (minor) A bridge pier with minor damage can be repaired without replacement of the concrete component
Severance of the longitudinal rebar and stirrups; plastic hinge formation in the pier;	Moderate: A bridge pier with moderate damage may have to be repaired with structural rehabilitation.
The crush of the bent; Flexural failure of the bent	Severe: A severely damaged bridge pier may pose a high risk of collapse of the bridge. Hence, the bridge may have to be demolished and reconstructed.

According to Zhou et.al. [38] in their study of a viaduct pier in Shanghai using a developed prototype of bridge pier (Figure 2-4) and Chinese model-Dongfeng truck developed using FEA-MISEL company. In this study Zhou et al. [38], the vehicle-pier collision numerical model was developed in LS-DYNA and validated using the nonlinear material constitutive laws considering strain-rate effect. The relationship between failure modes of the impacted piers and impact energy was analyzed and ESF as the impact force for pier design was also discussed. An impact mass of 1140 kg was dropped with speeds of 4.5 m/s on a 300 mm x 300 mm with a span of 4000 mm to be used in the verification and validation of the model.

The work by Fujikake et al. [34] consisted of three RC beams (twelve specimens of 250 mm x 150 mm and a span of 1700 mm) having varying longitudinal reinforcement ratio subjected to impact from a drop hammer. The 400 kg hammer as shown in Figure 2-4 was dropped from heights ranging from 0.15 to 1.20 m. Flexural failure was observed throughout all three specimens however the amount of local damage varied.

The study concluded that varying amounts of longitudinal reinforcement govern the amount of localized damage that can accumulate within a member. Testing has shown that localized damage in RC beams increases with higher amounts of tensile reinforcement due to the increase in stiffness. It was also found that the amount of localized failure can be reduced by providing more reinforcement in the compressive face of the beam.

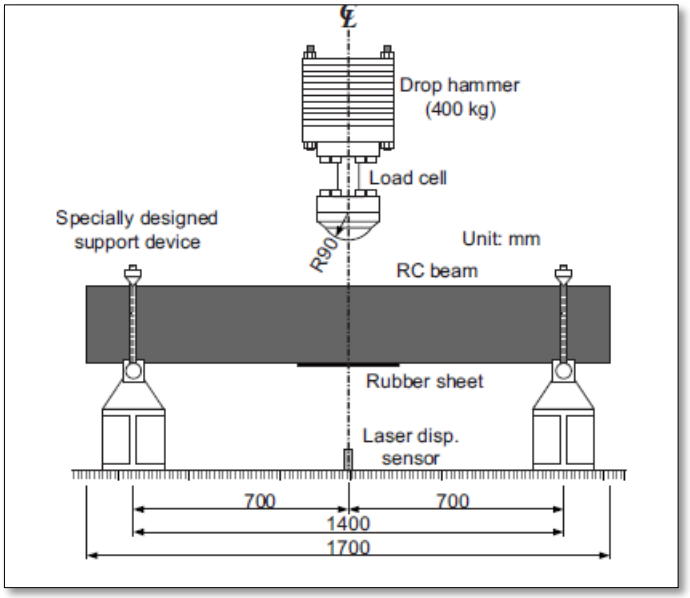

Figure 2-4 Drop Hammer Impact Test Setup [34]

Zhou and Li [37] numerically modelled and analyzed the vehicle–pier collision and concluded that the failure process of the impacted pier can be divided into four phases, that is, initial peak impact force phase, impact force of development phase, maximum peak impact force phase, and impact force of attenuation phase and defined the damage index as the ratio of the vehicle impact force to the shear capacity which can be used to assess the damage state of the impacted pier. Damage index was used to classify damage states as shown in Table 2-2.

In the study performed by Saatchi and Vecchio [35], it was found that under impact loding, shear mechanisms were the dominating factors in the primary behavior of beams. Even in beams that

were statically flexure-critical, shear failure was still of main concern under impact loading. Adequate transverse reinforcement in the shear critical sections of the beam prevented a portion of the beam from failing by shear. The study consisted of four RC beams with identical longitudinal reinforcement and varying transverse reinforcement ratios ranging from 0 – 0.3%.

Ozbolt and Sharma [36] studied concrete models that could accurately capture the rate and erosion effects of concrete under different loading situations. While it is crucial to develop validated models that can accurately capture a member's response under impact, it is equally important for in-depth analyses to be performed as well.

Table 2-2 Damage Index [37]

Damage Index Values/Damage State	Description of Results
0 - 0.2: Slight damage	Insignificant damage or microcracks occurred at the impact location. The impacted pier can be used without repairing
0.2 - 0.6: Moderate damage	Minor concrete fell off and reinforcement bent at the impact location. Small residual displacement remained at the impact location. The impacted pier can continue to be used with retrofit
0.6 - 1.0: Severe damage	The shear failure took place in the impacted Pier. Significant cracks occurred at the impact location with stirrups fractured. Obvious residual displacement at the impact location and small Vertical settlement at the top of the Pier remained.
Greater than 1: Collapse	Piers were destroyed with broken concrete and fractured stirrups. Excessive residual displacements and vertical settlement remained, resulting in superstructure being inclined badly or collapsed.

Table 2-3 Design Values of RC Piers [31]

Section dimensions /mm^2	Height /m	Compressive strength of concrete/MPa	Yield Stress of Steel/MPa	Reinforcement /mm	Stirrup /mm
1200 x 1500	6.5	31.467	414	54C32	C16@ 100/200

In a drop-weight impact test conducted by Xue-Chao [32], four different masses 0.875, 0.8, 0.675 and 0.5 kg, of steel hammers were used with a constant height of 400 mm, the hammer repeatedly fell on U-shaped concrete specimen until final failure occurred.

Brackin et al, [4] simulated heavy vehicle and a pier model where a rigid pier was modelled with fixed boundary conditions at the top and bottom making it possible to determine the maximum force that a pier might experience when hit. Two heavy vehicle models were used: a tractor-trailer and Single Unit Trucks (SUT) and 36 in. in diameter and 14 ft, tall were investigated.

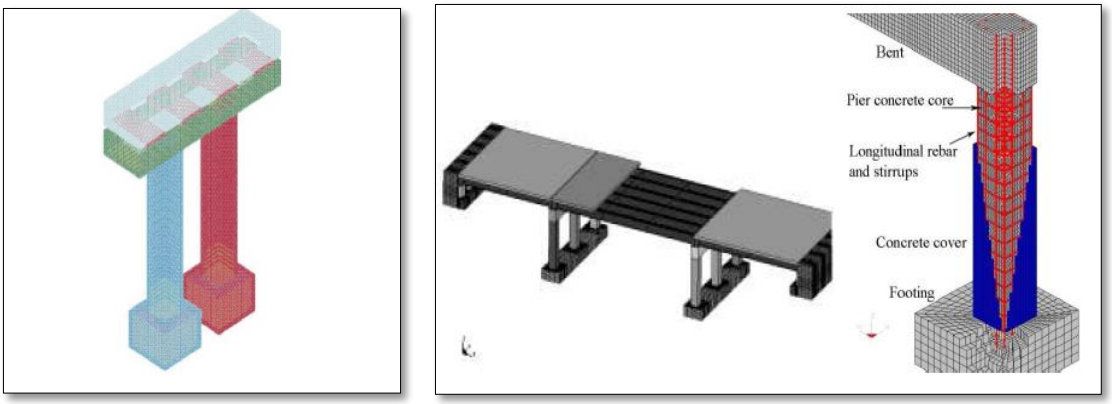

Figure 2-5 L-R Numerical Model of RC Pier; Whole Bridge Pier Model [21]

Gomez and Alipour [39] during their study, modeling controls, and material properties were verified by conducting an impact drop hammer experiment. The bridge pier collision models were validated by comparing vehicle damage and impact forces with published research results. Conservation of energy was also checked to assure stability within the impact simulation. Bridge piers subjected to vehicular collisions are exposed to significant shear forces that must be resisted by the concrete and steel reinforcement. A correlation was observed between the damage ratio of impact force over the shear resistance of a pier and the type of damage the pier experienced and were classified (Table 2-4).

Table 2-4 Damage Ratio and Classification [39]

Damage Ratio	**Damage Classification**
Less than 2	Minor
2.0 – 4.0	Moderate: Bridge remains operational
Greater than 4	Extensive: Bridge is out of operation with the possible collapse

Chen and Xiao [40] constructed a bridge model and a directly impacted pier was built with the detailed 3D nonlinear element, while the other piers, bent cap, and piles were modelled by elastic beam element, and nonlinear bar element with compression only response was used to represent soil. In their study they presented and discussed some simulations between medium-duty or heavy-duty truck and entire bridge or single pier; and the failure mode, deflection and impact force of each simulation.

2.3 Modeling and Simulation

2.3.1 Introduction

According to Sargent [41], simulation models are increasingly being used to solve problems and to aid in decision-making. Model verification is often defined as "ensuring that the computer program of the computerized model and its implementation are correct" while model validation is usually defined to mean confirmation that a computerized model within its domain of applicability possesses a satisfactory range of accuracy consistent with the intended application of the model. The cost of model validation is usually quite significant, especially when extremely high model confidence is required.

According to Zhou et.al. [31] validating a numerical model has different aspects like confirming the material models, contact types between different parts, failure modes of the impacted member, and hourglass control of the numerical result. The three chronological steps for model validation are;

1) To validate the material models and contact types.

2) To validate the failure mode and

3) To validate the hourglass control

There are three basic approaches used in comparing the simulation model output behaviour to either the system output behaviour or another model output behaviour: (1) the use of graphs to make a subjective decision, (2) the use of confidence intervals to make an objective decision, and (3) the use of hypothesis tests to make an objective decision.

Simulation modeling and analysis is becoming increasingly popular as a technique for improving or investigating process performance Chung [42]. It is a cost-effective method for evaluating the

performance of resource allocation and alternative operating policies. In addition, it may also be used to evaluate the performance of capital equipment before investment. These benefits have resulted in simulation modeling and analysis projects in virtually every service and manufacturing sector. Simulation modeling and analysis is the process of creating and experimenting with a computerized mathematical model of a physical system. Simulation modeling has specific benefits and these include:

- Experimentation in a compressed time
- Reduced analytic requirements
- Easily demonstrated models

2.3.2 Different techniques for impact load modeling

Freefall impact can be modelled in different Finite element software's using different techniques. One obvious way is to define an amplitude variation of impact load resulting from the test as an input. However, there are two easy techniques without prior knowledge of the impact load that are used for modeling.

- The drop weight can be modelled at its initial drop-height above the specimen and allow the software to calculate the motion under the influence of applied gravity acceleration. Studies show that weight falling testing apparatus is the best way to investigate shear, bending failures and deformations in structural members under impact effect according to Engin [24].
- The drop-weight can be modelled at a position very close to the specimen surface with a predefined initial impact velocity. The first option is less practical because of the large number of increments required to complete the falling part of the simulation. The latter is the most efficient technique that was used by Othman [28].

Here, by conservation of the energy, the speed on impact (V_f) is calculated by the equation of $V_{f;}$ -

$$\boldsymbol{mgh = \frac{1}{2} m V_f^2 - \frac{1}{2} m V_i^2 \; but \; Initial \; velocity \; V_i = 0} \quad \textbf{(1)}$$

$$\boldsymbol{V_f = \sqrt{2gh}} \quad \textbf{(2)}$$

where g is the acceleration due to gravity (9.806 m/s2), *h* is the free fall height (m),

2.3.3 Modeling of the Geometry

In general, the geometry of RC members should be modelled as close as possible to the real structure. The majority of numerical simulations of RC members have been carried out using two-dimensional idealization, which is valid for most cases involving static loading.

However, impact-contact problems require an adequate representation of local and global responses. 3D-FE modeling would enable accurate simulation of RC plates under impact load since stress and strain distributions are in three dimensions especially at impact zone as described by Belytschko et al. [43]. Additionally, three-dimensional modeling takes into account some critical aspect such as confinement effect, punching, transverse shear, and dilation of concrete, which are difficult to model using two-dimensional simplification.

According to Liu and Quek [44], there are numerous Computer Aided Design (CAD) software packages used for engineering design which can produce files containing the geometry of the designed engineering system. These files can usually be read in modeling software packages, which can significantly save time when creating the geometry of the models. In many cases, finely detailed geometrical features play only an aesthetic role and have negligible effects on the performance of the engineering system.

2.3.4 Material Property and modeling

The adopted material constitutive model must be capable of tracing the development and propagation of the yielding and inelastic flow of the material up to the failure point. In addition, the strain rate effect is another important issue that must also be simulated properly. The elastic behavior of a material is specified by defining elastic modulus and Poisson's ratio. The inelastic behavior is defined using the true stress-logarithmic plastic strain curve. According to Liu and Quek [44], Young's modulus and shear modulus are required for the stress analysis of solids and structures, whereas the thermal conductivity coefficient will be required for thermal analysis.

According to Liu and Quek [44], solids and structures are stressed when they are subjected to *loads* or *forces*. The *stresses* are, in general, not uniform, and lead to *strains*, which can be observed as either *deformation* or *displacement*. Materials can be *anisotropic*, meaning that the material property varies with direction. Deformation in anisotropic material caused by a force applied in a particular direction may be different from that caused by the same force applied in another direction. Composite materials are often anisotropic. Many material constants have to be used to define the material property of anisotropic materials. Many engineering materials are,

however, *isotropic*, where the material property is not direction-dependent. Isotropic materials are a special case of an anisotropic material. There are only two independent material constants for isotropic material. Usually, the two most commonly used material constants are Young's modulus and Poisson's ratio.

According to Subhashini et al. [45], plasticity is a characteristic for describing the behavior of ductile materials that experience permanent deformations. Nevertheless, plasticity theory can also be used in finite element analysis of brittle behavior. Concrete also shows some ductility under compression loading and confining pressure. It ought to be noted that when tension is present, such as shear in reinforced concrete structures, plasticity theory is usually employed in the compression zone and that the constitutive behavior of concrete is very tedious to capture by using elastic damage models or elastic plastic laws since irreversible strains cannot be captured. On the other hand, when elastic plastic relation is adopted the strain will be overestimated since the unloading curve will follow the elastic slope.

Constitutive relations define the behavior of the material in terms of stress-strain relations, function F (σ, ε), in a material and corresponding material stiffness. They reflect the non-linear material effects and failure, such as the concrete cracking or the reinforcement yielding. The above formulation is typically incremental. The forces, displacements, strains, and stresses are linearized increments within each load step.

Cracking is the most important property of brittle materials such as masonry, concrete or rock. Therefore, the complete response of a structure to a given imposed loading can be obtained by such an analysis including stages of crack propagation in the pre-peak serviceability state, the failure load and failure mode and the post-peak behavior. The response of concrete can be divided into four stages; uncracked, cracked, yielding of the reinforcement and failure according to Michael and Josefine [46] as shown in Figure 2-6

In the uncracked stage, the reinforcement has small influence and the flexural rigidity is mostly governed by the concrete. The response is relatively stiff and linear in this stage. This is referred to as state I.

When the tensile strength of the concrete is reached in a section, a crack is formed. In the early stages of cracking the concrete between the cracks has a large contribution to the stiffness, this is called tension stiffening. When the cracks propagate in the structure the stiffness decreases

until the structure can be regarded as fully cracked and the stiffness is to a high degree governed by the reinforcement. The stiffness of the fully cracked section is referred to as state II stiffness.

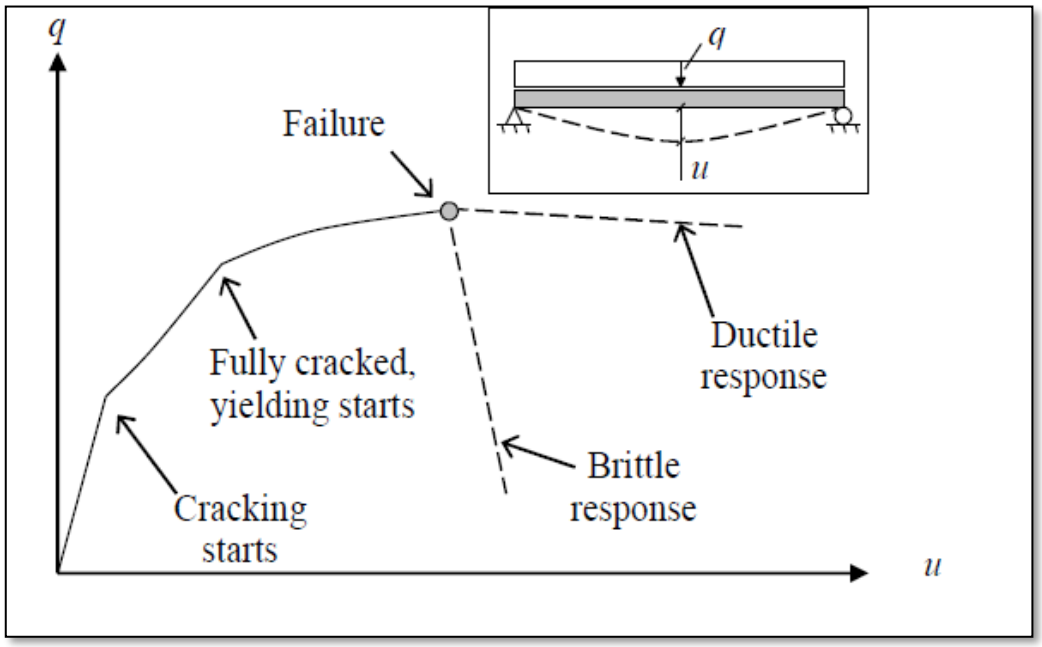

Figure 2-6 Modified Structural behavior of Concrete [46]

In the third stage, the reinforcement will start to yield and the response of the structure changes drastically. The strain hardening of the steel allows the load on the structure to be increased beyond the yield strength of the steel. The failure of the structure can be brittle or ductile depending on the properties of the section, e.g. the amount and the ductility properties of the reinforcement. A formation of a plastic hinge will develop if the response of the reinforcement is ductile and a suitable reinforcement configuration, with regard to cross-section and concrete strength, is present.

2.3.5 Strain rate effects

The rate at which a strain is applied to a structure affects the response of the materials. When a strain is applied fast, materials tend to be stiffer and stronger. According to Michael and Josefine [46], the strain rate effect on concrete can be explained by viscous and structural effects as shown in Figure 2-7.

The viscous effects have an impact on the formation of cracks in the material. During static loading, the crack propagates through the material slower and has time to find the weaker path. At high strain rates, on the other hand, the crack propagates without having time to make use of the same weaknesses within the material. This gives rise to a stiffer and stronger response.

At higher strain rates, the structural effects are influencing the strength. This is mainly due to inertia forces that develop at the tip of the crack. When concrete is subjected to compression, faster than it responds, a confinement effect will arise. This leads to a stress state close to plain strain which increases the strength of the concrete.

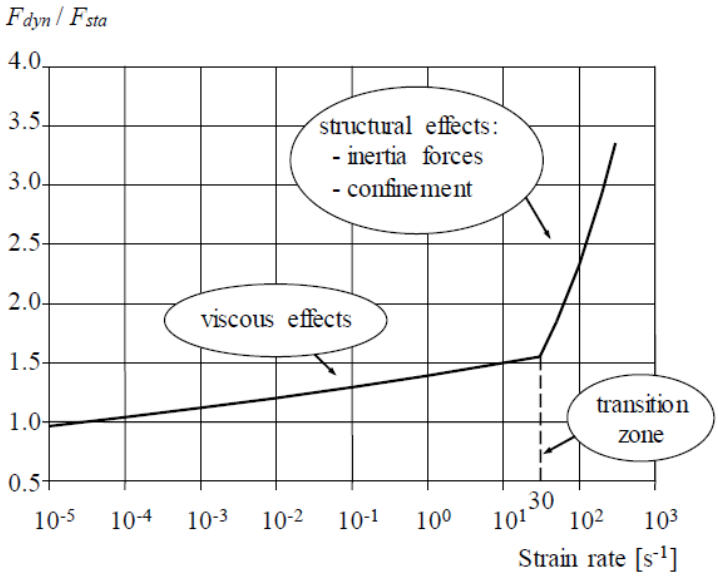

Figure 2-7 Strain rates for Viscous and Structural effects are influence concrete in compression [46]

The material strain rate is the rate of strain change of a material with respect to time. Any increase in concrete properties under dynamic loading is typically reported as a dynamic increase factor (DIF). DIF is the ratio of dynamic concrete strength to static concrete strength; it is calculated from both the strain rate and concrete static properties.

$$DIF = \frac{F_{dyn}}{F_{Sta}} \quad \textbf{(3)}$$

2.3.6 Mesh size dependency

Meshing is performed to discretize the geometry created into small pieces called elements or cells, according to Liu and Quek [44]. One of the complexities associated with FE analysis of RC structures is mesh dependency of results. Several numerical studies reported that both tensile and compressive post-peak behavior of concrete is mesh size dependent, in which the numerical results do not converge to a unique solution as the mesh is refined Othman[28]. It is more affected by the in-elastic uniaxial tensile response rather than compression softening behavior. This problem is not limited to the static or low loading rates cases but manifests identically in

the dynamic loading case. Mesh dependency typically occurs when a constitutive model based on smeared cracking approach is used to trace the damage progression in material with a stress-strain softening response.

According to Engin et al. [24], two aspects should be considered to determine if a mesh is good or not. The first has to deal with the representation level of the domain (RLD). This variable is measured as the difference between the areas or volumes of the actual domain and the final mesh. The second aspect is quality. This is evaluated in terms of aspect ratio, warping ratio, element quality and Jacobian ratio. The idea of putting a lot of emphasis on quality is because bad quality elements can lead to several computational errors in the simulation.

Logan [47] stated that aspect ratio is the ratio of the longest dimension to the shortest dimension of a quadrilateral element. In many cases, as the aspect ratio increases, the inaccuracy of the solution increases.

2.3.7 Energy balance

The law of conservation of energy explains that energy inside a system cannot be created or destroyed, and it can be transferred from one form into another without changing the total amount of energy Tony and Jason [48]. In general, the total energy (E_{total}) of any system remains constant since the energy cannot disappear but can only be transformed. Therefore, checking the total energy of the system is a good way to verify the stability of the analysis. In numerical analysis, the total energy is not completely constant and varies with time Othman [28]. As a vehicle moves with a particular velocity, it contains an inherent amount of kinetic energy. Energy dissipation through heat and sound are neglected as they account for a relatively small amount of the total energy in the system. Vehicles are designed to protect the passengers by dissipating energy through crumple zones; where the material in parts of the vehicle are designed to yield without causing damage to the passenger compartment. Once the vehicle itself cannot absorb any more energy through deformation, the remainder of the energy is transferred into the bridge pier. The amount of energy absorbed by the bridge pier is proportional to the pier's stiffness and inertia at rest. Because bridge piers often possess a large amount of inertia, the force required to cause a displacement of the column is very large. As the column displaces due to the impact, work is done.

In addition to monitoring the total energy time history, it is important to check different components of internal energy. The internal energy (E_I) is equal to the summation of recoverable

elastic strain energy (E_E), the energy dissipated through inelastic plasticity processes (E_P), the energy dissipated through viscoelasticity or creep (E_{CD}), and the artificial strain energy or hourglass energy (E_A). The artificial strain energy is used to suppress hourglass modes and it includes energy stored in hourglass resistances and transverse shear in shell and beam elements. The artificial energy is another useful quality check and it should be minimal, typically not exceeding 5% of internal energy. Large values of artificial strain energy indicate that mesh refinement is necessary. Energy briefs that include internal energy, total energy, and specific energy are explained as follows according to Tony and Jason [48];

Internal energy: In theory, the internal energy is equal to the work (E) done by external forces on the system, which is equal to the product of the exerted force (F) and the distance (d) through which the force moves.

Total energy: The total absorbed energy is the amount of energy that the specimen absorbed during the entire impact test – from start to end. This value may be the same as energy to maximum load when the specimen abruptly fails at the maximum load point. The value is calculated from the time the load begins to rise until the first occurrence of zero loads after the maximum point. This value can be used as an indicator to a materials ductility or toughness – the higher the value the stronger the material. However, care needs to be taken to ensure that when the data collection ends, the load has fallen below the zero thresholds. If it hasn't, this value is no longer a valid number to be used. The total energy is calculated by the summation of energy before the crash and after the crash of the different materials.

Specific energy: Fundamentally, the key requirement of crash protection is to absorb and dissipate energy. In an impact, the crash structure must dissipate the energy of the impact whilst ensuring that the occupants of the vehicle are not subjected to excessive accelerations/forces and that the "survivable" zone within the car remains intact (i.e. the crash structure does not ingress too far into the vehicle). This energy dissipation is achieved through plastic work done in deforming the material in the crash structure known as specific energy.

Hourglass Energy: According to Bala and Day [49], hourglassing refers to nonphysical, zero-energy modes of deformation in solid, shell, and thick shell elements with a single integration point. Hourglass modes result in zero strain and no stress modes, this can affect solution accuracy by interfering with the structure's true response. Hourglassing can be eliminated from the solution by implementing fully integrated elements but at the expense of longer analysis time.

Single point integration elements are more commonly used because they are much faster to analyze, and with the implementation of hourglass control algorithms hourglass is minimized to a tolerable amount; usually, less than 10% of the total energy of the system as discussed by Bala and Day [49]. The hourglass control algorithms apply internal forces to resist the hourglass modes and result in hourglass energy that is taken away from the physical energy of the system. Hourglass energy is controlled by viscous and stiffness formulations. Viscous and stiffness hourglass control formulations generate hourglass forces proportional to components of nodal velocity and displacement, respectively. Viscous forms are recommended for high velocity and high strain rate problems such as explosives. Stiffness forms are recommended for low strain rate problems such as crash simulations.

2.4 Methods of Analysis under Numerical formulations

According to Liu and Quek [44], structural analysis is typically performed for any given structure to evaluate local effects such as internal forces or stresses, or global effects which involve displacements and reactions. For this analysis to function properly and produce decent results, well-defined geometry, material properties, and boundary conditions of the studied member have to be provided. There are three analysis methods which are commonly used by researchers: empirical, analytical, and numerical. Many complex engineering problems cannot be analyzed using the first two methods, and more practical analysis is usually carried out using numerical approaches. This method involves breaking down a structure (domain) into smaller pieces (sub-domains).

2.4.1 Finite Difference Method (FDM)

The finite difference method is a numerical technique frequently used to obtain approximate solutions of problems governed by differential equations Hutton [50]. This method generally involves breaking the structure into nodal regions and the governing equations are replaced by finite difference equations, then these equations are solved simultaneously to obtain a solution. However, the major drawbacks of this method is that it is impractical to apply the procedure to structures with complicated geometries, boundary conditions, and problems of fast-changing variables as in the case of stress concentration.

2.4.2 Boundary Element Method (BEM)

As implied by the method's name, elements are only formed on the boundary of the structure. The method applies Green's theorem as the response of the differential equation to determine

quantities of interest such as displacements and stresses within the closed boundary. Despite the efficiency of this method in terms of computation, large matrices are sometimes expected which makes the techniques difficult to use in nonlinear problems and structures with non-homogeneous media Hutton [50].

2.4.3 Finite Element Method (FEM)

FEM is a numerical method seeking an approximated solution of the distribution of field variables in the problem domain that is difficult to obtain analytically Liu and Quek [44] . This method is based on the laws of mechanics and depending on the nature of the problem, it can be associated with solid or structural mechanics, fluid mechanics, or thermo-mechanics. The modeling procedure of the finite element analysis can be simply described as a loop. The first step involves modeling the physical problem numerically by using the appropriate differential equations (also known as shape functions) to create the finite element model that is a close representation of the structure. Loads are then applied to the model and displacements are quantified at the nodes, followed by stress and strain analyses of the system. The results obtained from this numerical modeling is validated against real data.

In summary **Figure 2-8** depicts the precedence of the finite element method that involves the choice of elements (such as truss, beam, 2D or 3D continuum), mesh, and boundary conditions. Understanding the boundary conditions imposed on the problem can, at times, be a difficult task Logan [47]. Also, it is often difficult to determine the kinds of loads that must be applied to a body and their magnitudes and locations. The combined solutions of all the elements form the solution of the entire part. This method is typically utilized to analyze structures with complex features and various material properties. It also offers an effective analytical tool for studying the structural behavior of reinforced concrete members. Cracking, tension stiffening, nonlinear material properties, interface behavior, and other mechanisms that are ignored or treated approximately by other numerical methods can be modelled rationally using the finite element method. Nevertheless, the reliability of this method relies on the accuracy of the original model and the degree of agreements between the numerical results and the actual data from the prototype structure. Finally, the tremendous advantages of this technique made it the method of choice in the numerical analysis segment of this research study.

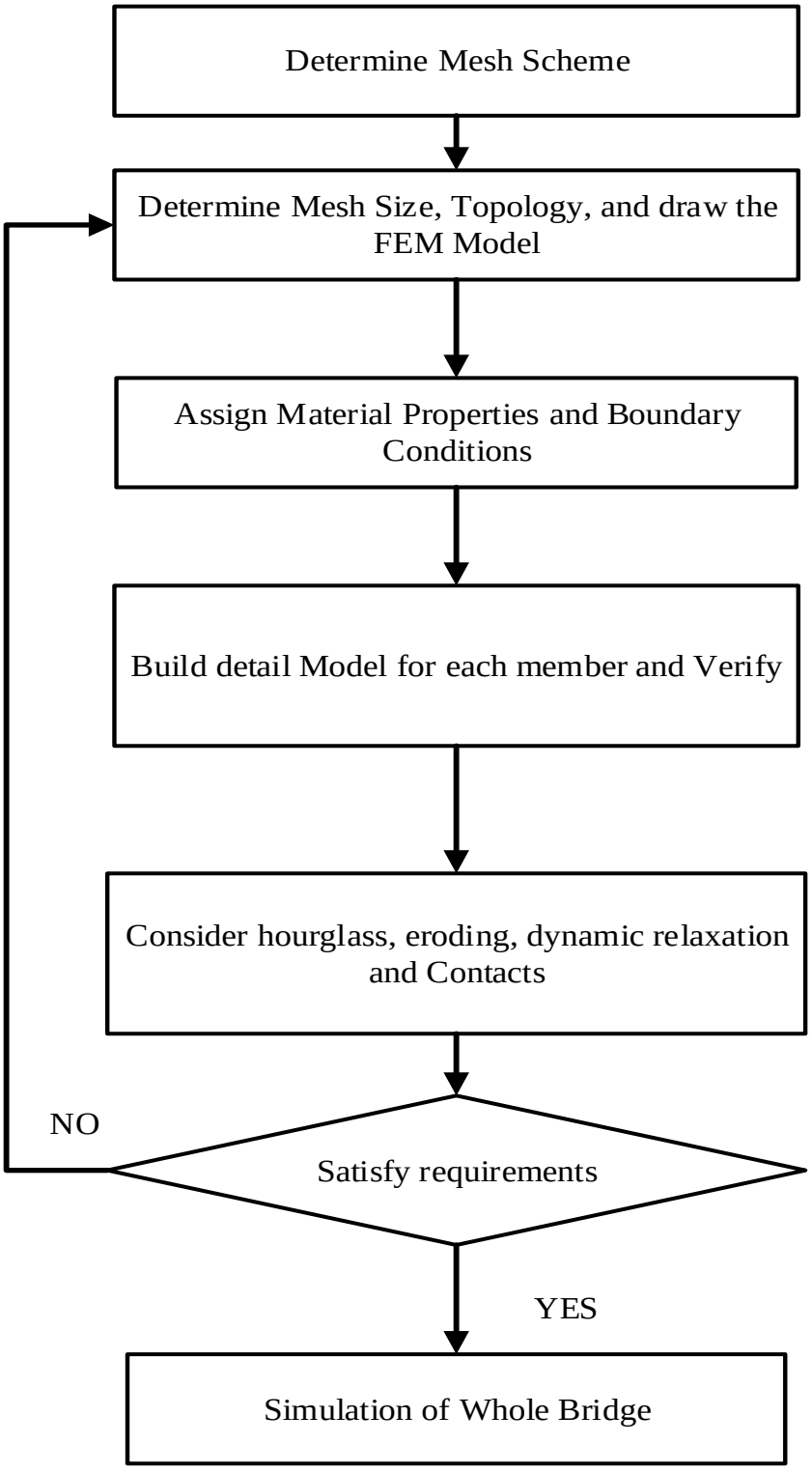

Figure 2-8 Procedure of FEM Modelling of Highway Bridges/Model Validation [6]

2.5 SAMPLING

2.5.1 Introduction to Sampling

The purpose of sampling is to obtain data that enables the estimation of some statistical parameter, or spatial predictions of some properties over an area. Sampling is constrained by financial and available resources; thus, an efficient sampling strategy is sought, Minasny and McBratney [51].

2.5.2 Types of Sampling

There are basically two major categories of Sampling [52] [53]and these are as follows; -

Probabilistic sampling; this consists of Simple random sampling; Systematic sampling; Stratified random sampling; Cluster sampling and Area sampling.

Non- Probabilistic Sampling: This consists of Convenience sampling; Purposive sampling; Quota sampling and Snowball sampling.

2.5.2.1 Systematic Sampling

According to Zhang [54], Systematic sampling is a widely used technique in survey sampling. It is easy to execute, whether the units are to be selected with equal probability or with probabilities proportional to auxiliary sizes. It can be very efficient if one manages to achieve favorable stratification effects through the listing of units. The main disadvantages are that there is no unbiased method for estimating the sampling variance and that systematic sampling may be poor when the ordering of the population is based on inaccurate knowledge. It is shown that in a number of common situations, where Systematic sampling has on average the same efficiency as the corresponding random sampling alternatives under an assumed model for the population, the sampling variance fluctuates much more with the Systematic sampling. The use of Systematic sampling is associated with a risk that in general increases with the sampling fraction. This can be highly damaging for large samples from small populations in the case of single-stage sampling, or large sub-samples from small sub-populations in the case of multi-stage sampling. Systematic sampling technique is operationally more convenient than Simple random sampling. It also ensures at the same time that each unit has an equal probability of inclusion in the sample.

2.5.2.2 Latin Hypercube Sampling (LHS)

An important part of the analysis of any engineering structure is to calculate the probabilities of failure or of unacceptable structural performance, Olsson et al. [55]. Since modern structures require more critical and complex designs, the need for accurate approaches to assess uncertainties in loads, geometry, material properties, analysis processes, and designing has increased significantly. However, computational structural mechanics has evolved to a level of sophistication that merits consideration of newer methods for incorporating uncertainty in the design process, Bhattacharjee et al. [56] and this usually comes with some degree of uncertainty. Chu et al. [57] stated that uncertainty is an inevitable issue in the process of manufacture, infrastructure, and engineering design. Quantifying and propagating the uncertainty in the simulation or design process is a key component of risk analysis, robustness evaluation or reliability-based optimization that attracts the attention of researchers and designers. In all engineering structural system design, uncertainties are unavoidable due to the stochastic nature of the material and imperfect nature of the mathematical model. These uncertainties can be accounted through reliability analysis *i.e.*, through failure probability distribution of load and resistance Bhattacharjee et al. [56].

The traditional deterministic model is not effective for structural analysis because of avoiding the effects of uncertainties in the parameters. Uncertainties and randomness associated with both loads and structural characteristics introduce variability in structural response. The predicted response of structure based on mathematical and statistical models with imperfect knowledge tends to depart from reality, Bhattacharjee et al. [56]. Recent developments in the area of probabilistic methods and statistical inference offer a mathematical basis that will enable the designer to incorporate the influence of variability and uncertainties arising from a variety of sources more effectively into the design process.

To consider parameter fluctuation in the real operation environment, Monte Carlo simulation (MCS) is chosen to perform stochastic simulation. When the probabilities of failure are small, however, as they usually are in reliability analysis, such an analysis is extremely time-consuming and expensive in terms of computer resources due to a very large number of iterations that are performed. Alternative methods such as Latin Hypercube Sampling should, therefore, be considered since it is one of the most popular discrete algorithm for uncertainty analyses and used with increasing frequency results through systems of linked models. According to Novak

et al. [58], Latin hypercube sampling technique appeared to be a very efficient technique in this context because it requires rather a small number of simulations for accurate results.

LHS has been a powerful tool for sampling statistical distributions in uncertainty analyses for more than 15 years. Key to its success has been its flexibility, the ability to perform traditional Monte Carlo uncertainty analyses and more advanced Latin hypercube sampling and to perform both using either random or restricted pairing techniques. The upgraded capabilities such as the added distribution types, the computation of point estimate values, and the ability to identify individual random variables by user-defined names, enable LHS to remain a viable uncertainty analysis tool for many years to come.

LHS program has been successfully used to generate multivariate samples of statistical distributions. Its ability to use either LHS or MCS with both random and restricted pairing methods has made it an important part of uncertainty analyses in areas ranging from probabilistic risk assessment (PRA) to complex simulation modeling according to Wyss and Jorgensen [59]. LHS is a widely-used method to generate controlled random samples. McKay et al. [60] in their study that involved comparison of three methods (Random sampling, Stratified sampling and Latin Hypercube sampling) for selecting values of input variables in the analysis of output from a computer code, Latin Hypercube Sampling method was found to be a good method to use for selecting values of input variables because it improves upon simple random sampling when certain monotonicity conditions hold. To obtain the Latin hypercube sample the range of each input variable Xi with i = 1, 2……. n was stratified into 2^n intervals of equal probability. In Latin Hypercube Sampling approach, the range of all random input variables is divided into n intervals with equal probability, which is restricted within the respective interval to avoid the disadvantage of clustering together, Chu et al. [57].

LHS is a stratified random procedure that provides an efficient way of sampling variables from their multivariate distributions. The goal of Latin hypercube sampling is to spread out the sample points so that low, high and moderate values of each variate are all contained in the sample.

In general, Latin hypercube sampling performs well whenever the quantity to be averaged is a sum of univariate functions and also requires estimators of the mean, the variance, and the population distribution function of the output of a computer code when the inputs are treated as random variables [60] [58] [61]. The basic idea is to make sampling point distribution close to probability density function (PDF), Larson et al. [62].

In order to obtain an analytical model that can be used to predict intricate relationships between input variables and a certain output, broad numerical study of estimates of commonly used statistical parameters accomplished by Florian [63].

LHS ensures that the entire range of each input variable is completely covered without regard to which single variable or combination of variables might dominate the computer model response(s).The three related measures of dispersion, standard deviation, mean and Coeffiecient of variation are helpful in obtaining parameters for use by LHS. To provide a measure of dispersion, it is convenient to define a value that is expressed as a fraction or percentage of the mean value. The most commonly used measure of dispersion is the coefficient of variation (V), which is the standard deviation (σ) divided by the mean value ($\bar{x}$):

2.6 Sensitivity Analysis

According to Saltelli A [64], sensitivity analyses help to identify key model features, effects of uncertainty, unnecessary model detail, and important areas for future data collection. Sensitivity studies are also used to predict outcomes for parameter sets which have not been used as input to the simulation program, and parameter modifications which will achieve optimal or desired simulated outcomes. These analyses are increasingly important as model complexity grows, and questions about the validity, interpretation, and usefulness of the model arise. The identification and representation of the implications of uncertainty are widely recognized as a fundamental component of analyses of complex systems Helton et al. [65] [66]. The study of uncertainty is usually subdivided into two closely related activities referred to as uncertainty analysis and sensitivity analysis, where

1) Uncertainty analysis involves the determination of the uncertainty in analysis results that derives from uncertainty in analysis inputs. There are two types of uncertainty: parameter uncertainty and model uncertainty.

- **Parameter uncertainty:** In statistics, a measure of uncertainty in the parameter estimation is the standard error (this should not be confused with the standard deviation). Parameter uncertainty can reduce if a larger sample is used; the standard error also depends on the standard deviation.
- **Model Uncertainty:** Model uncertainty is the uncertainty around the assumptions of the model. While models tend to report single summary outcomes, the interpretation of those results will largely depend on the level of **confidence** or **uncertainty** in various factors.

2) Sensitivity analysis involves the determination of relationships between the uncertainty in analysis results and the uncertainty in individual analysis inputs.

Sensitivity analysis is generally conducted to rank the predictors (input parameters) in terms of their contribution to the uncertainty in each of the responses (model outcomes). In simple terms, it is essentially the study of how changes in model inputs affect model outputs This can be achieved in several ways involving primarily the calculation of correlation coefficients and regression analysis and variance-based methods. According to Othman,[28], sensitivity analysis has to be carried out to identify the factors that most contribute to high probabilities of failure of a given structure.

A variety of approaches to uncertainty and sensitivity analysis are in use [65], [66] including; -

(i) Differential analysis, which involves approximating a model with a Taylor series and then using variance propagation formulas to obtain uncertainty and sensitivity analysis results
(ii) Response surface methodology, which is based on using classical experimental designs to select points for use in developing a response surface replacement for a model and then using this replacement model in subsequent uncertainty and sensitivity analyses based on Monte Carlo simulation and variance propagation.
(iii) Fourier amplitude sensitivity test (FAST) and other variance decomposition procedures, which involve the determination of uncertainty and sensitivity analysis results on the basis of the variance of model predictions and the contributions of individual variables to this variance.
(iv) Fast probability integration, which is primarily an uncertainty analysis procedure used to estimate the tails of uncertainty distributions for model predictions.
(v) Sampling-based (i.e. Monte Carlo) procedures, which involve the generation and exploration of a probabilistically based mapping from analysis inputs to analysis results. Additional information on uncertainty and sensitivity analysis.

Types of sensitivity analyses [65]**:**

1) Deterministic: This involves choosing and changing values for one or more parameters at a time keeping the rest constant. The standard way of presenting one-way sensitivity

analyses results is to plot the parameter you are changing in the x-axis and output of interest on the y-axis

2) Probabilistic: This involves assigning parameters a probability distribution and use simulations to compute new combinations. This type of sensitivity analysis assumes that a parameter has a probability distribution and thus assigns a probability to each possible outcome of a random variable. It can be described using the probability parameters for example, a normal distribution can be described by its mean and variance (two-parameters).

Tests for Hypothesis

A statistical hypothesis is a statement about the parameters of one or more populations. Statistical hypothesis testing and confidence interval estimation of parameters are the fundamental methods used at the data analysis stage of a **comparative experiment,** in which the engineer is interested, for example, in comparing the mean of a population to a specified value. These simple comparative experiments are frequently encountered in practice and provide a good foundation for the more complex experimental design problems. The hypothesis can be a two-sided alternative hypothesis. or one-sided alternative hypothesis [53] [52]**.**

A procedure leading to a decision about a particular hypothesis is called a **test of a hypothesis.** Hypothesis-testing procedures rely on using the information in a random sample from the population of interest. If this information is consistent with the hypothesis, we will conclude that the hypothesis is true; however, if this information is inconsistent with the hypothesis, we will conclude that the hypothesis is false.

Stepwise results/Regression based Analysis

Stepwise regression is probably the most widely used variable selection technique. The procedure iteratively constructs a sequence of regression models by adding or removing variables at each step [53].The standardized rank regression coefficient (SRRC) is used as a measure of variable importance during sensitivity analysis. Inspection of the results obtained with the individual replicates is supposed to be very consistent. This similarity includes the order in which variables are selected in the stepwise process, the SRRCs associated with individual variables, and the R^2 value of the final regression model, Helton [65].

Sensitivity analysis without regression

Some analyses are quite good, with R^2 values above 0.9 and others not quite so good, with R^2 values in the range from 0.6 to 0.8. This implies that the failure to account for uncertainty as measured by R^2 values probably derives from the sensitivity analysis technique in use (i.e. stepwise regression analysis with rank-transformed data) rather than from an overly small sample size Helton et al.[65].

When regression-based approaches to sensitivity analysis do not yield satisfactory insights, important variables can be searched for by attempting to identify patterns in scatterplots between sampled and predicted variables with techniques that are not predicated on searches for linear or monotonic relationships. Possibilities include use of (i) the F-statistic to identify changes in the mean value of y across the range of x, (ii) the c2-statistic to identify changes in the median value of y across the range of x, (iii) the Kruskal–Wallis statistic to identify changes in the distribution of y across the range of x, and (iv) the c2-statistic to identify a non-random joint distribution involving y and x .

When the relationship between variables is not monotonic or when measurements are arbitrarily or irregularly distributed, regression analysis is more appropriate than simple correlation coefficients, Hoare et al. [67]. A regression equation provides an expression of the relationship between two (or more) variables algebraically and indicates the extent to which a dependent variable can be predicted by knowing the values of other variables, or the extent of the association with other variables.

In effect, the regression model is a surrogate for the true computational model. Accordingly, the coefficient of determination, R^2, should be calculated with all regression models and the regression analysis should not be used if R^2 is low (arbitrarily, less than ~ 0.6). R^2 indicates the proportion of the variability in the data set that is explained by the fitted model and is calculated as the ratio of the sum of squares of the residuals to the total sum of squares. The adjusted R^2 statistic is a modification of R^2 that adjusts for the number of explanatory terms in the model. R^2 will tend to increase with the number of terms in the statistical model and therefore cannot be used as a meaningful comparator of models with different numbers of covariants (e.g., linear versus quadratic). The adjusted R^2, however, increases only if the new term improves the model more than would be expected by chance and is therefore, preferable for making such comparisons Hoare et al. [67].

Regression analysis seeks to relate a response, or output variable, to a number of predictors or input variables that affect it, Hoare et al. [67]. Although higher-order polynomial expressions can be used, constructing linear regression equations with interaction terms or full quadratic responses is recommended. This is in order to include direct effects of each input variable and also variable cross interactions and nonlinearities; that is, the effect of each input variable is directly accounted for by linear terms as a first-order approximation but we also include the effects of second-order nonlinearities associated with each variable and possible interactions between variables.

One of the values of regression analysis is that results can be inspected visually. If there is only a single explanatory input variable for an outcome variable of interest, then the regression equation can be plotted graphically as a curve; if there are two explanatory variables then a three-dimensional surface can be plotted. For greater than two explanatory variables the resulting regression equation is a hypersurface. Although hypersurfaces cannot be shown graphically, contour plots can be generated by taking level slices, fixing certain parameters. Further, complex relationships and interactions between outputs and input parameters are simplified in an easily interpreted manner, Hoare et al. [67].

Although regression analysis can be useful to predict a response based on the values of the explanatory variables, the coefficients of the regression expression do not provide mechanistic insight nor do they indicate which parameters are most influential in affecting the outcome variable. This is due to differences in the magnitudes and variability of explanatory variables, and because the variables will usually be associated with different units. These are referred to as unstandardized variables and regression analysis applied to unstandardized variables yields unstandardized coefficients. The independent and dependent variables can be standardized by subtracting the mean and dividing by the standard deviation of the values of the unstandardized variables yielding standardized variables with a mean of zero and variance of one. Standardized coefficients should be interpreted carefully – indeed, unstandardized measures are often more informative, Helton et al.[65].

The regression equation can provide more meaningful sensitivity than correlation coefficients as it can be shown that an x% decrease in one parameter can be offset by a y% increase/decrease in another, simply by exploring the coefficients of the regression equation. It must be noted that this is true for the statistical model, which is a surrogate for the actual model. The degree to

which such claims can be inferred to the true model is determined by the coefficient of determination, R^2.

According to Manache and Melching [68], the sensitivity contribution of the model input variables to the model output can be quantified by various measures. For the uncertainty analysis, the mean, standard deviation, and other statistics of the model output are calculated and used to parameterize assumed probability distributions for the model output. These probability distributions can then be used to estimate the probability that design or planning goals will be achieved.

Chapter 3 : AALRT BRIDGE PIERS VULNERABILITY

3.1 Introduction

This stage of the study involved identification and categorization of vulnerable bridge piers at risk of being subjected to vehicular impact load along AALRT. The identification, categorization, and ranking of vulnerable piers was done according to section 2.2.2.2 of NYSDT [69].

3.1.1 Vulnerability assessment

The vulnerability assessment process is used to determine the relative vulnerability to collision impact damage failure of bridges. The process consists of a classification step and rating step.

The classifying step used information such as impact factors, exposure factors, characteristics of traffic and geometries of the structure and its approaches to evaluate the vulnerability of the pier to collision. The result of this step is a vulnerability classification score and a high, medium or low vulnerability class is later on assigned to individual piers. The classification score quantified the collision vulnerability class for a structure as indicated in APPENDIX A. The vulnerability classes describe the relative potential a structure has for failure due to collision impact damage, and it is used to determine the vulnerability rating for a structure.

The rating step is intended to provide a uniform measure of a structure's vulnerability to failure on the basis of the likelihood of a failure occurring and the consequences of failure. There are six possible ratings usually done for the entire bridge structure, from 1 to 6, with 1 being the worst possible rating and 5 being the best. Structures for which this assessment procedure is not applicable are rated 6. These indicate what types of corrective actions are needed and the urgency in which these actions should be implemented. Based on the rating, an interim action such as load posting or closing a bridge may be necessary until an evaluation can be completed and vulnerability reduction measures taken.

3.1.2 Collision Vulnerability Classes

The higher the vulneralibility class for a given pier the more the risk it has to collision. This however does not mean that low class is not susceptible to collision, though the probability of such an occurance is too minimal.[69]. The bridge rating was not done because this study was only focused on bridge pier vulnerability assessment for simulation purpose.

High: Conditions exist on a structure which create a significant potential for failure due to collision impact damage. Bridges in this class will typically have primary members exposed to direct vehicle, water vessel or railroad impact. If a protection system exists, it has failed or is inadequate. It is quite likely that during the structure's remaining life it may receive an impact capable of causing failure.

Medium: Conditions exist on a structure which create a recognizable potential for failure due to collision impact damage. Bridges in this class will typically have primary members exposed to direct vehicle, water vessel, or railroad impact. A protection system exists, but may not protect the primary member from severe impact damage, possibly causing failure, and may thereby need to be upgraded or enhanced.

Low: Conditions exist on a structure which reveal little or no potential for failure due to collision impact damage. These bridge types, while recognized as having primary members susceptible to a collision impact damage failure, have adequate protection to protect against failure.

3.2 Bridge Pier Vulnerability Classification

Pier vulnerability classification was done following data collection. The data that was collected was of two categories and these were primary and secondary data. Primary data was collected through field surveys that required making the required observations and measurements along the study route while secondary data was collected from review of existing data from different agencies, previous research, and published documents and literature.

3.2.1 Preliminary investigation and desktop study

3.2.1.1 Route segmentation

AALRT route was divided into four main segments so as to be able to separately understand the level of vulnerability of piers in each section for the safety analysis of the piers. The segments under which the piers were categorized are: -

1. Tangent Section
2. Round-about Section
3. Signalized Intersection
4. Curved Section

3.2.1.2 Pier designation

Piers were generally designated as line- pier number, for the purpose of this research the following were adopted for the different categories; Lines were categorized into three; - NS; EW and NS-EW.

- North-South (NS): - applicable to stretches from Atikiltera to Darmar; Stadium to Nefas Silk2;
- East-West (EW): - applicable to stretches from Coca-Cola to St-Lideta and Stadium to Bambis.
- Common Line (NS-EW): -applicable to the common stretch which is from St-Lideta to Stadium.

A total of 276 piers were considered for the purpose of this research with; 93 piers designated NS-01 to NS-93 being found between Atikiltera and Darmar; 28 piers designated NS-207 to NS-234 being found between Stadium and Nefas Silk2; 6 piers designated EW-235 to EW-240 being found between Coca-Cola and St-Lideta; 36 piers designated EW-241 to EW-276 being found between Stadium and Bambis and 113 piers designated NS-EW-94 toNS-EW-206 from St-Lideta to Stadium.

3.2.2 Main Stage Investigation

3.2.2.1 Field visits

Preliminary visual inspection of all the piers was done in order to identify bridge pier particularities such as the structural system, possible damages and all the stipulated parameters based on (Appendix A) so as to complete the bridge pier vulnerability evaluation and classification. Upon classification of the piers, a supplementary field visit was done to enable picking of coordinates and as built dimensions of the vulnerable piers so as to draft a Vulnerability Pier Map

3.2.2.2 Supplementary information

Traffic Characteristics: For the purpose of complete assessment, review of documentation related to vulnerability classification was undertaken. Average Daily Truck Traffic (ADTT) data was obtained from Addis Ababa Transport Authority and thereafter adopted for the bridge pier vulnerability classification in this work.

Weight of the Superstructure: The weight classification was assumed as follows:

- Light:- All double track areas except for stations and turn out areas.
- Medium: - All Station platform areas
- Heavy: - The two main turn out areas (next to Stadium and St-Lideta)

3.3 Pier Vulnerability Ranking, Sampling, and Mapping

3.3.1 Pier Vulnerability Ranking

Out of the 276 piers that were visually inspected and classified, it was found out that 6 piers corresponding to 2.174 % are highly susceptible to vehicle impact, while 269 piers (97.463%) are moderately exposed and 1 pier (0.3623%) was found to be of low exposure to impact.

Further analysis of the highly and moderately exposed piers shows that by location, 35.273% are located along curved sections while 56.727% are located along the tangent section, 4.727% are located along roundabouts and 3.273% are at intersections as summarized in Figure 3-1 . Whereas by the availability of protective barrier for the highly exposed piers also showed that; 59.091% had no protection at all while 40.909% had a sub-standard protective measure. A detailed consideration of the ranking is attached in APPENDIX A.

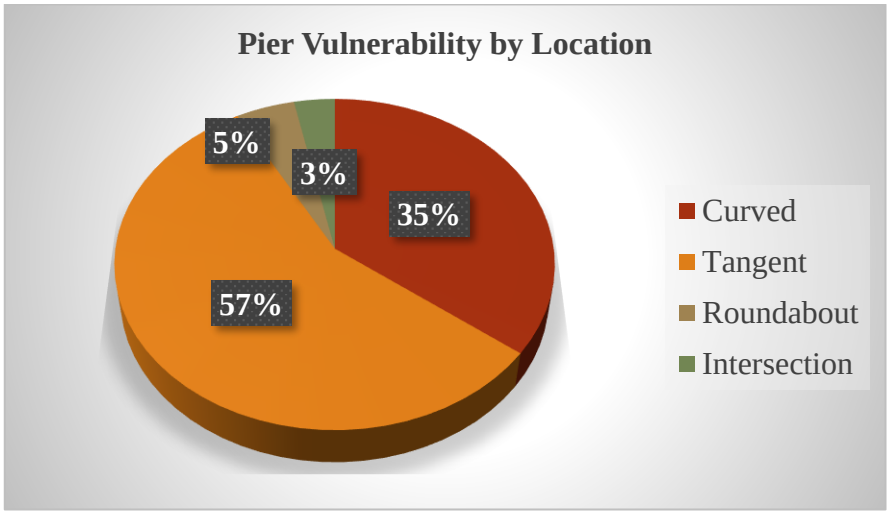

Figure 3-1 AALRT Pier Vulnerability by Location

3.3.2 Pier Sampling

Upon ranking of the piers in the different created strata as shown in Table A-1 in Appendix A, the most vulnerable piers were systematically chosen from each category. The chosen piers were then considered for the drafting of the Pier Vulnerability Map.

3.3.3 Pier Vulnerability Map

A GPS was used to pick coordinates of the identified piers as in Table 3-1. The accuracy of the ground-truthed GPS points were confirmed by importing the coordinates to Google Earth Maps which confirmed the points as being along AALRT. Using ArcGIS, the Vulnerability Map was generated as shown in Figure 3-2.

Table 3-1 Vulnerable Piers for Simulation

S/NO	TYPE OF SECTION	PIER CODE	Structural Redundancy	PIER TYPE	NUMBER OF PIERS
1.1	TANGENT	NS-EW-96	Simple	Frame Type	3
		NS-EW - 97			
		NS-EW - 98			
1.2	TANGENT	NS-EW-102	Simple	Solid Hammered Head	4
		NS-EW-103			
		NS-EW-104			
		NS-EW-105			
2	CURVED	NS-EW-190	Simple	Frame Type	4
		NS-EW-191			
		NS-EW-192			
		NS-EW-193			
3	ROUNDABOUT	NS-EW-138	Simple	Solid Hammered Head	4
		NS-EW-139			
		NS-EW-140			
		NS-EW-141			
4.1	INTERSECTION 1	EW-255	Simple	Solid Hammered Head	4
		EW-256			
		EW-257			
		EW-258			
4.2	INTERSECTION 2	NS-30	Simple	Frame Type	3
		NS-31	Simple	Solid Hammered Head	
		NS-32	Continuous		
4.3	INTERSECTION 3	EW-241	Simple	Solid Hammered Head	3
		EW-242			
		EW-243			

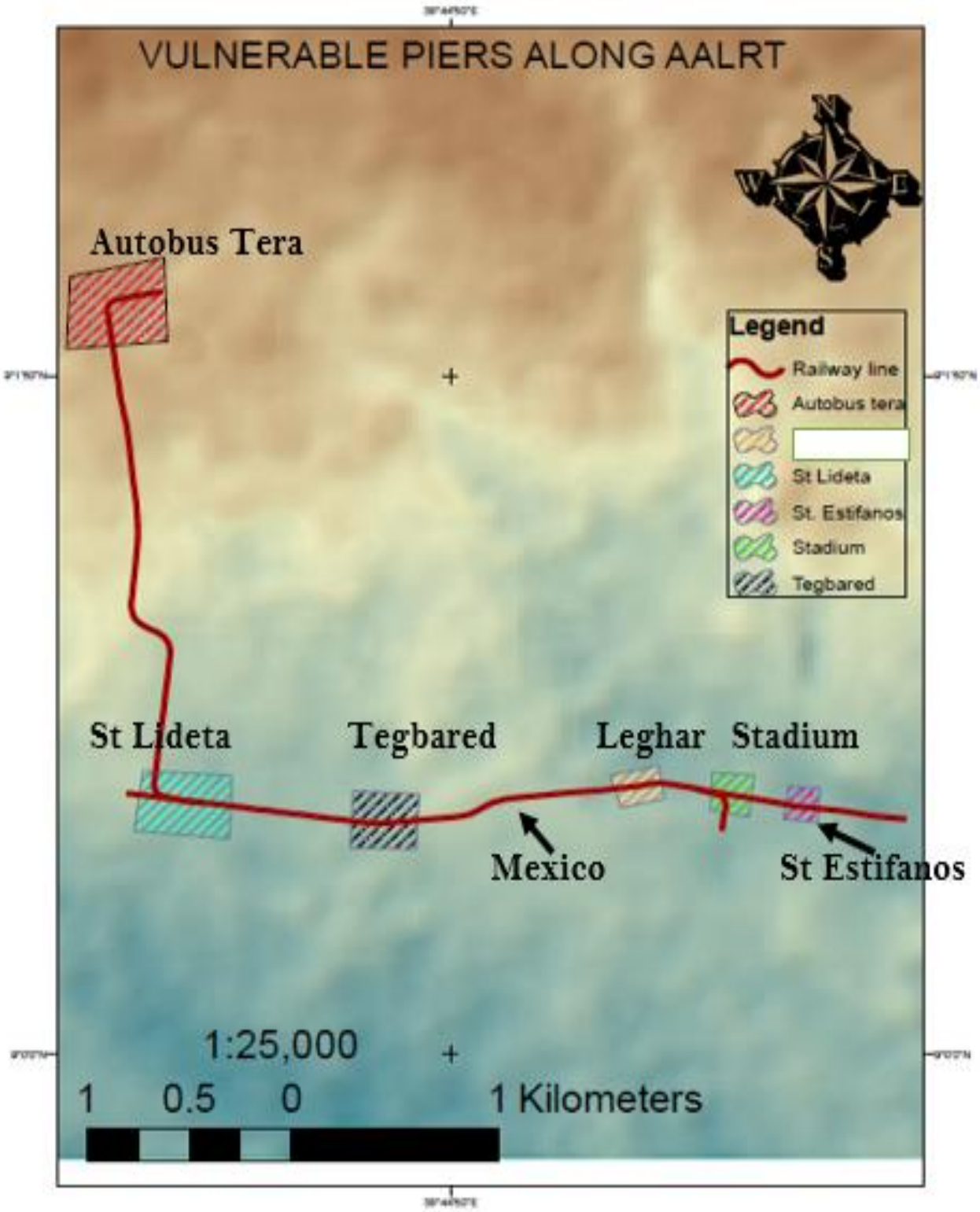

Figure 3-2 AALRT Pier Vulnerability Map

Chapter 4 : FINITE ELEMENT MODELLING AND VALIDATION

4.1 Introduction

Validation is required when using any given software so as to ensure that the finite element analysis for the model accurately represents what is being depicted. Physical characteristics that include boundary conditions, material properties, and geometry, have to be modelled to match to a greater extent that of the experimental test setup being used. The model can be validated by matching displacements and forces with experimental results and at times by comparing the crack patterns. Since experimental data for vehicle collisions with bridge piers was very limited, an experiment representing a similar impact phenomenon was used for validation purposes. For the purpose of this study the experiments conducted by Fujikake et al.[34] were used for validating the finite element controls and material properties for the vehicle-pier impact simulations. The experiment consisted of a reinforced concrete beam subjected to a drop hammer that was being dropped at different heights where crack patterns were captured and used for validation. The following finite element models were created in units of N, mm, and seconds.

4.2 Beam Impact Experiment Setup

250 mm depth, 150 mm and 1700 mm length different sets of reinforced concrete beams as prepared by Fujikake et al. [34] were subjected to impact loads. The beams have a clear span of 1,400 mm and were supported by two specially designed support devices which allowed free rotation of the beam but prevented the beam from displacing longitudinally and vertically as shown in Figure 2-8.

A concrete cover of 40 mm was provided around the reinforcement cage, except at the ends which had 25 mm of cover and all beams consisted of four longitudinal reinforcing bars, with two for tension and two for compression and with 22 transverse reinforcing bars 75mm apart as shown in Figure 4-1. The longitudinal reinforcing bars which consisted of D13, D16, and D22 with yield strengths of 397, 426, and 418 MPa, respectively as shown in Table 4-1, while the transverse reinforcing bars consisted of D10 bars with a yield strength of 295 MPa. The concrete compressive strength at the time of testing was 42.0 MPa.

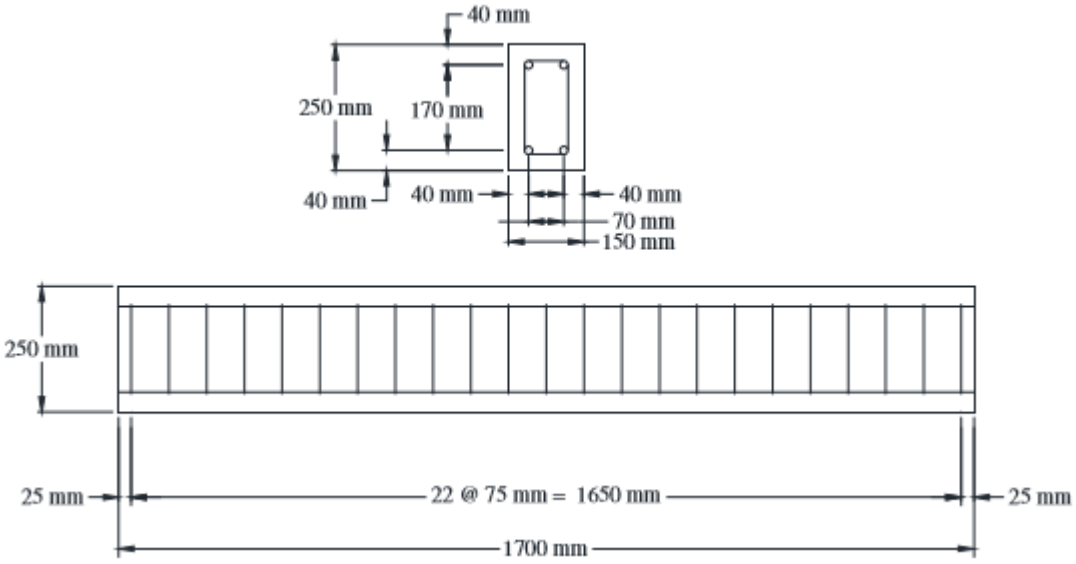

Figure 4-1 Beam Cross Section (Top) and Longitudinal Section (Bottom) [34]

Table 4-1 Beam Test Series [34]

Beam Designation	Compression Bars	Tension Bars	The ratio of longitudinal reinforcement to the gross cross-sectional area of the beam % - ρ
S1616	2 D16	2 D16	2.12
S1322	2 D13	2 D22	2.40
S2222	2 D22	2 D22	4.13

The reinforced concrete beam specimens were subjected to impact loads using a drop hammer impact loading machine. The drop hammer had a hemispherical striking head with a radius of 90 mm and a mass of 400 kg. The hammer was dropped freely onto the top surface of the reinforced concrete beam at mid-span from varying heights as shown in Table 4-2.

Table 4-2 Drop Heights for Different Beam Series [34]

HAMMER DROP HEIGHTS FOR DIFFERENT BEAMS (m)	
S1616	S1322 & S2222
0.15	0.3
0.3	0.6
0.6	1.2
1.2	2.4

ANSYS is a general-purpose finite element modeling package for numerically solving a wide variety of mechanical problems. These problems include static/dynamic structural analysis (both linear and non-linear), heat transfer and fluid problems, as well as acoustic and electromagnetic problems, UOA [70], [71]. A general-purpose Multiphysics software-ANSYS was chosen because of having an Explicit dynamic component which is great in simulating high energy dynamic conditions in addition to its availability and ease of application. Explicit dynamics of ANSYS- workbench was chosen because it models and analyses extremely well impact load simulations. The modeling is done in two main stages and these are; - Pre-processing and Post-Processing. Pre-processing consists of creating the geometry, assigning material models, boundary conditions, and all other required parameters. The post-processing mainly involves analyzing the results Hutton[50].

4.2.1 Geometry

The reinforced concrete beam geometry was created with the DesignModeler in Explicit Dynamics tool of workbench. The beam was created with the following mesh results-Element Quality of 0.5721-1, Aspect ratio of 1-3.7171 and with a Jacobian ratio of 1 – 3.6106. which clearly signifies a good mesh quality of element size 5 mm with a total number of 663,780 elements and 705,436 nodes while the drop hammer was modelled using eight nodes, constant stress, single-point integration solid elements. The drop hammer consisted of 133,579 nodes and 125,580 solid elements.

A major portion of the beam impact test setup which consisted of the beam, supports and impactor were created using the SOLID body type with an automatic shared topology in DesignModeler. The steel reinforcement cage was created as line bodies and later assigned cross-sectional area as per the required diameter corresponding to that of a given beam designation based on Table 4-1 series.

As a way of ensuring that the reinforcement cage created and the concrete act as a single component of reinforced concrete, a new body interaction in the connection of ANSYS AUTODYN Prepost is created and assigned as REINFORCEMENT type of interaction. This enables ANSYS to consider all line bodies created within the SOLID bodies as reinforcements for simulations to run.

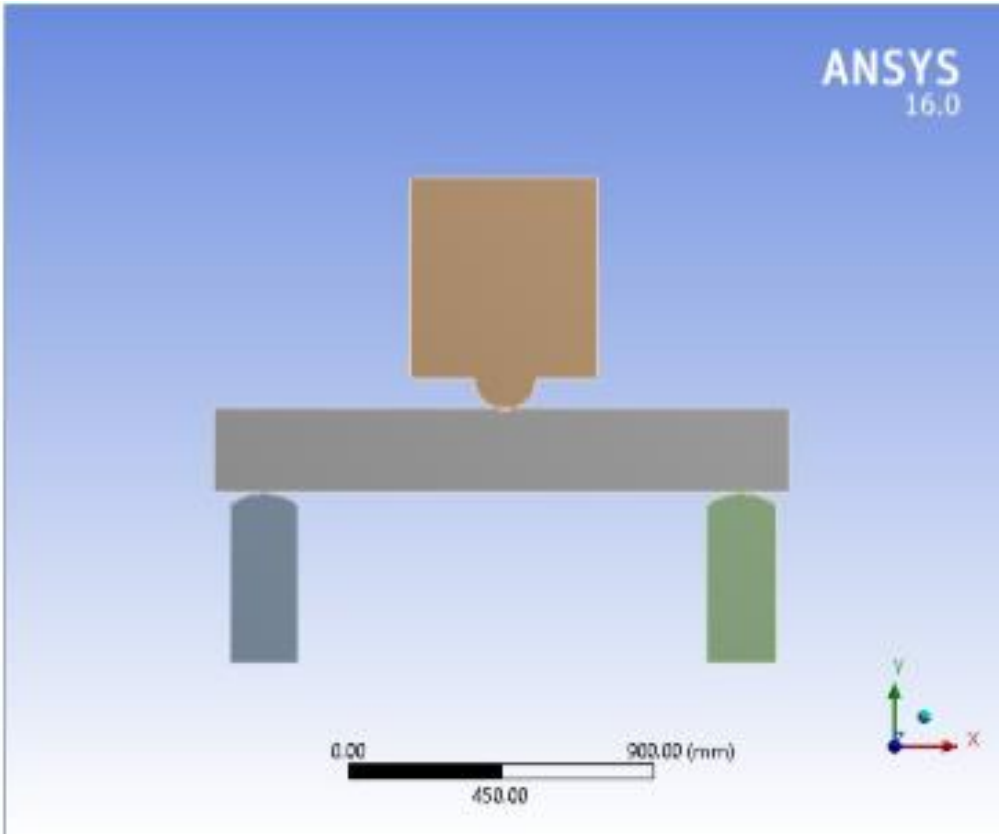

Figure 4-2 FE Model Used in the Impact Test

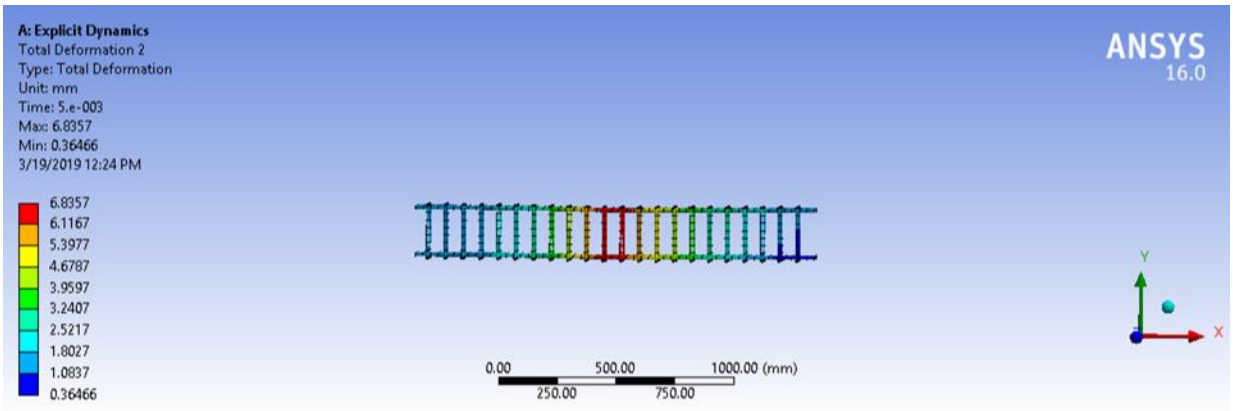

Figure 4-3 Reinforcement Cage for Impact Test Model

4.2.2 Material Models

All materials used during the study were defined with a Lagrangian reference frame and flexible stiffness behavior. They were assigned non-linear and thermal strain effects for the purpose of this study.

Concrete: The concrete behavior of the beam was modelled using Explicit material Model 37 (CONC-35MPA) from the Engineering Data Sources-5 (Explicit materials) as outlined by

Riedel et al. [72]. This is a continuous elastic surface cap model that is available for use as an Explicit Material in the Engineering Data of ANSYS Workbench. The material model defined the required strength, stiffness, hardening, softening, and rate effect parameters as a function of concrete density, specific heat, compressive and tensile strength, failure surface, fracture strength and damage constant, among others. Damage to the concrete elements is tracked through ductile and brittle damage parameters. Ductile damage occurs when stress is applied to the element in compression. Brittle damage occurs when stress is applied to the element in tension. The damage parameters range from 0 - no damage to 1- complete damage. Damage is initiated when strain-based energy terms exceed a specified damage threshold. The strength and stiffness of an element will be equal to zero when one of the damage parameters approaches a value of 1. The concrete that was modelled had a mass density of 2,274 for the Hammer test and 2,400 kg/m^3 for all the other simulations, an unconfined compressive strength of 42 MPa with damage constants D1 and D2 as 0.04 and 1 respectively.

Steel Reinforcement: Based on the Engineering data sources available in ANSYS general materials, material model 12 was chosen and used for modeling the steel reinforcements. It is an elastoplastic material model that accounts for a stress-strain curve and strain rate dependency. The main material property that was varied for the study was the tensile and compressive yield strength of the reinforcement bars that is D10; D13; D16 and D22 as 295, 397, 426, and 418 MPa, respectively. The following material properties were left constant input for each different size reinforcement bar include mass density (7,850 kg/m^3), Tensile Ultimate Strength (460 MPa); Modulus of elasticity (200 GPa), Poisson's ratio (0.3).

Drop Hammer: The drop hammer was modelled using material model 12 but with a higher stiffness though as a flexible material-modulus of elasticity of 400 GPA and Poisson's ratio 0.1. The drop hammer had a volume of approximately 0.014239 m^3 and a mass of 400 kg, mass density of 28,091.86 kg/m^3.

4.2.3 Finite Element Modeling Controls

The accuracy of the finite element model is highly dependable on the finite element controls, such as boundary conditions, initial conditions, contact between objects, and analysis controls. The following section describes how these conditions were accounted for in the modeling process.

4.2.3.1 Boundary Conditions

The modelled beams used for the beam impact experiment were assumed to be automatically constrained through the automatic contact generated at the supports between the beam and the supports while the bases of the support were fixed.

4.2.3.2 Initial Conditions and Loads

The Pre-stress environment was set to none and pressure initialization was set to 'from deformed state' Initial velocity was applied and the drop hammer was selected as the body corresponding to the drop height for a particular simulation. Impact velocities shown in Table 4-3 were calculated using **Equation- 2** (as shown in chapter 2) based on the corresponding drop hammer free fall heights.

Table 4-3 Drop Test Impact Velocities

DROP HEIGHT (m)	IMPACT VELOCITY (mm/s)
0.15	1720
0.30	2432
0.60	3440
1.20	4865
2.4	6880

4.2.3.3 Contact

ANSYS software automatically generates a connection between bodies. The contact relation between two closely placed bodies is automatically generated together with the nature of body interaction between the different bodies. Under the body interaction in order to have a realistic simulation a friction coefficient (0.3), dynamic coefficient (0.3) and decay constant of 0.001 were applied for the entire bodies.

4.2.3.4 Analysis Control

Explicit dynamics like any other simulation software requires an end time to determine whether the analysis has run for a sufficient amount of time to acquire the desired solution. An end time of 0.005 seconds was selected because it efficiently generated the desired output for the impact and its response in a timely manner from the drop hammer experiment. Erosion is a numerical mechanism for the automatic removal (deletion) of elements during a simulation. The primary

reason for using erosion is to remove very distorted elements from a simulation before the elements become inverted (degenerate). This ensures that the stability timestep remains at a reasonable level and solutions can continue to the desired termination time. Erosion can also be used to allow the simulation of material fracture, cutting and penetration. There are a number of mechanisms available to initiate erosion of elements and these are;- geometric strain, timestep, material failure and retained inertia**.** The erosion options can be used in any combination. Elements will erode if any of the criteria are met [41] [70].

4.2.3.5 Hourglass Energy Control

The hourglass damping was automatically done in Explicit dynamics however the maximum energy error coefficient had to be fixed to 0.01. At all times the energy summary from the solution output was observed to ensure that the error was within acceptable levels, errors for case (b) were always adopted as they provided slightly better results as compared to those shown in (a) in Figure 4-4.

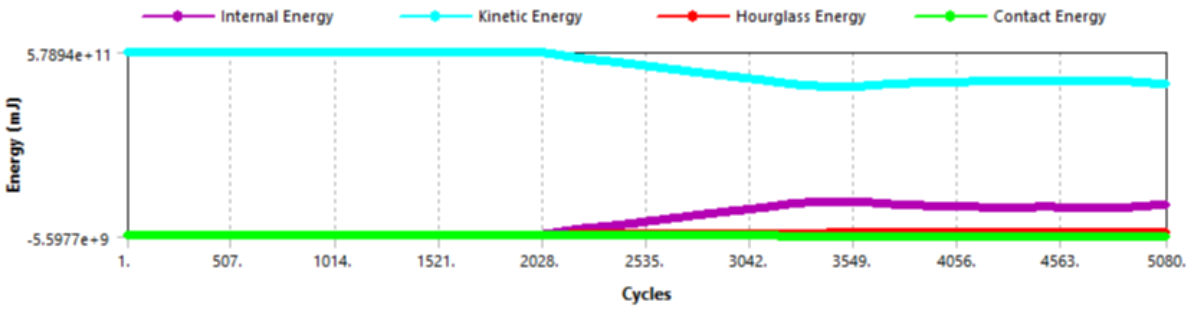

(a)

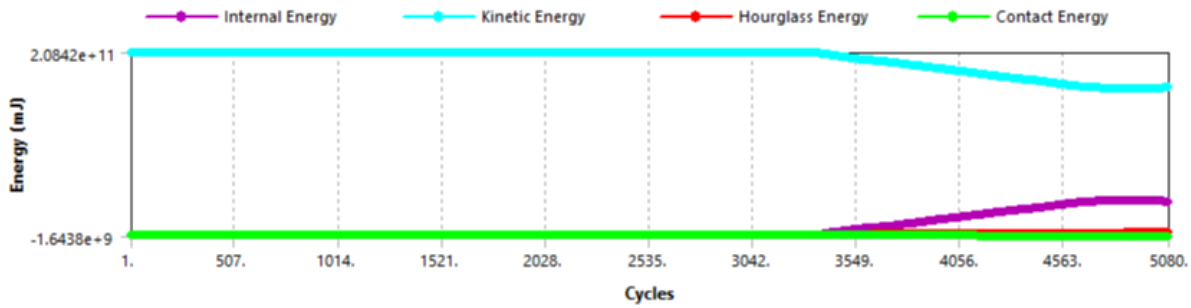

(b)

Figure 4-4 (a) and (b) Typical Hourglass Energy from the Energy Summary

4.3 Numerical Results

The experimental results reported by Fujikake et al. [34] were compared with the numerical simulation for mid-span crack patterns as a way of validating the models. The analytical results for maximum mid-span deflection were compared for the different experiments as shown in Figures 4-5, 4-6, 4-7, the crack profiles of the analytical and experimental results were compared. Where (a),(c),(e) and (g) are experimental results while (b), (d),(f) and (h) are simulation results as shown in Figures 4-8; 4-9 and 4-10.

Upon comparison of the different cracks generated it is worth noting that the validation of the beam impact experiment has been done and therefore, it was concluded that the finite element procedures used in this study can be applied to develope vehicle impact simulations with bridge piers based on the selected material models. Explicit material model 37 [72] and General material model 12 can be used to represent the material properties of concrete and steel reinforcement, respectively, under dynamic impact loading simulations. Therefore, the generated automatic connections that comprise of contacts and body interactions effectively represent the interaction between the two impacting objects. The allowable maximum energy error coefficient of 0.01 represents an allowable energy glass hour.

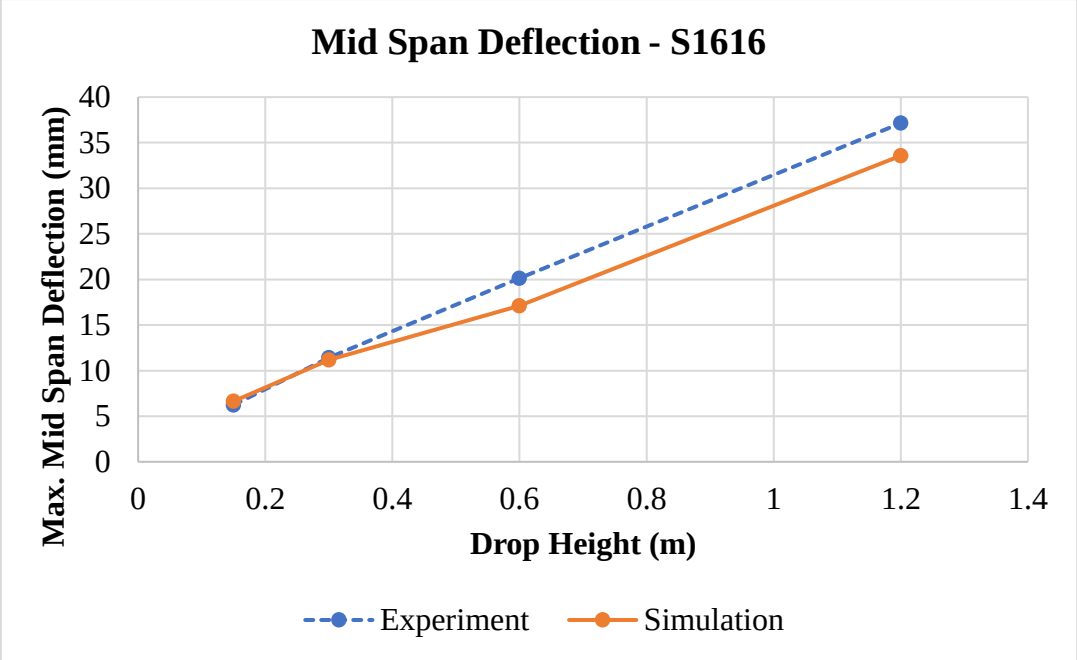

Figure 4-5 Maximum Mid Span Deflection -S1616

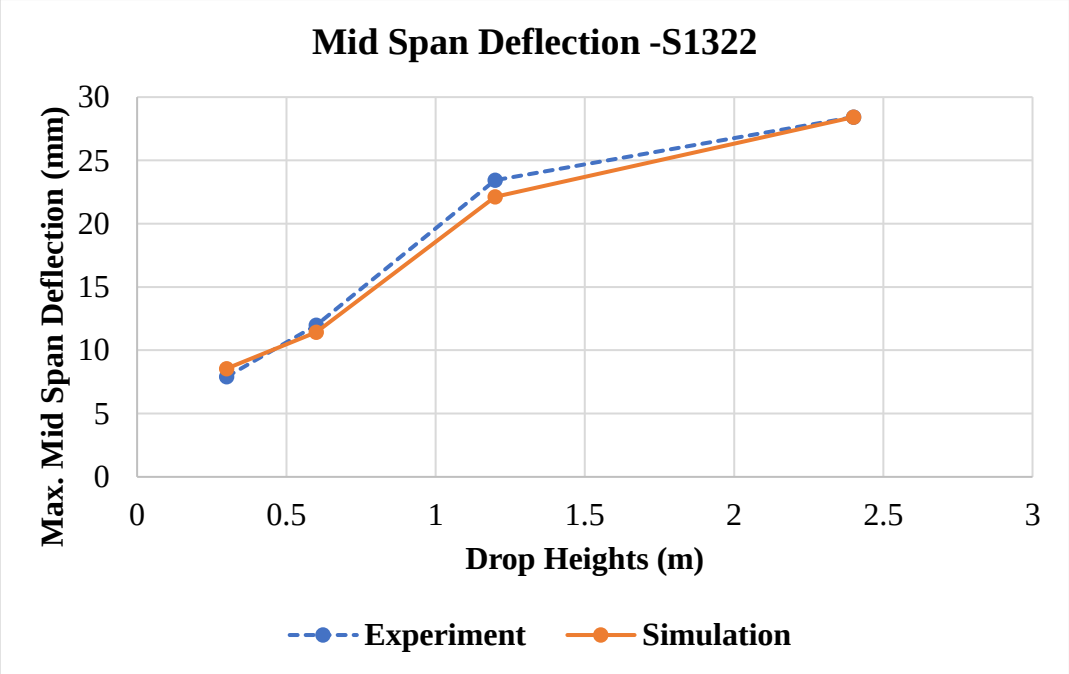

Figure 4-6 Maximum Mid Span Deflection S1322

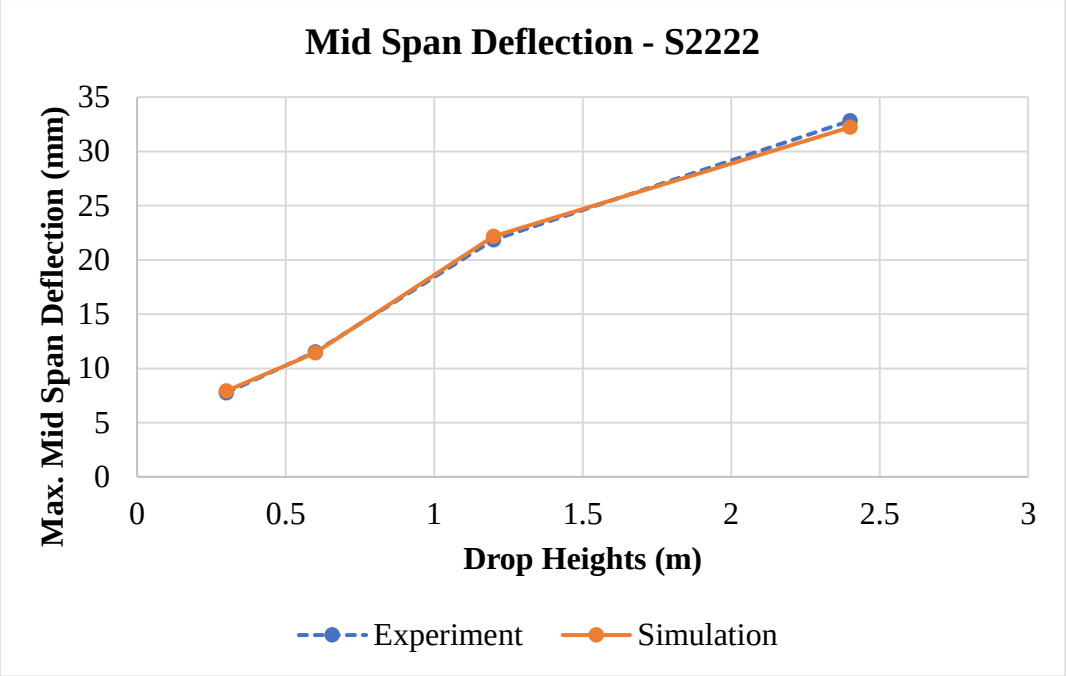

Figure 4-7 Maximum Mid Span Deflection – S2222

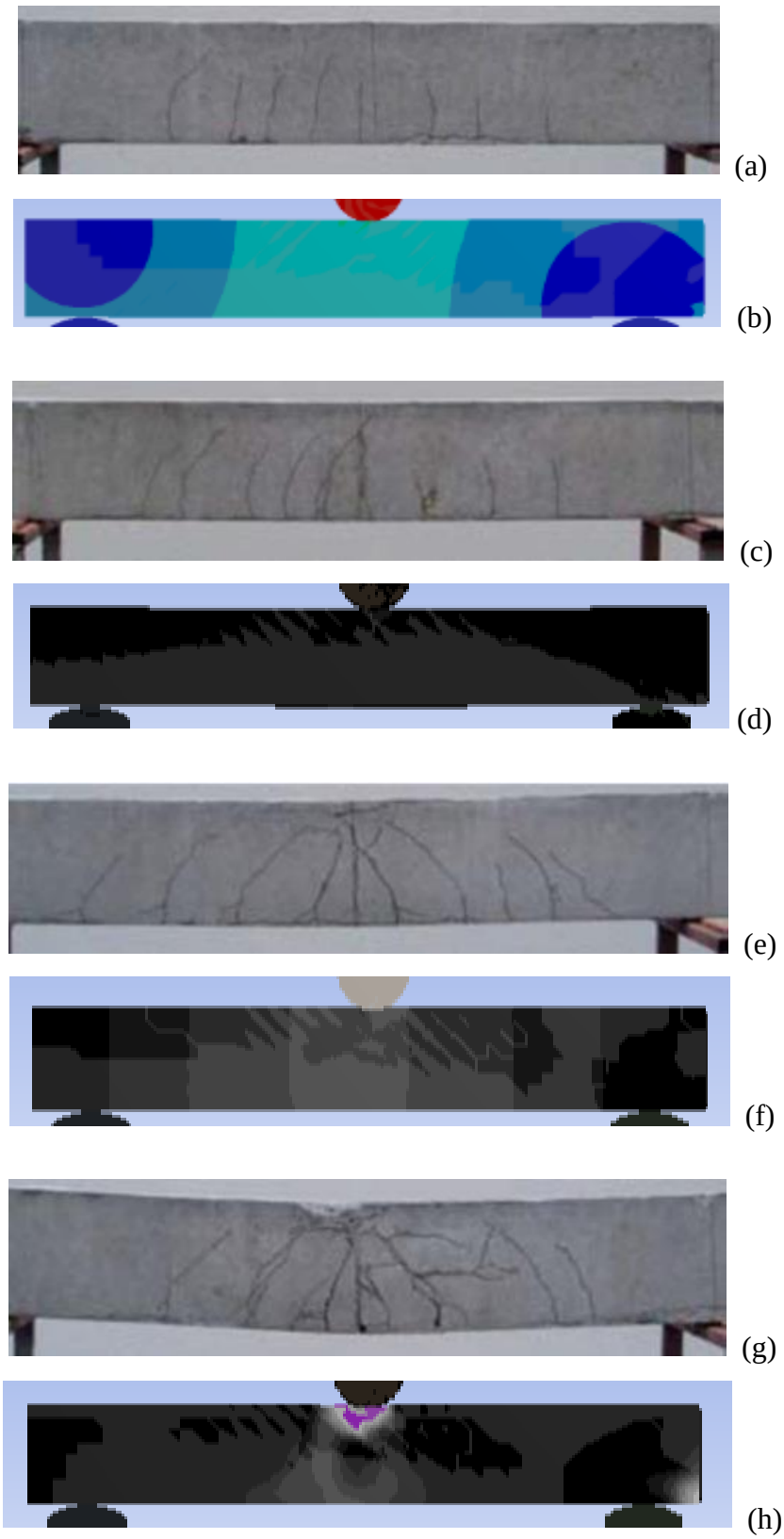

Figure 4-8 S1616 Crack Patterns at different drop height

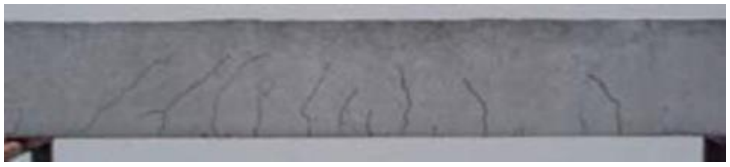
(a)

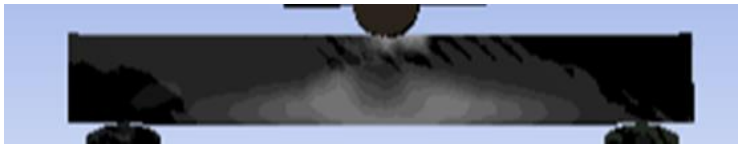
(b)

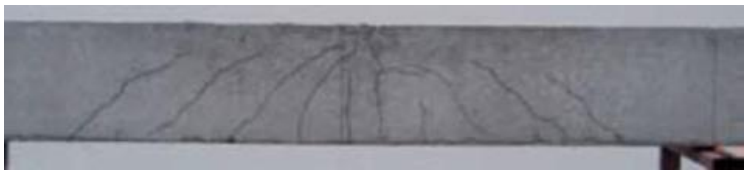
(c)


(d)

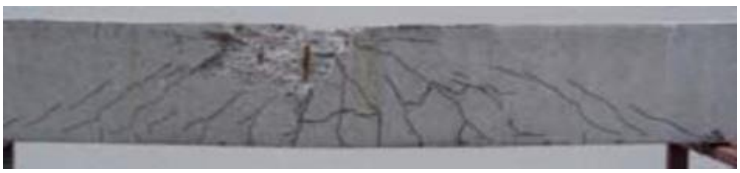
(e)

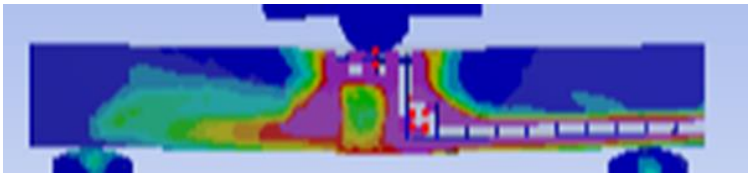
(f)


(g)

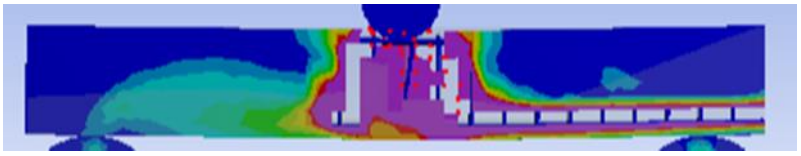
(h)

Figure 4-9 S1322 Crack Patterns at different drop Heights


(a)


(b)

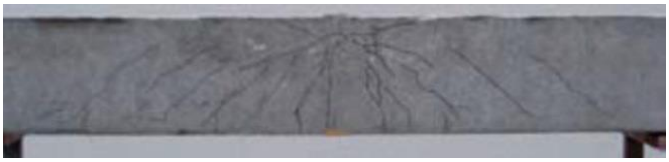
(c)


(d)

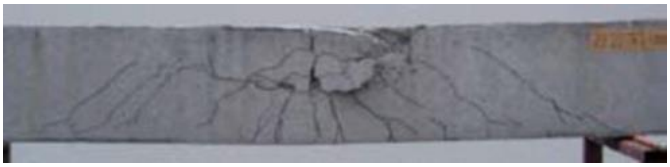
(e)

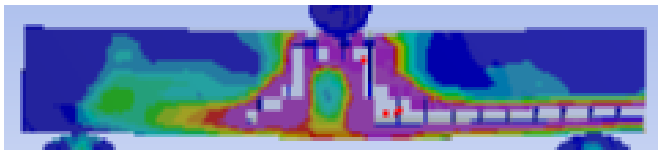
(f)


(g)

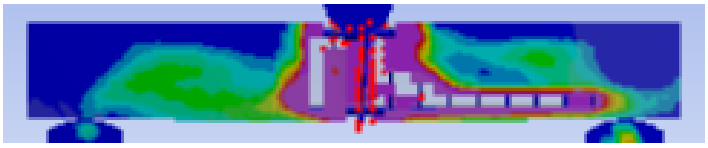
(h)

Figure 4-10 S2222 Crack Patterns at different drop heights

4.4 Finite Element Modeling of Vehicle Collisions with Bridge Piers

The following section outlines the process and results of the finite element modeling of the vehicle collision with bridge pier simulations. These simulations are an efficient and cost-effective way of studying vehicle collisions with bridge piers. This is because many simulations can be conducted to fully understand all the mechanics involved in a collision event. No vehicle model validation was done during the study since the interest was the pier behavior in relationship to a vehicle (impacting object) in terms of its mass, velocity and impact angle which were used during modeling of vehicle collisions with bridge piers. The vehicle impact simulations were validated by comparing results to published reports using relevant simulations but with keen interest to the shear failure mode and deformation.

4.4.1 Vehicle -Pier Collision Validation

4.4.1.1 Pier Geometry

The vehicle geometry was generated to a shape as shown in Figure 4-10 and the pier geometry was as described by El-Tawil et al. [23]. The validation exercise consisted of the vehicle models crashing into a circular reinforced concrete column at 110 km/h. The piers investigated consisted of circular reinforced concrete columns, 1,075 mm in diameter, 9,930 mm in height, and reinforced with fourteen No. 36 longitudinal bars and No. 16 transverse hoops spaced at 127 mm on center. The column rests on a pile cap 1,075 mm in depth and embedded 830 mm into the ground. The top of the column is loaded with a 32.5 Metric Tonne block to represent the mass of the supported superstructure. The concrete had cylinder compressive strength of 23 MPa and was modelled using Explicit material model 37. The steel reinforcement had a yield strength of 420 MPa and was modelled using General material model 12. Because the impact forces were the only result of interest for validation, the base of the column was constrained and assumed fixed rather than modeling the whole pile foundation. The simulation based Shear failure model as shown in Figure 4-10 was compared to that of Figure 4-8 and Figure 4-9 and used as a basis for validation of the Vehicle-Pier collision.

4.4.1.2 Boundary Conditions and Initial Conditions and Loads

The foundation of the column was constrained in the horizontal and vertical directions along the length of the section and over the entire base.

Vehicle impact simulations were conducted with a speed of 110 km/h. The initial translational velocities were applied to the vehicles in the global x-direction using the initial velocity

4.4.1.3 Contact

Automatic surface-to-surface contact algorithms were utilized to model the interactions between the vehicles and the bridge piers. All the other parameters were not varied as they were kept constant from the impact test experiment.

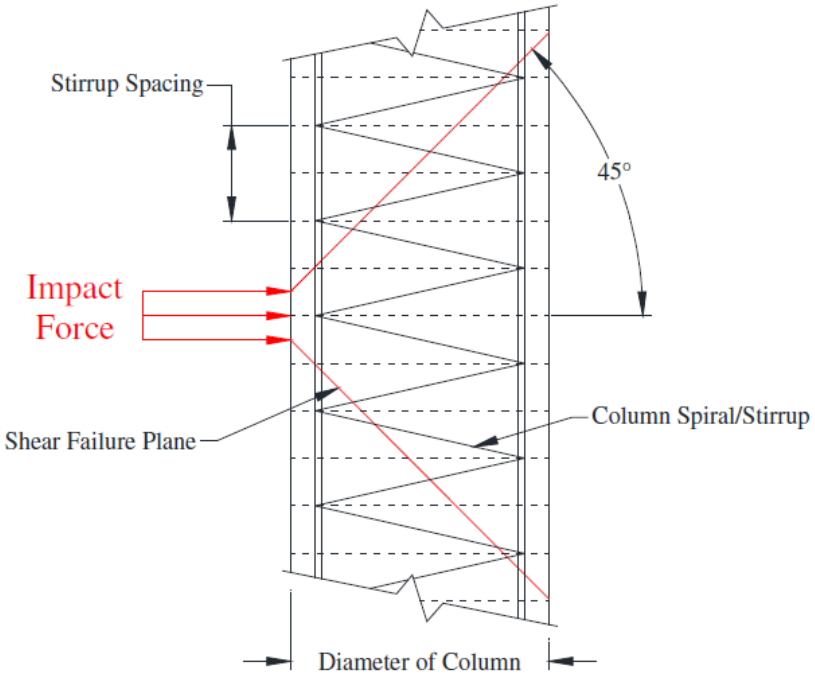

Figure 4-11 Shear failure mechanism due to vehicle Impact force [4]

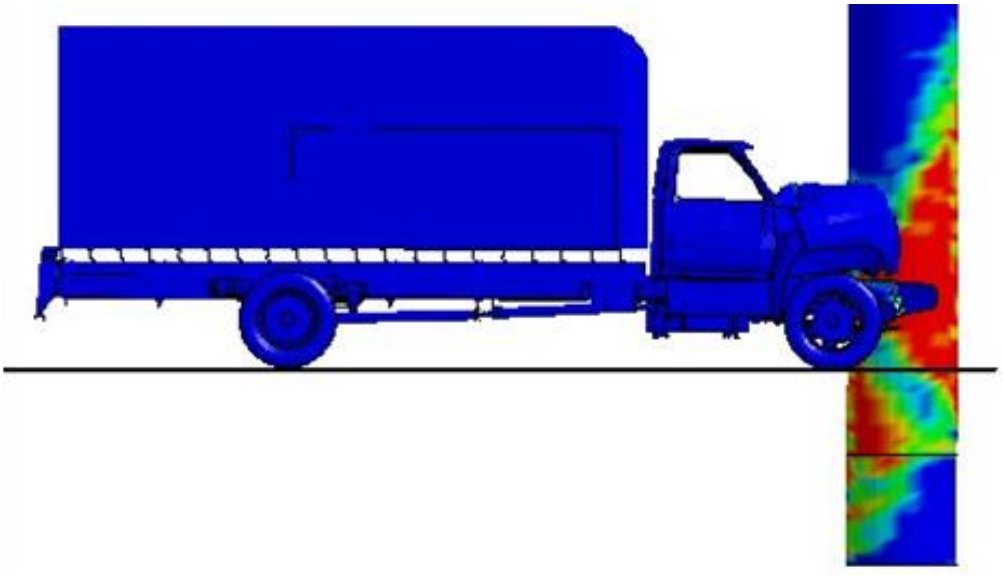

Figure 4-12 Plastic Strain Contours for the F800 SUT [23]

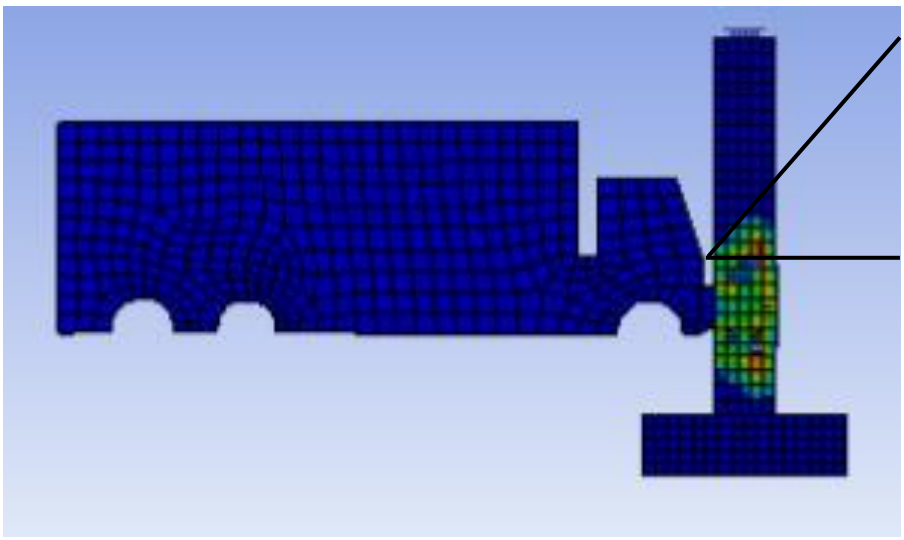

Figure 4-13 Vehicle -Pier impact Shear response

Chapter 5 : VEHICLE-BRIDGE PIER RESPONSE -AALRT

5.1 Introduction

Bridges should be designed to avoid undesirable structural or psychological effects due to their deformations. The level of acceptable damage should be proportionate to the size of attack. For example, linear behavior and/or local damage should be expected under a small-size attack, while significant permanent deformations and significant damage and/or partial failure of some components should be acceptable under larger size attacks. AASHTO [73]. For this study the structural strength of the AALRT piers will be assessed depending on their ability to resist damage from impact loads due to vehicular collision. The piers identified in Chapter 3 were subjected to a 70.6 tonne mass for speeds of 70 Km/hr (Vehicle mass and speed values obtained from Chapter 6). based on the validation parameters obtained in chapter 4 especially for developing the model. It is important to note that this study was based on a combination of field measurements and preliminary design reports and not as-built designs.

5.2 AALRT Vehicle- Bridge Pier Response

Eight different pier cross-section dimensions as obtained from the field visits were prepared as shown in Table 5-1 and these were corresponding to the vulnerable piers identified in Chapter 3. An average pier height of 6000 mm was used for the various simulations since the actual height could not be easily ascertained, and a uniform superstructure span of 25000 mm obtained from the design location plan was adopted.

A vehicle model of 12500 mm long X 4600 mm height X 2600 mm wide in geometry was developed with a yield strength of 460 MPa was adopted and used in the simulations. All geometrical models were developed in AUTOCAD and later imported into ANSYS and edited for the addition of reinforcement, assigning of materials, meshing, boundary conditions, loads and final processing.

Simulation Speeds adopted

70 Km/hr is the maximum speed obtained from the travel time speeds study for periods between (8:00 Am to 10:00 Pm) as shown in Table 7-5 APPENDIX C and this was adopted as the the currently existing worst-case scenarios of speeding around AALRT.

However to cater for off peak hours, several speeds from 75 to 120 Km/hr were randomly used during simulations to check the behavior of the piers in case the vehicle was moving at speeds before impact. More detailed input and output data for the different simulations are as shown in Appendix B.

Impact angle adopted

Though it was greatly observed from the field investigation that the orientation of the piers in relationship to the direction of traffic flow limits the occurance of vehicular impact occurring at an angle of zero due to being parallel on a great length across AALRT route, zero impact angle was adopted for this study simply because it provides maximum possible deformation there would be incase such an even occurred, therefore zero impact angle of impact was adopted for this study.

Table 5-1 Dimensioned Vulnerable Piers for Simulation

DIMENSIONED VULNERABLE PIERS FOR SIMULATION								
S/NO	**TYPE OF SECTION**	**PIER CODE**	**Structural Redundancy**	**PIER TYPE**	**NUMBER OF PIERS**	**LOCATION**	**Pier Dimension & Number**	
							Dimension	Simulation Number
1.1	TANGENT	NS-EW - 96 NS-EW - 97 NS-EW - 98	Simple	Frame Type	3	Darmar to St Lideta	2.1 X1.6	PIER 8
1.2	TANGENT	NS-EW-102 NS-EW-103 NS-EW-104 NS-EW-105	Simple	Solid Hammered Head	4	St-Lideta to Tegbared	1.8 X 1.5	PIER 5
2	CURVED	NS-EW-190 NS-EW-191 NS-EW-192 NS-EW-193	Simple	Frame Type	4	Leghar to Stadium	1.8 X 1.5	PIER 7
3	ROUND ABOUT	NS-EW-138 NS-EW-139 NS-EW-140 NS-EW-141	Simple	Solid Hammered Head	4	TEGBARED to Mexico	1.7 X 1.3	PIER 3
4.1	INTERSECTION 1	EW-256 EW-257 EW-258	Simple	Solid Hammered Head		Stadium to St - Estifanos	2 X 1.5	PIER 2
4.2	INTERSECTION 2	NS-30 NS-31 NS-32	Simple Simple Continuous	Frame Type Solid Hammered Head	3	Gojam Berenda to Autobustera Autobus Tera to Sebatagna	2.8 X 1.8 1.8 X 1.5 1.8 X 1.5	PIER 4 PIER 5 PIER 5
4.3	INTERSECTION 3	EW-241 EW-242 EW-243	Simple	Solid Hammered Head	3	Stadium to St - Estifanos	2 X 1.5	PIER 2
		OTHERS						
	CURVED	NS-EW-94		Solid Hammered Head		Darmar to St-Lideta	1.4 x 1.2	PIER 1
	CURVED	NS-EW-166		Solid Hammered Head		Mexico to Leghar	1.7 x 1.3	PIER 3
	TANGENT	NS-EW-204		Frame Type		Leghar to Stadium	2.4 X 1.8	PIER 6

Table 5-2 AALRTs' Deformation and Damage Ratios (extracted from Table 7-2)

PIER & CONNECTION	Deformation (mm)	Damage Ratio	Pier Condition
PIER 1 1400 X 1200			
SIMPLE	3.87530	0.080	Excellent
	3.84500	0.078	Excellent
	4.30680	0.083	Excellent
PIER 2 2000 X 1500			
SIMPLE	0.00000	0.000	Excellent
	0.00000	0.000	Excellent
	0.00000	0.000	Excellent
PIER 3 1700 X 1300			
SIMPLE	4.67450	0.092	Excellent
	4.14740	0.075	Excellent
	4.11250	0.048	Excellent
PIER 4 2800 X 1800 (WITH 1200 X 1800 2N0 COMBINED PIERS)			
SIMPLE	2.58540	0.057	Excellent
	2.58540	0.057	Excellent
	2.82880	0.058	Excellent
PIER 5 1800 X 1500			
SIMPLE	5.72910	0.098	Excellent
	5.73310	0.098	Excellent
	5.77350	0.099	Excellent
PIER 5 1800 X 1500			
CONTINOUS	5.10617	0.054	Excellent
	5.43210	0.054	Excellent
	5.64938	0.054	Excellent
PIER 6 2400 X 2200			
CONTINOUS	0.68875	0.000	Excellent
	0.63370	0.000	Excellent
	0.48223	0.000	Excellent
PIER 7 1800 X 1500			
SIMPLE	5.39958	0.120	Excellent
	5.45783	0.123	Excellent
	6.38814	0.138	Excellent
PIER 8 2100 X 1600			
SIMPLE	4.12226	0.092	Excellent
	4.41271	0.099	Excellent
	5.28473	0.118	Excellent

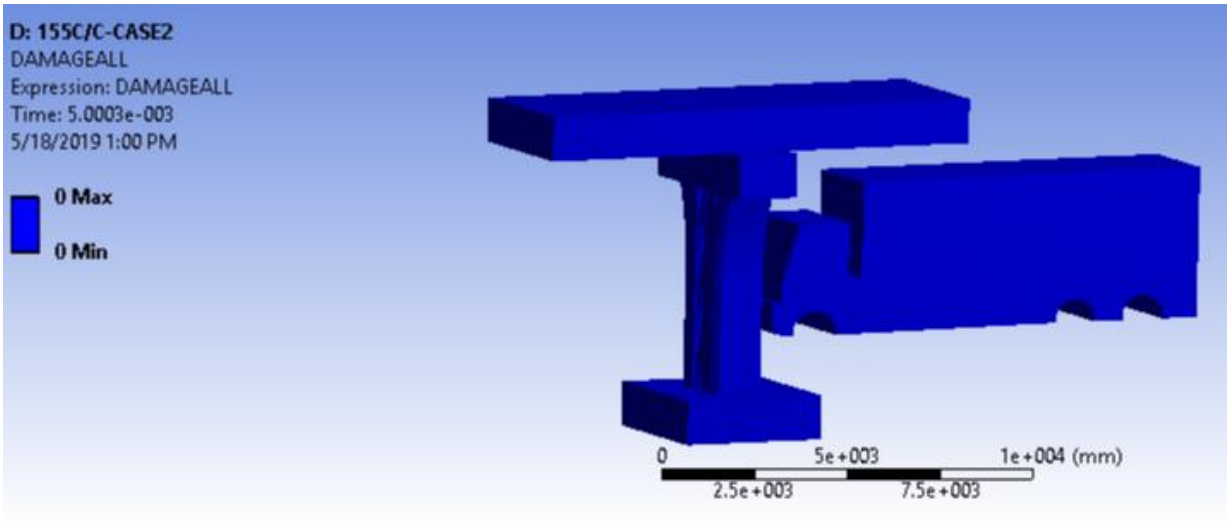

Figure 5-1 Pier 2 Damage Ratio Response

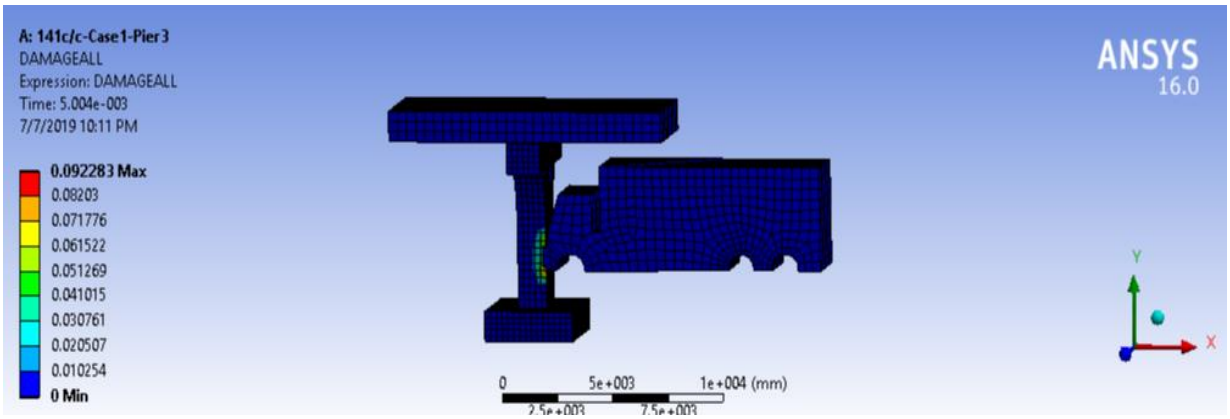

Figure 5-2 Pier 3 Damage ratio at 70 Km/hr

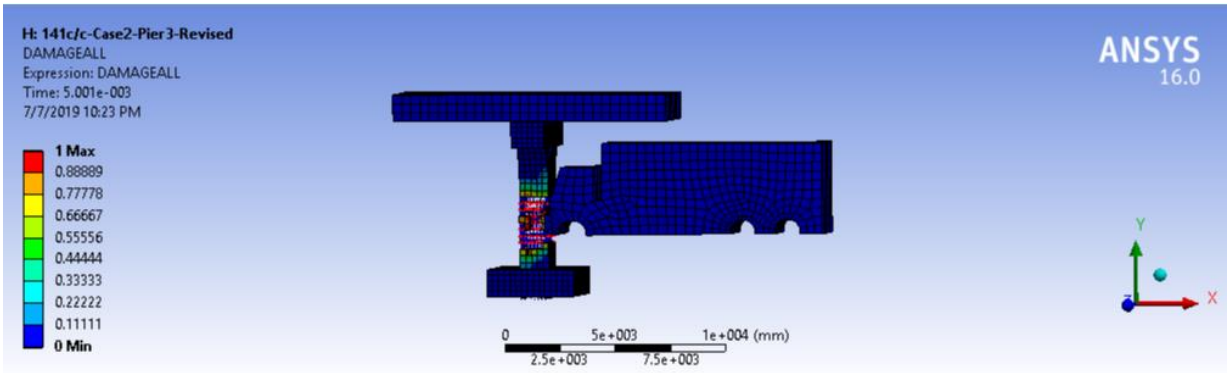

Figure 5-3 Pier 3 Damage Ratio at 120 Km/hr.

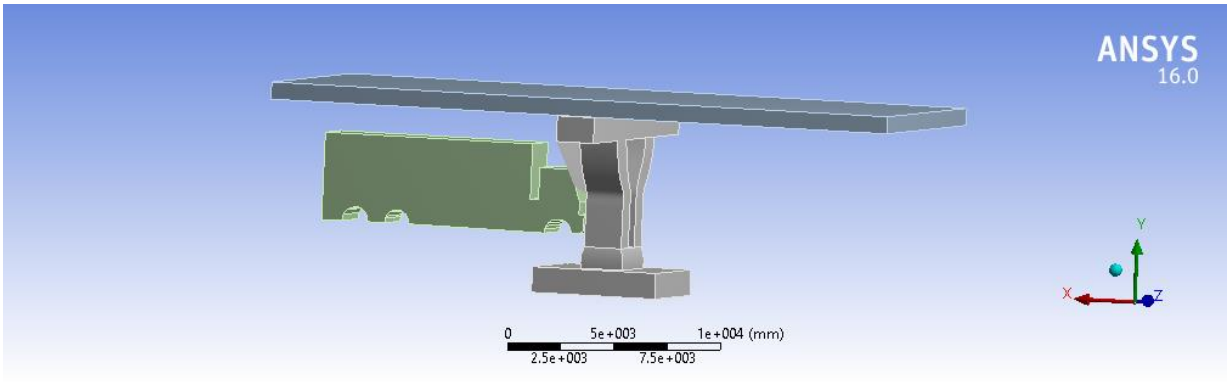

Figure 5-4 Typical of Pier 4

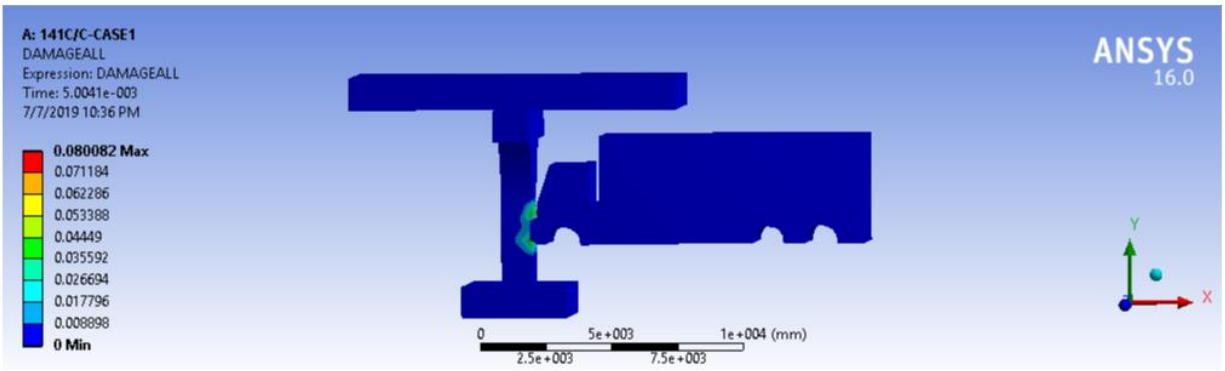

Figure 5-5 Pier 1 Damage Ratio (Stirrup @ c/c 141)

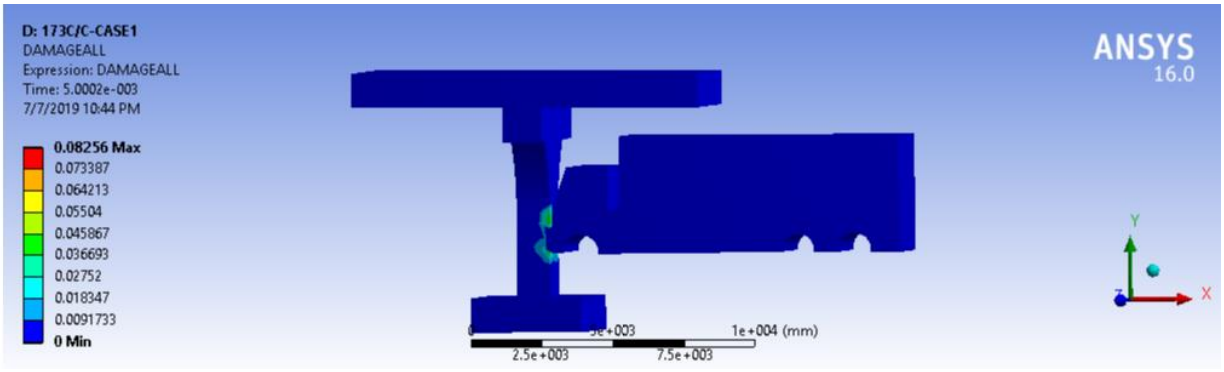

Figure 5-6 Pier 1 Damage at 70 Km/Hr. (Stirrup @ 173 c/c)

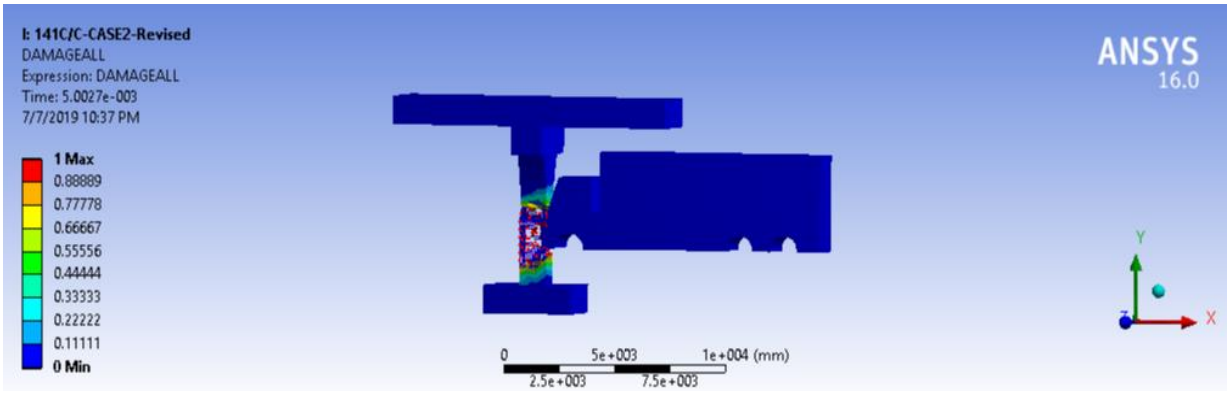

Figure 5-7 Pier 1 Maximum Damage at 120 Km/Hr.

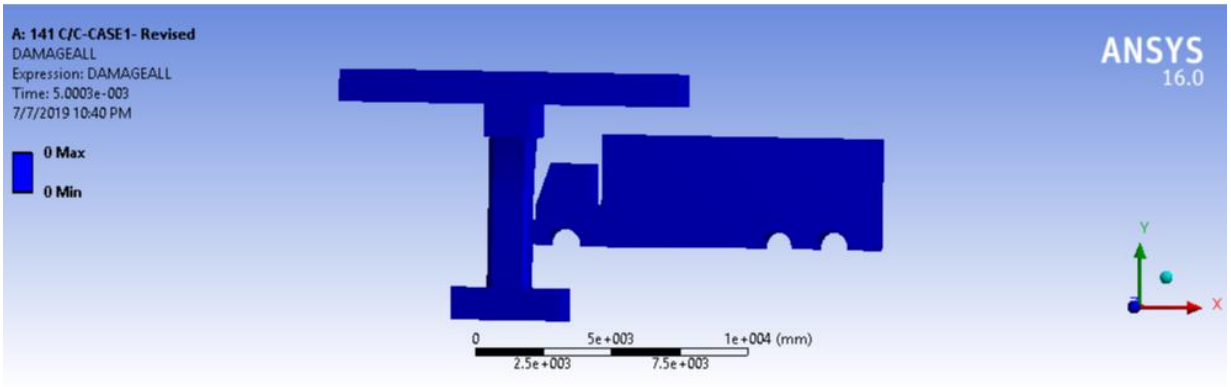

Figure 5-8 Pier 2 Damage Ratio at 70 Km/hr.

5.3 Findings:

The average damage ratio obtained from the 25 investigated simulations for the 8 different piers along AALRT gave a damage ratio of 0.066 on a scale of 1 as shown in Figure 5-9 is a very insignificant damage only capable of causing micro cracks at the impact location which is a clear indicator that the piers can be repairable (minor) without replacement of the concrete component or any major effect on the operation of the train. Based on deformation as a serviceability requirement for structural performance, a deformation of up to a maximum of 6.4 mm is equally too small to lower the confidence of the train users.

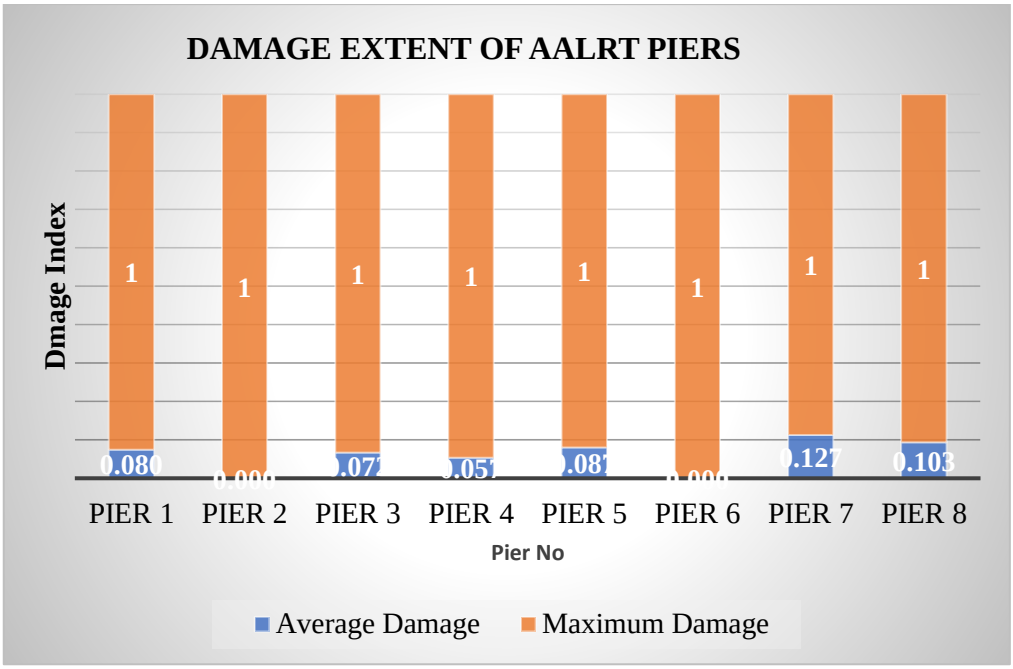

Figure 5-9 Damage extent of AALRT Piers

Only a combination of 70.6 tone vehicle traveling at speeds of 120 km/hr and over are capable of causing total failure of the piers without sudden warning. This combination itself makes it even more difficult to have such a failure as a result of the vehicle -bridge pier collision.

Chapter 6 : PARAMETRIC STUDY AND SENSITIVITY ANALYSIS

6.1 Introduction

To evaluate the influence of different parameters, such as vehicle mass, vehicle velocity, concrete compressive strength, stirrup spacing and varying number of longitudinal reinforcements required the generation of different models with probabilistic inputs generated using Latin Hypercube sampling software. Pier deformation and damage ratios were considered as ideal for this study in relation to bridge safety. Deterministic studies such as vehicle impact angle, pier cross section (circular Vs rectangular) and foundation-pier-superstructure connection to vehicle-pier response were also conducted.

6.2 Deterministic Approach

6.2.1 Effect of Vehicle Impact Angle

Impact angles of 0; 2.5, 7.0, 10, and 12.5 degrees were considered for this study at fixed vehicle mass of 60 Tones with varying speeds of 75, 140 and 240 Km/hr.

The diameter of the circular pier was taken as 1500 mm and cross section area of 1500 mm X 1180 mm for the rectangular pier both with a fixed connection at footing-pier and pier-superstructure. Explicit material model 37 was used with a density of 2400 Kg/m^3 and compressive strength of 20 MPa keeping all other Parameters constant.

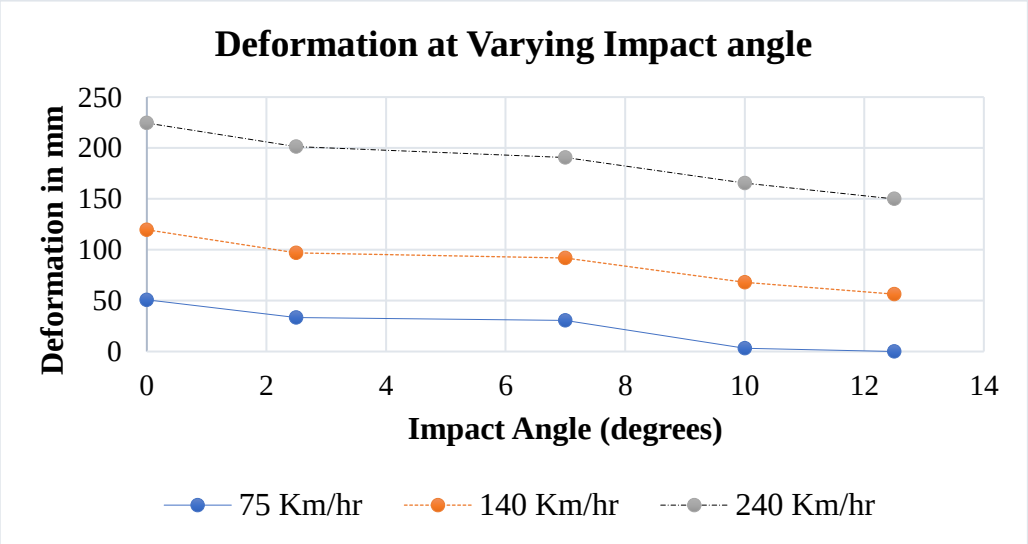

Figure 6-1 Deformation for Changing Impact Angle-Circular Pier

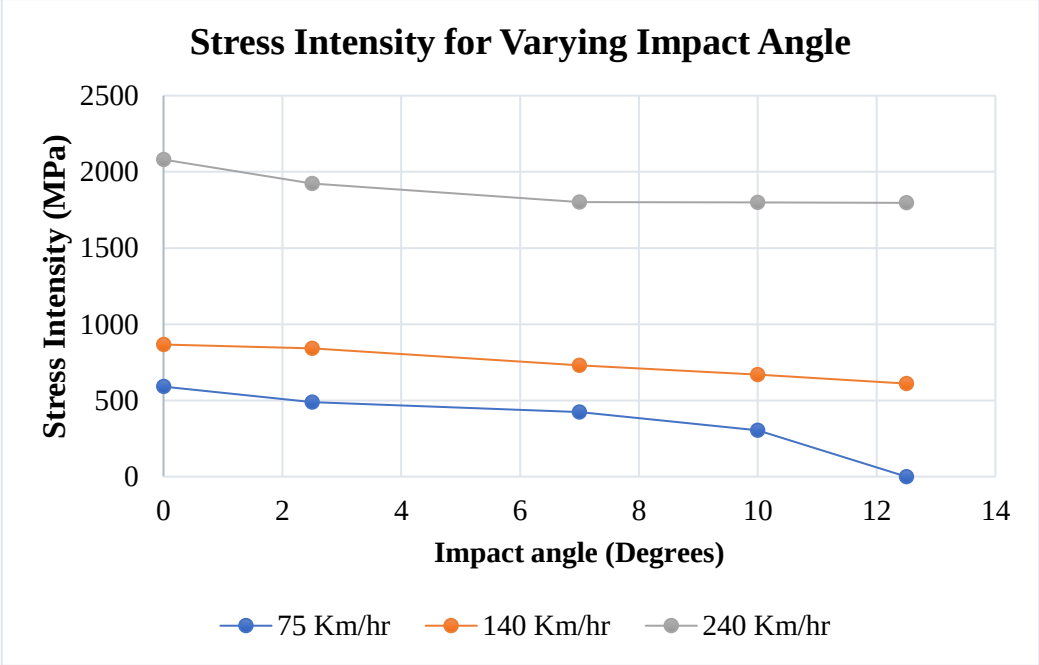

Figure 6-2 Stress Intensity- for Changing Impact Angle - Circular Pier

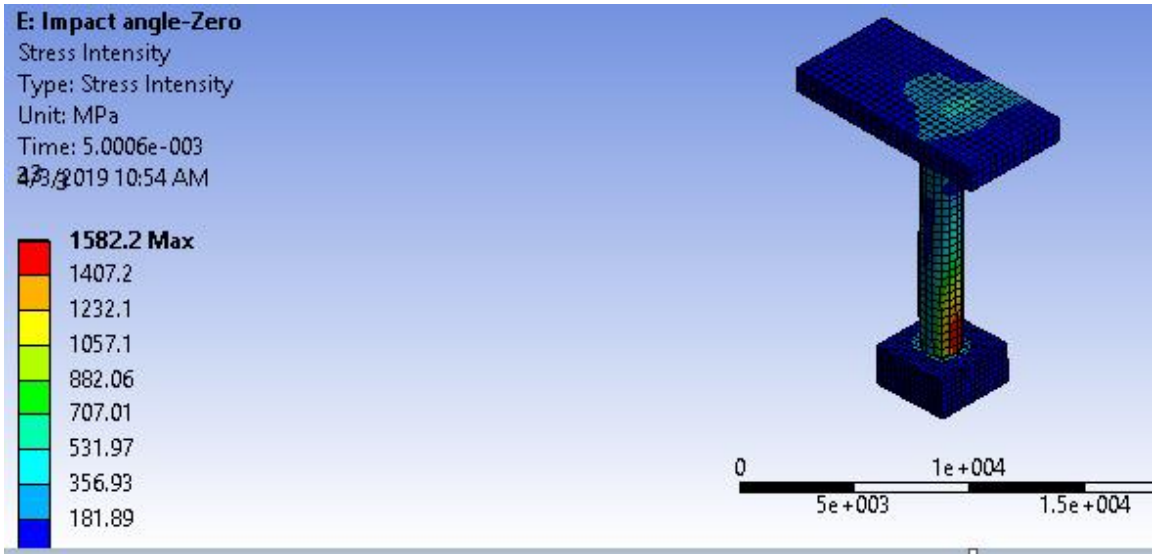

Figure 6-3 Zero Degree Impact Angle Deformation of Circular Pier

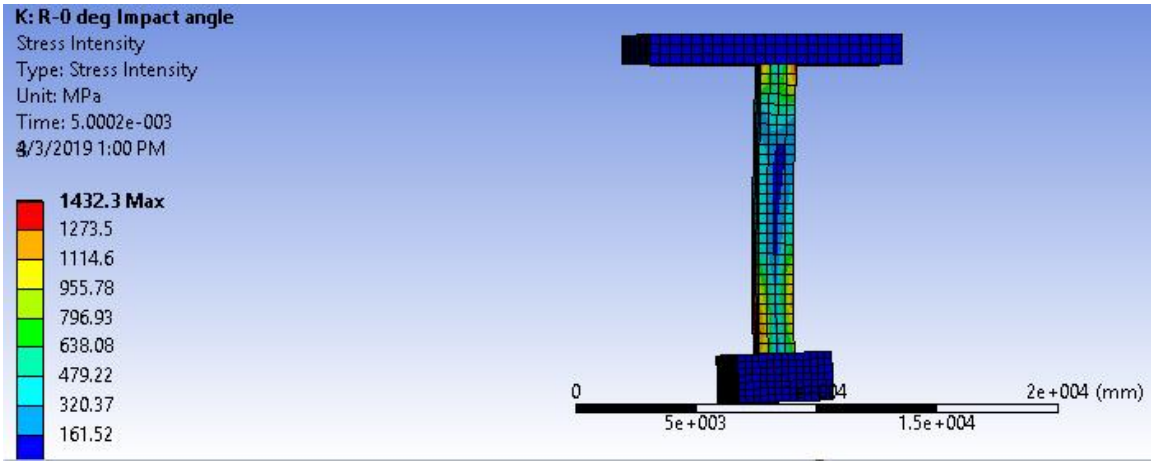

Figure 6-4 Zero degrees Impact angle deformation of rectangular Pier

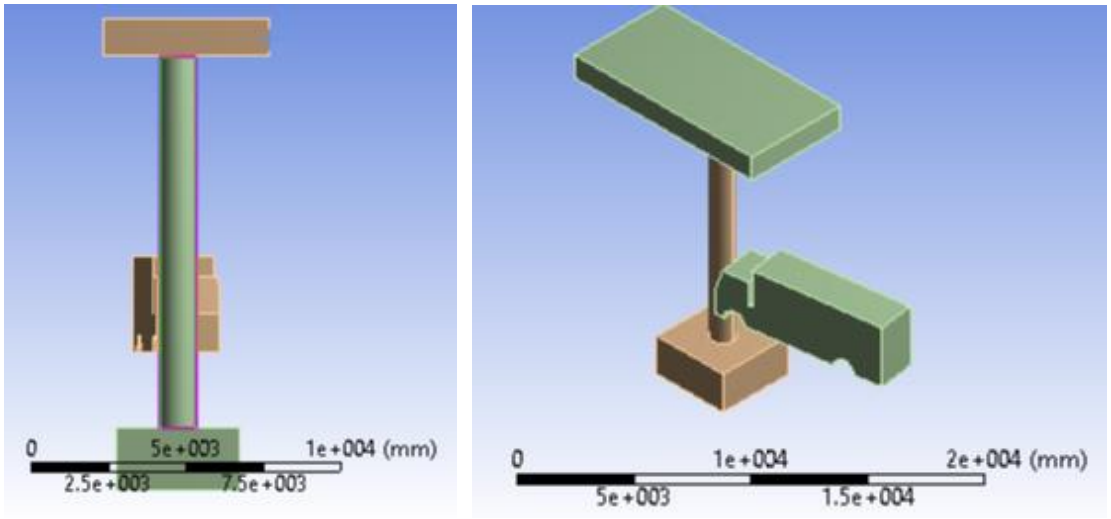

(a) – 2.5 Degrees (b) 7.5 Degrees

Figure 6-5 Impact Angle Model

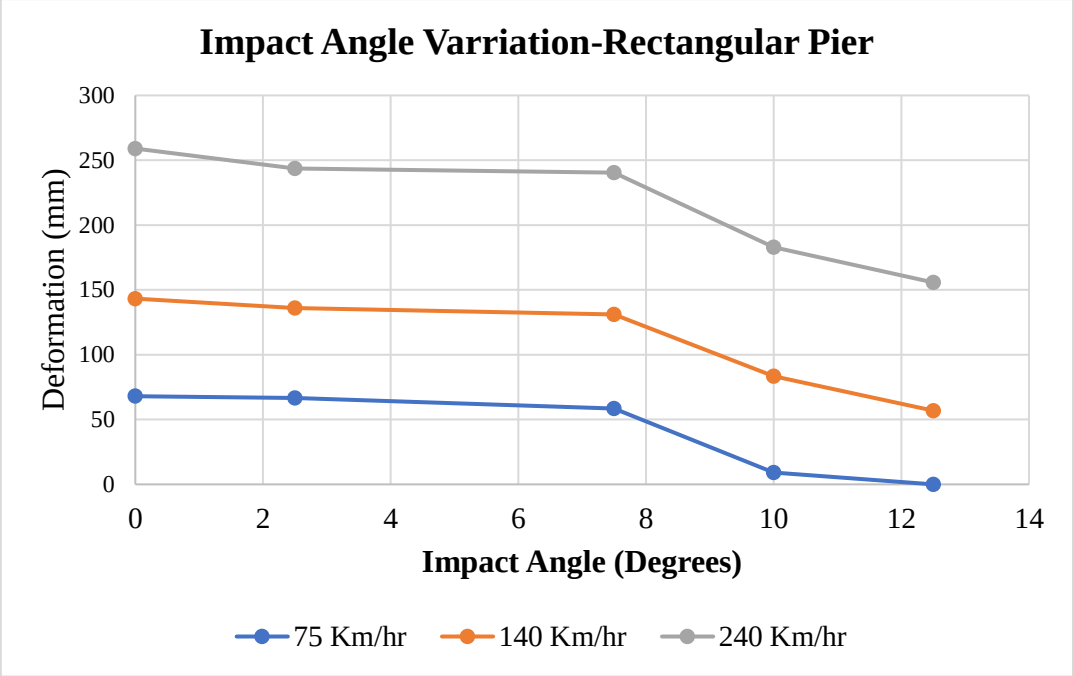

Figure 6-6 Changing Impact Angle and Rectangular Pier Deformation

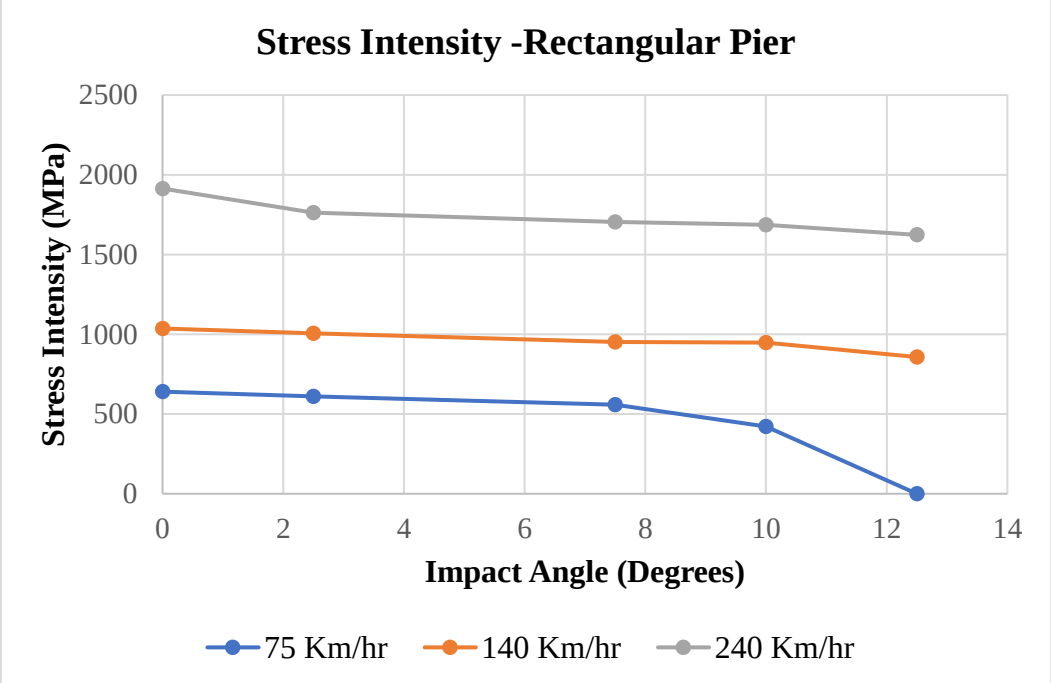

Figure 6-7 Stress Intensity- Rectangular Pier at Different Speeds

6.2.2 Effect of compressive strength on Damage time

The effect of compressive strength of concrete and speed were also studied in terms of time required to cause maximum damage to the pier elements.

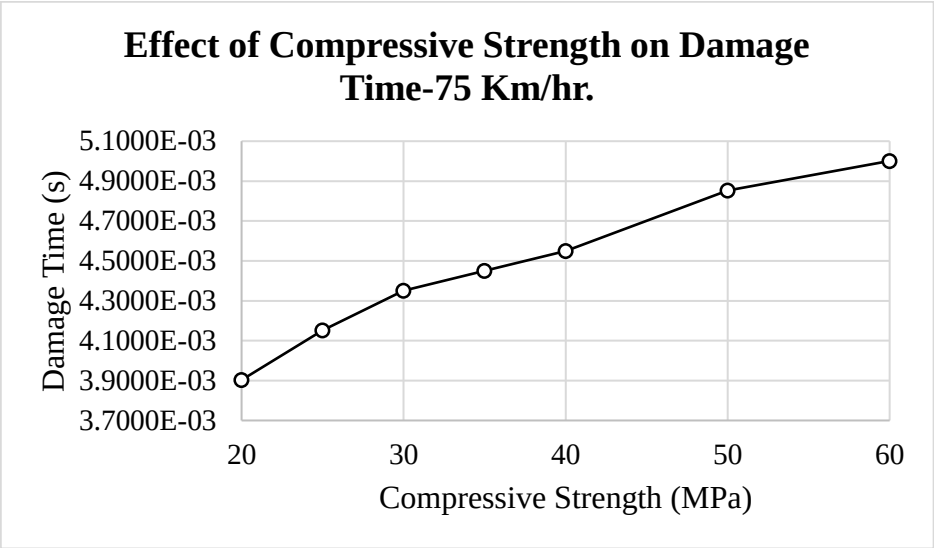

Figure 6-8 Effect of Compressive Strength on Damage Time 75 Km/hr

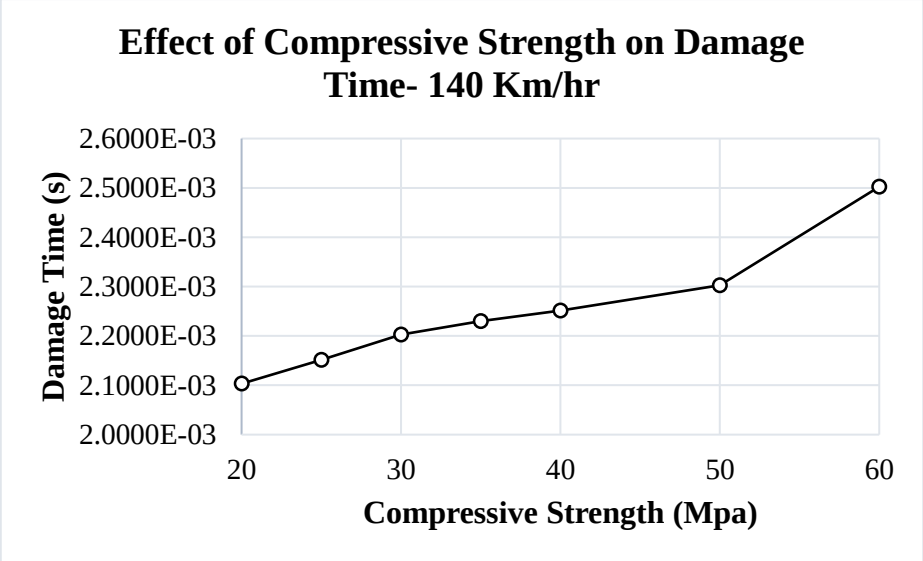

Figure 6-9 Effect of Compressive Strength on damage time (140 Km/hr.)

6.2.3 Effect of Connection (Foundation-Pier-Superstructure)

In order to understand the effect of the nature of the connection between the foundation-Pier-Superstructure, three different arrangements were developed. The three cases that were modelled are;

Pinned - Pinned: The connection between the foundation and pier is pinned and is similar to that between the pier and superstructure. In the geometry that was used this resulted in three different bodies that make up the complete model.

Fixed – Pinned: This type of connection allows for a fixed connection between the footing and pier while the superstructure and pier have got a pinned connection. In the model, this resulted in two main bodies as a component of the pier Geometric model used in the simulation. This type of connection is assumed to be a connection where a bridge bearing is used between the superstructure and pier and was found to be the most common type of connection for Addis Ababa Light Rail Transit.

Fixed - Fixed: This is a type of connection where both ends of the Pier are fixed. This type of connection results in one single geometry being used for simulation. This kind of connection was observed along curved areas, turnouts and switches.

A circular pier of diameter 1200 mm was used keeping the height as described before in section 6.2.1. Only Explicit material Model 37 was revised and compressive strength of 35 MPa was used with other parameters kept constant.

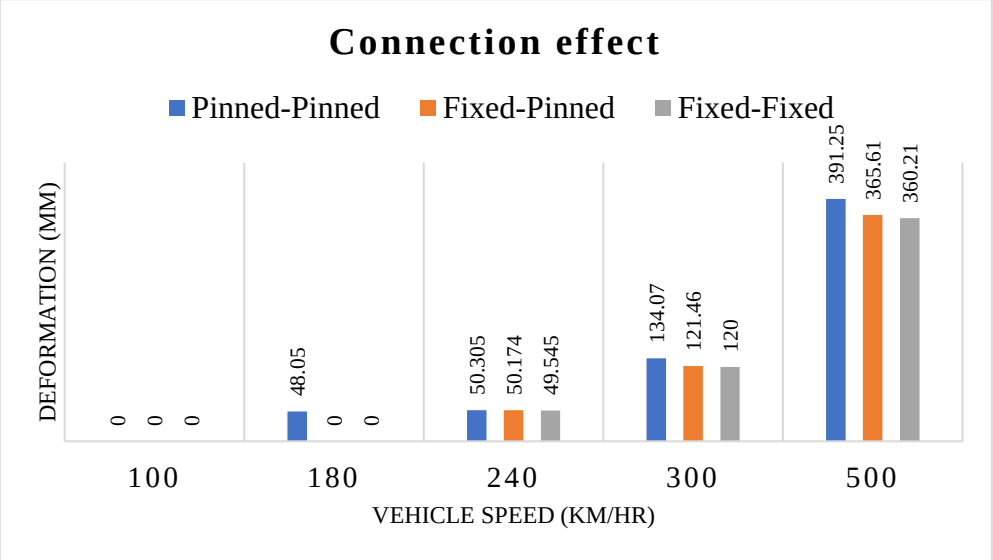

Figure 6-10 Comparison of deformation based on Geometry connection

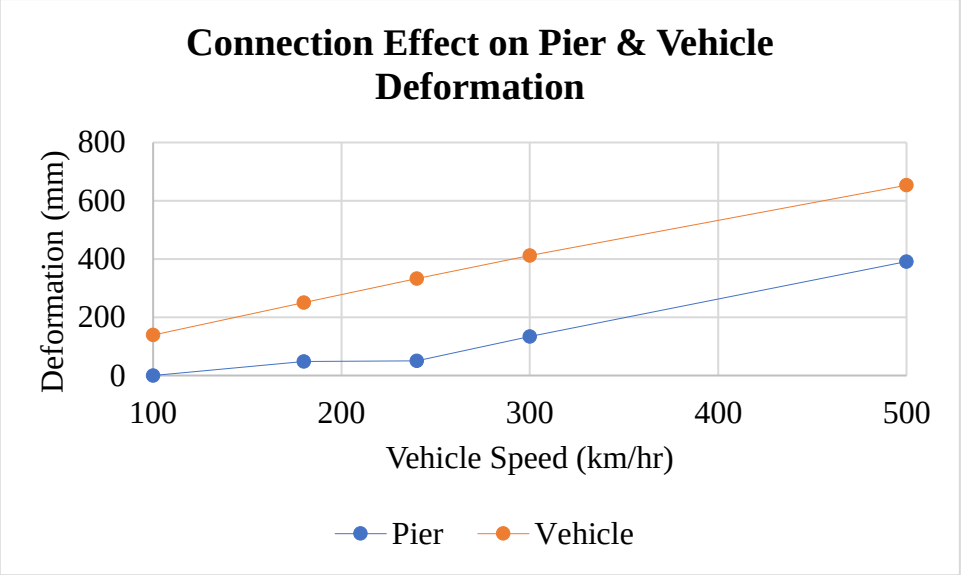

Figure 6-11 Pinned-Pinned Connection

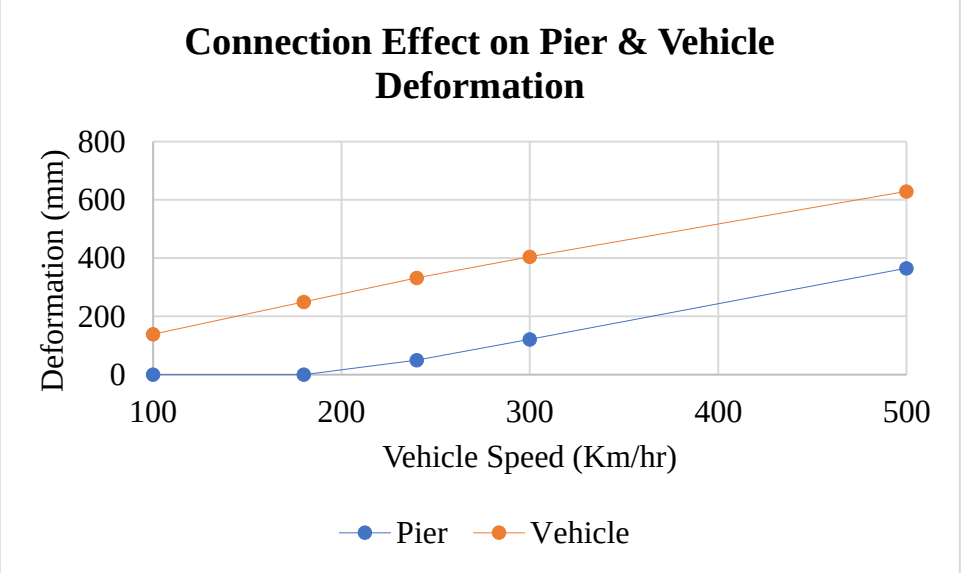

Figure 6-12 Fixed-Pinned Connection

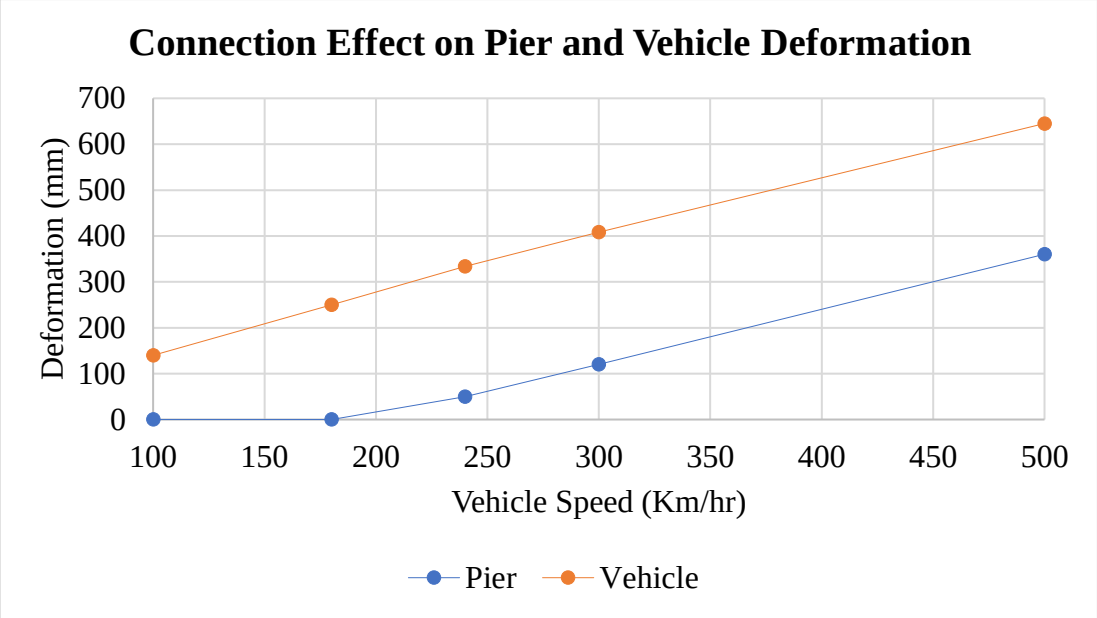

Figure 6-13 Connection effect on Pier-Vehicle Deformation

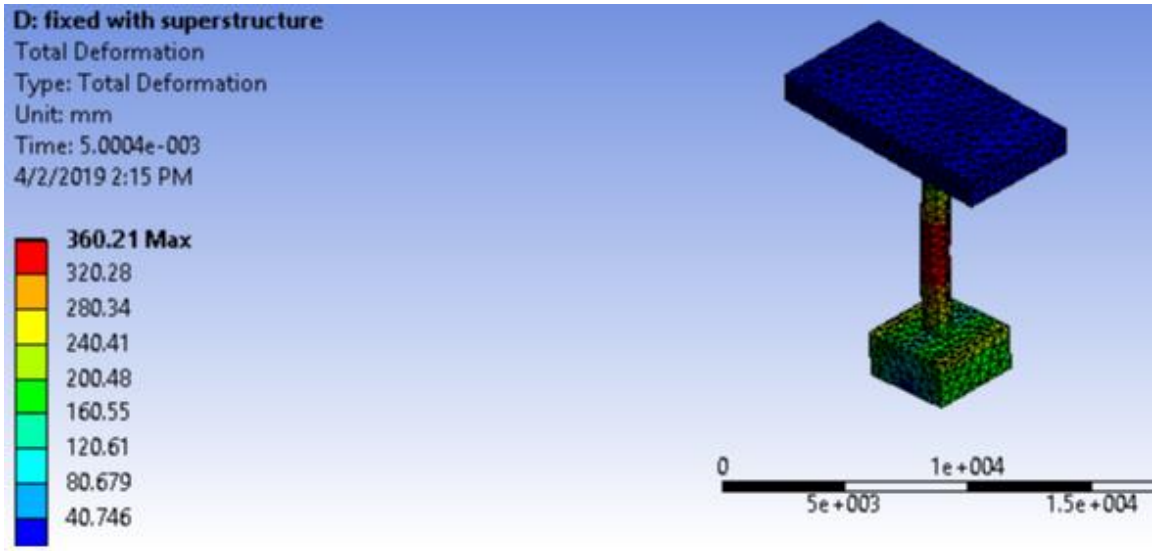

Figure 6-14 Deformation of Fixed-Fixed connection Pier

6.2.4 Effect of Pier cross section (Circular Vs Rectangular)

Six different sizes of equal cross- sections were prepared (see Table 6-3) to study the effect of varying cross-section on deformation and at the same time to be able to compare rectangular and circular cross-sections in terms of resistance to deformation. The vehicle model was modified to have a mass of 60 tones with modulus of elasticity of 200 GPa. The rectangular sections were developed into two different arrangements in relation to the position of the vehicle and thus rectangular sections 1 and 2 as indicated in Table 6-3.

Table 6-1 Pier Cross Section used in deterministic Modelling

Pier Code	Rectangular 1 Dimension (mm)	Rectangular 2 Dimension (mm)	Circularr Diameter (mm)
S1	1500 X 1180	1180 X 1500	1500
S2	1200 X 942.5	942.5 X 1200	1200
S3	1075 X 845	845 X 1075	1075
S4	900 X 710	710 X 900	900
S5	800 X 630	630 X 800	800
S6	600 X 475	475 X 600	600

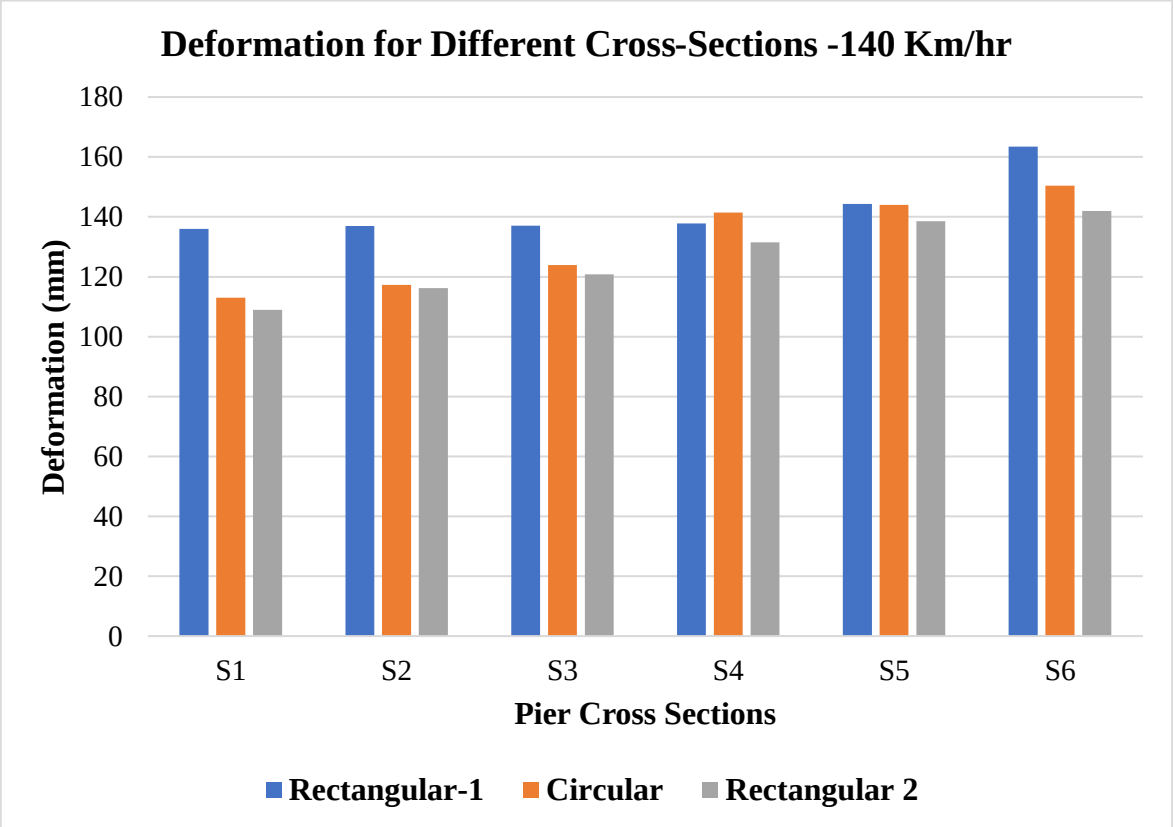

Figure 6-15 Deformation of Different Cross- Sections -140 Km/hr.

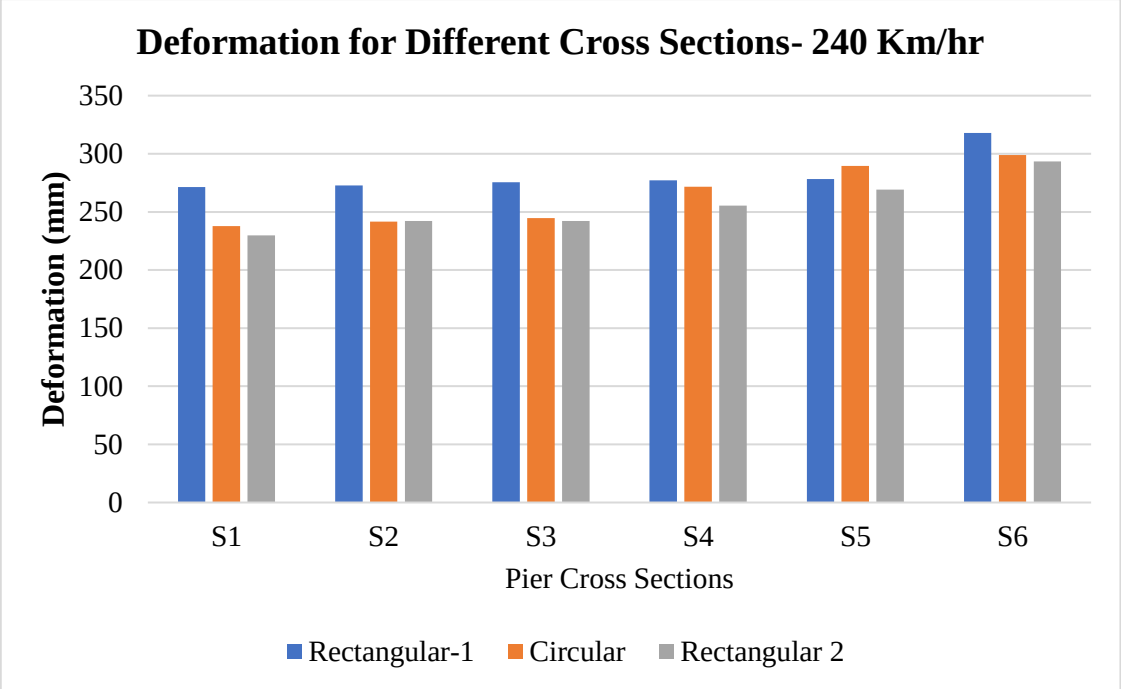

Figure 6-16 Deformation of different Cross Sections -240 Km/hr.

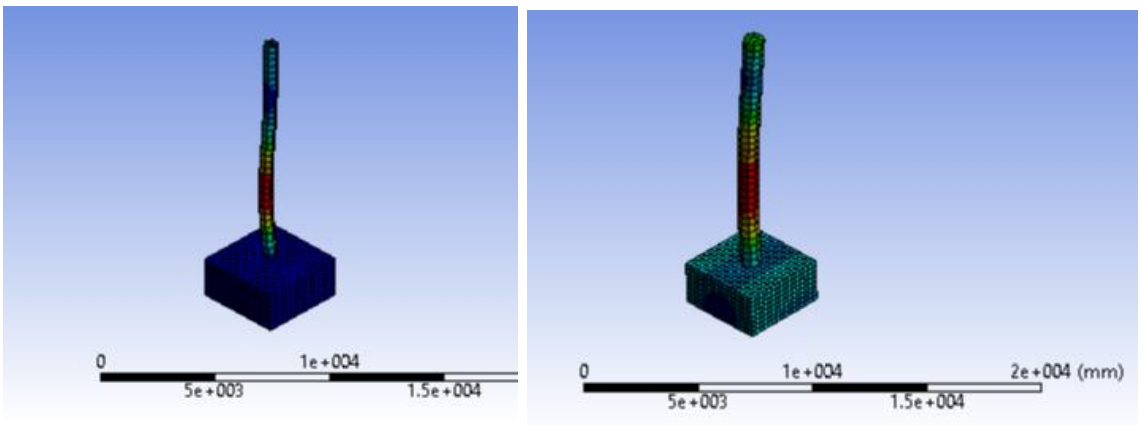

Figure 6-17 L-R Deformation of 600 mm; 900 mm Modelled Circular Piers

6.3 Probabilistic approach

6.3.1 Pier and Vehicle Geometry:

The bridge pier models that were used for the study consisted of the following components: the footing, bridge pier, super-structure, and vehicle as shown in Figure 6-1. The pier that was used for this study was rectangular in nature of 1400 mm X 1200 and 6100 mm high on a 2000 mm x 2000 mm x 1200 mm deep footing that is fixed on all its faces as between the pier and the super structure was represented by 4000 mm X 4000 mm X 2000mm deep block. The vehicle

model had a constant volume of 119 m^3. The vehicle model was generated at a distance of 2000 mm above the footing top surface. A distance of 1524 is provided as the distance recommended as per AASHTO while a distance of 476 mm is allowed to cater for fill material onto the footing. All models were generated using AUTOCAD and later exported as IGES files into ANSYS for modeling.

The pier cap and pile cap footing were considered as unreinforced while the pier reinforcement was made up of 32 mm diameter longitudinal steel and 10 mm diameter stirrup. The quantiy of both the longitudinal steel and stirrup was varied according to the combinations generated by LHS for the different simulations done.

6.3.2 Probabilistically Generated Input Parameters

According to Novak et al. [58], Latin Hypercube Sampling software requires the mean and standard deviations of the parameters to be used are provided so that it can generate the required number of inputs in terms of a different number of combinations. Since the number of parameters that is vehicle speed, vehicle mass, unconfined concrete compressive strength, stirrup spacing and area of longitudinal bars was the chosen parameters to be studied, their means and standard deviations were obtained as discussed in the following paragraphs. The required number of parameters ultimately gave the minimum number of layers or combinations to be generated by LHS, that is 2^n where n = 5; the generated input combinations were therefore 32.

Vehicle Speed

Based on a spot speed study conducted by Emebet [74], mean speed and standard deviation of 49.125 Km/hr. and 9.476 Km/hr. were obtained respectively. These were compared to the spatial travel time corresponding speeds that were obtained using a stop clock between three main sections (CBE New headquarters building to Stadium-0.82 km, UNECA Headquarters to Estifanos 0.31 Km and Dembel to Estifanos 0.61 km) obtained randomly, the mean speed and standard deviations from this approach were 46.439 Km/hr. and 10.896 Km/hr. respectively. Therefore, comparing the coefficient of variations of 0.193 and 0.235 for the first and second data sets, the first was adopted due to its lower coefficient of variation.

Vehicle Mass

A combination of weights adopted from 2 weighbridges at Modjo and Holeta as investigated by Biniam [75] were adopted and integrated with some COMESA regional countries permissible

maximum combination for determination of mean masses and their corresponding standard deviations. The mean and standard deviations were thus obtained as 56342 Kgs and 6635.21 Kg respectively.

Concrete Compressive Strength

Based on the required cube strength for AALRT of 45 MPa a corresponding cylinder strength of 36 MPa was adopted and standard deviation of 2.33 MPa was adopted in comformity to AREMA article 1.12.5.3 volume 2 which were adopted for this study.

Stirrup Spacing

A 10 mm diameter bar was adopted for use in this study on article 2.11.2 AREMA [77], and based on article 5.10.6.2 of AASHTO [73], 152.4 mm was adopted as the average stirrup spacing. [Working with a 95% level of confidence, using a Wararit [78] table 3 as shown in Table 7-3 in APPENDIX C]. A corresponding value of coefficient is interpolated between 0.05; 0.9502 and 0.10; 0.9494 at 0.95 was obtained as 0.062. Using this coefficient of variation, a corresponding standard deviation of 9.525 mm was obtained and used in conjunction with the mean spacing of 152.4 mm.

Longitudinal Steel Reinforcement Ratio

This was obtained in terms of the area and was based on Article 2.11.1 of AREMA [77]. Since the reported steel ratio of 0.0157 provided is acceptable, it was considered as the mean longitudinal steel reinforcement ratio. This mean ratio of reinforcement of 0.0157 and using a coefficient of variation of 0.062 obtained from Table 7-3, generated a standard deviation of 9.734E-4.

Table 6-2 LHS Input Parameters

ID	**Parameter**	**Mean**	**Standard Deviation**	**Units**
1	Vehicle Speed	49.125	9.476	Km/hr.
2	Vehicle Mass	56342.143	6635.207	Kg
3	Compressive Strength	36	2.33	MPa
4	Stirrup Spacing	152.400	9.525	mm
5	Longitudinal Steel Reinforcement Ratio	0.0157	9.734X10^-4	x Gross Area(mm^2)

Based on the above inputs (As shown in Table 6-2) 32 different combinations of vehicle speed, mass, compressive strength, stirrup spacing, and longitudinal steel reinforcement ratio were generated and used to develop different simulations as shown in Table 6-3.

Masses of the vehicle were attained by varying the density of General Material Model 12 shown in Table 6-3 all the other vehicle parameters like Modulus of elasticity were kept constant except for the yield strength that was set to 460 MPa. The vehicle mass was taken to impact the pier at an impact angle of 0 degrees. During this study, only the compressive strength and tensile strength of the concrete as Explicit Material Model 37 were varied keeping all other parameters constant. Tensile strength of concrete according to AS3600 [79] was calculated using Equation 4. With all the other Explicit material model 37 properties being kept constant density being considered such as the density 2400 kg/m3, the compressive strength The Tensile Strength ratio f_t/f_c which was computed for different classes as indicated in Table 6-3.

$$\boldsymbol{f_T^1 = 0 \cdot 4\sqrt{f_C^1}} \quad \textbf{(4)}$$

f_c^1 is the specified compressive strength of concrete at 28 days.

6.4 Regression-Based Sensitivity Analysis

Sensitivity analysis was done by conducting a multiple regression-based analysis and checking the corresponding level of significance in terms of their relationship with the outcome (deformation). A hypothesis test for individual parameters was conducted based on [52] [53];

Null Hypothesis, H_o; $\beta_i = 0$

Alternative Hypothesis, H_a; $\beta_i \neq 0$

Reject the null hypothesis Ho; if P-Value ≤ Level of significance (α), else fail to reject the null hypothesis when P-Value > Level of significance (α).

Where;

β_i is the slope of the i^{th} parameter being investigated. If H_0: $\beta j = 0$ is not rejected, this indicates that the regressor X_i can be deleted from the model.

The backward eleimination step-wise multiple linear regression analyses were conducted at the level of confidence of 99% and the Adjusted R^2 value was observed since many regression users prefer to use an **adjusted** R^2 statistics [53].

Based on how significantly each parameter (vehicle speed, vehicle mass, compressive strength, stirrup spacing and longitudinal steel ratio) was related to deformation during the vehicle-pier

collision, individual parameters were eliminated until two parameters remained. Vehicle speed was found to be the most critical parameter at a level of confidence of 99% while stirrup spacing is a leading deformation resisting component of the pier at a level of confidence of 95%. The sensitivity process based on the level of significance in terms of the relationship between the different parameters and deformation are as shown in Table 6.3 and the ANOVA output values obtained during the different multiple regression analyses are as indicated in APPENDIX D.

Function:

$$Deformation = -8.322218284 + 0.14186516 * S + 1.42117E - 06 * VM - 0.003416035 * CS + 0.058624075 * SS - 38.11216896\, SR$$

Where; S Vehicle Speed; VM- Vehicle Mass; CS- Compressive strength(Cylinder) , SS- Stirrup Spacing , SR- Longitudinal Steel Ratio

Table 6-3 LHS Output (Column 1;2;4;7; & 8) ANSYS output (Column 12 & 13)

NO.	1		2	3	4	5	6	7	8	9	10	11	12	13
Data Set	Vehicle Speed Km/hr		Vehicle Mass (Kg)	Vehicle Density	Concrete Compressive Strength (Mpa)	0.4*Sqrt(f'_c)	Tensile Strength	10mm(2.11.2 AREMA) Stirrup Spacing (mm)	#5#16 Rebar (2.11.1-AREMA 2010-Vol2) Area of Rebars	1200*1400	Equivalent Area	Area of 1 Bar (200mms) No of Bars	Deformation (mm)	Damage
1	56.99	15831.92	51535	432	33.49	2.31	0.07	141	0.01552	1680000	26077.98	32	7.33	0.111
2	41.26	11459.74	60496	507	32.70	2.29	0.07	154	0.01681	1680000	28235.55	34	5.93	0.105
3	40.15	11153.69	62624	525	32.10	2.27	0.07	166	0.01645	1680000	27631.73	34	6.36	0.106
4	50.99	14164.64	64502	541	38.21	2.47	0.06	144	0.01610	1680000	27048.99	33	6.76	0.111
5	38.91	10809.57	50060	420	35.35	2.38	0.07	145	0.01473	1680000	24746.8	30	5.14	0.111
6	55.06	15293.87	56082	470	34.31	2.34	0.07	154	0.01459	1680000	24516.45	30	7.88	0.113
7	50.24	13955.83	49193	412	37.24	2.44	0.07	161	0.01530	1680000	25703.01	31	7.61	0.117
8	37.47	10408.57	55034	461	36.84	2.43	0.07	158	0.01538	1680000	25831.48	32	5.54	0.112
9	43.19	11997.80	57650	483	36.09	2.40	0.07	159	0.01545	1680000	25956.13	32	6.46	0.112
10	55.99	15552.92	70633	592	35.73	2.39	0.07	148	0.01419	1680000	23841.98	29	7.70	0.110
11	45.71	12697.89	50832	426	30.98	2.23	0.07	139	0.01559	1680000	26197.93	32	5.75	0.107
12	48.01	13335.84	54500	457	35.54	2.38	0.07	146	0.01505	1680000	25280.53	31	6.45	0.112
13	48.75	13542.71	67462	566	39.90	2.53	0.06	164	0.01764	1680000	29632.66	36	7.58	0.112
14	69.54	19315.32	55561	466	39.30	2.51	0.06	136	0.01698	1680000	28519.71	35	8.67	0.116
15	28.71	7976.36	63491	532	34.96	2.37	0.07	151	0.01721	1680000	28910.02	35	3.99	0.103
16	52.54	14593.78	52803	443	36.27	2.41	0.07	142	0.01581	1680000	26554.06	32	6.82	0.113
17	59.34	16482.09	58185	488	33.13	2.30	0.07	152	0.01602	1680000	26920.51	33	8.41	0.110
18	42.26	11738.75	56602	474	34.76	2.36	0.07	153	0.01514	1680000	25429.34	31	5.98	0.110
19	33.24	9234.39	46935	393	34.06	2.33	0.07	157	0.01618	1680000	27182.51	33	4.83	0.110
20	44.91	12474.24	61149	513	37.04	2.43	0.07	173	0.01626	1680000	27322.66	33	7.47	0.113
21	51.76	14376.78	58732	492	37.69	2.46	0.07	132	0.01566	1680000	26316.76	32	6.13	0.111
22	53.34	14817.43	52188	437	33.79	2.33	0.07	157	0.01588	1680000	26674.01	33	7.86	0.112
23	46.49	12914.89	57124	479	37.94	2.46	0.06	156	0.01595	1680000	26795.87	33	6.75	0.113
24	49.50	13748.95	59295	497	36.46	2.42	0.07	147	0.01495	1680000	25120.27	31	6.71	0.112
25	35.69	9913.88	45222	379	38.87	2.49	0.06	149	0.01667	1680000	28005.2	34	4.83	0.114
26	47.26	13127.03	53953	452	38.51	2.48	0.06	143	0.01574	1680000	26435.23	32	6.17	0.113
27	58.10	16137.97	59881	502	35.16	2.37	0.07	163	0.01522	1680000	25569.48	31	8.93	0.114
28	60.78	16883.10	61853	519	37.46	2.45	0.07	155	0.01442	1680000	24232.29	30	8.81	0.116
29	62.56	17377.79	48182	404	35.91	2.40	0.07	160	0.01376	1680000	23119.34	28	9.41	0.120
30	65.01	18057.28	65749	551	41.02	2.56	0.06	150	0.01655	1680000	27807.53	34	9.04	0.116
31	54.18	15049.89	53389	448	34.54	2.35	0.07	168	0.01485	1680000	24944.47	30	8.68	0.115
32	44.07	12241.78	42051	353	36.65	2.42	0.07	151	0.01635	1680000	27471.47	34	6.09	0.115

Table 6-4 Regression based sensitivity Analysis

RUN NO	Parameters Considered	Adjusted R Square	Parameter P-Value	Level of Significance - α	Hypothesis Test Result	Decision Taken
1	Vehicle Speed	0.99785	3.01523E-35	0.01	P < α	The parameter with the highest P-Value is neglected in the next level because it has a low level of significance when it comes to its relationship with deformation, therefore, Compressive Strength is neglected.
	Vehicle Mass		0.448908374	0.01	P > α	
	Compressive Strength		0.533423941	0.01	P > α	
	Stirrup Spacing		1.16331E-26	0.01	P < α	
	Longitudinal Steel Ratio		0.013915248	0.01	P > α	
2	Vehicle Speed	0.953895	3.01523E-35	0.01	P < α	The parameter with the highest P-Value is neglected in the next level because it has a low level of significance when it comes to its relationship with deformation, therefore, vehicle mass is neglected.
	Vehicle Mass		0.448908374	0.01	P > α	
	Stirrup spacing		1.16331E-26	0.01	P < α	

	Longitudinal Steel ratio		0.013915248	0.01	P > α	
3	Vehicle Speed	0.955416	3.01523E-35	0.01	P < α	The parameter with the highest P-Value is neglected in the next level because it has a low level of significance when it comes to its relationship with deformation, therefore, Longitudinal steel ratio is neglected.
	Longitudinal Steel ratio		0.013915248	0.01	P > α	
	Stirrup Spacing		1.16331E-26	0.01	P < α	
4	Vehicle Speed	0.956836	3.01523E-35	0.01	P < α	Vehicle speed from the impactor and stirrup Spacing from the resisting side are the two critical parameters,
	Stirrup Spacing		1.16331E-26	0.01	P < α	

Chapter 7 CONCLUSIONS AND RECOMMENDATIONS

7.1 CONCLUSIONS

A total of 276 piers were investigated to ascertain the extent of the vulnerability, it was found out that 6 piers corresponding to 2.174 % are Highly susceptible to vehicle impact, while 269 Piers (97.464%) are moderately exposed and 1 pier (0.362%) was of low exposure to vehicle collision. Further analysis of the highly and moderately exposed piers shows that by location, 35.273% are located along curved sections while 56.727% are located along the tangent section, 4.727% are located along roundabouts and 3.273% are at intersections.

Though most of the piers were found to be moderately and highly vulnerable to vehicle impact collision this study has found out that they are highly resistant to failure as a result of damage from vehicular impact load of a 70.6-ton vehicle traveling at speeds of upto 100 km/hr as evidenced in the average damage index of 0.066 which does not in any way affect the load-carrying capacity of the Pier. The obtained deformation of up to a maximum of 6.4 mm is too small to cause to be noticed.

It is worth noting that the bridge piers located along AALRT route are satisfactorily strong to avoid any form of catastrophe as a result of bridge pier-vehicle collision. This could be due to factors such as the sizes of the piers being greater than 1200 mm x 1400mm, the nature of pier-super structure being fixed and the parallel nature of orientation of the piers as much as possible in areas where high vehicular impacts are expected.

Regression-based sensitivity analysis of the five main parameters that were considered (vehicle speed, vehicle mass, compression strength, stirrup spacing and longitudinal steel ratio) showed that vehicle speed as an aspect of the impacting force was to a level of confidence of 95%. This is the most sensitive parameter for causing deformation while for the pier resisting aspect, stirrup spacing to a level of confidence was responsible for resisting deformation. This is similar to the findings of Gomez and Alipour [39] who concluded that, the spacing of transverse hoop reinforcement was observed to have a significant impact on the performance of the bridge piers subjected to vehicular collisions. Close spacing 100 to 165 mm of the transverse reinforcement provided greater shear resistance in the pier and resulted in only minor damage to the concrete cover.

It was also observed that an increase in the longitudinal steel resulted into increased damage which is similar to the findings reported by Fujikake et al.[34] who reported that localized damage in RC beams increases with higher amounts of tensile reinforcement due to the increase in stiffness.

7.2 RECOMMENDATIONS

Minimum pier cross-section size of 1200 mm X 1400 mm with a fixed- continuous superstructure connection between the pier and superstructure with a minimum compressive strength of 35 MPa, with a minimum longitudinal steel ratio of 0.0157 and stirrup spacing of 150 mm was found to be adequate when subjected to vehicular impact loads.

As much as possible for rectangular piers, the pier length must be made parallel to the direction of vehicle traffic to minimize the effect of damage to the pier. Vehicle speeds should be restricted in areas where highly susceptible piers are identified to a maximum of 50 Km/hr.

7.3 FUTURE WORK:

The effect of vehicular impact can be studied to cater for the effect of variation of Stirrup diameter, slenderness ratio, effect of pier surrounding soils on impact resistance by the pier and repeated impact loading including the effect of spirals and ties in resisting damage. Similar study can also be conducted to include the effect of environmental change on the performance of concrete.This study can also be re-done for AALRT based on the as-built drawings.

A soft impact study in which the deformation of the vehicle is also considered can be conducted to determine the response of the piers along AALRT.

REFERENCES

[1] C. R. G. LIMITED, "ADDIS ABABA LRT PROJECT EAST-WEST LINE PROJECT STUDY REPORT," Addis Ababa, 2009.

[2] C. R. G. LIMITED, "ADDIS ABABA LRT PROJECT NORTH-SOUTH LINE PROJECT STUDY REPORT," Addis Ababa, 2009.

[3] K. Z, "Vehicle Accident Impacts on Bridges Report," Statyba, 1997.

[4] M. S. Brackin, A. Abu-Odeh, C. E. Buth, W. F. Williams, G. T. Fry, and G. Freeby, "Impact Forces from Heavy-Vehicle Collisions with Bridge Piers," *Transp. Res. Rec. J. Transp. Res. Board*, vol. 2313, no. 1, pp. 42–51, 2013.

[5] WisDOT, *Bridge Manual*. Wisconsin, 2018.

[6] A. K. Agrawal and X. Xu, "Finite Element Simulation of Truck Impacts on Highway Bridge Piers," 2016.

[7] E. B. Williamson and D. G. Winget, "Risk Management and Design of Critical Bridges for Terrorist Attacks," *J. Bridg. Eng.*, vol. 10, no. 1, pp. 96–106, 2004.

[8] A. El-Newihy, "Application of Impact Resonance Method for Evaluation of the Dynamic Elastic Properties of Polypropylene Fiber Reinforced Concrete," 2013.

[9] I. E. Harik, A. M. Shaaban, H. Gesund, G. Y. S. Valli, and S. T. Wang, "United States Bridge Failure, 1951-1988," *J. Perform. Constr. Facil.*, vol. 4, no. 4, pp. 272–277, 1991.

[10] K. Wardhana and F. C. Hadipriono, "Analysis of Recent Bridge Failures in the United States," *J. Perform. Constr. Facil.*, vol. 17, no. 3, pp. 144–150, 2003.

[11] WHO, "Global status report on road safety 2015," 2018.

[12] [UNECA] United Nations. Economic Commission for Africa, "Case study: road safety in Ethiopia." UNECA, Addis Ababa, 2009.

[13] T. A. Abdi, B. H. Hailu, T. A. Adal, P. H. A. J. M. Van Gelder, M. P. Hagenzieker, and C.-C. Carbon, "Road Crashes in Addis Ababa, Ethiopia: Empirical Findings between the

Years 2010 and 2014," *African Research Review*, 2017. [Online]. Available: https://www.researchgate.net.publications. [Accessed: 18-Nov-2018].

[14] Fesseha Hailu and Teshager Sileshi, "The neglected health problem in Amhara National Regional State , Ethiopia," *Ethiop. J. Heal. Dev. 2014;28(1)*, vol. 28, no. 7, 2014.

[15] G. S. Tulu, S. Washington, and M. J. King, "Characteristics of Police-reported Road Traffic Crashes in Ethiopia over a Six Year Period," in *Proceedings of the 2013 Australasian Road Safety Research, Policing & Education Conference 28th – 30th August, Brisbane, Queensland*, 2013, pp. 1–13.

[16] G. L. Mosis, "Analysis of Road Traffic Violations in Addis Ababa City, The Case of Arada Subcity," Addis Ababa, 2018.

[17] L. Daudeville and Y. Malécot, "Concrete structures under impact," *Eur. J. Environ. Civ. Eng.*, vol. 15, no. sup1, pp. 101–140, 2012.

[18] Haimes.Y.Y, "Protection of Critical Complex Transportation Infrastructure," 2001.

[19] BBC, "M6 Closed in Lacanshire as Lorry Crashes into Bridge," 2018. [Online]. Available: https://www.bbc.com/news/uk. [Accessed: 14-Nov-2018].

[20] R. I. Gilbert, "The serviceability limit states in reinforced concrete design," in *The Twelfth East Asia- Pacific Conference on Structural Engineering & Construction*, 2011.

[21] A. K. Agrawal, G. Y. Liu, and S. Alampalli, "Effects of Truck Impacts on Bridge Piers," *Adv. Mater. Res.*, vol. 639–640, pp. 13–25, 2013.

[22] SB-LRA, "Sustainable Bridges Assessment for Future Traffic Demands and Longer Lives," Sweden, 2007.

[23] S. El-Tawil, E. Severino, and P. Fonseca, "Vehicle Collision with Bridge Piers," *J. Bridg. Eng.*, vol. 10, no. 3, pp. 345–353, 2005.

[24] E. Gücüyen, R. T. Erdem, E. Kantar, and M. Bağcı, "Determination of the Impact Behavior of Concrete and Reinforced Concrete Beams," *Math. Comput. Appl.*, vol. 18, no. 3, pp. 502–510, 2013.

[25] Q. M. Li, S. R. Reid, H. M. Wen, and A. R. Telford, "Local impact effects of hard missiles on concrete targets," *Int. J. Impact Eng.*, vol. 32, no. 1–4, pp. 224–284, 2006.

[26] Y. Chen and I. M. May, "Reinforced concrete members under drop-weight impacts," *Proceedings of the Institution of Civil Engineers - Structures and Buildings*, vol. 162, no. 1. pp. 45–56, 2009.

[27] CEB-FIB, "Concrete Structures Under Impact and Impulsive Loading," Lausane, 1988.

[28] O. H and M. H, "An Experimental Investigation on the effect of steel Reinforcement on Impact Response of reinforcement," *Int. J. Impact Eng.*, vol. 18, no. 1, pp. 12–21, 2016.

[29] M. O, "Comparison of different Constitutive Models for Concrete in Abaqus/Explicit for Missile Impact Analysis," 2010.

[30] S. N. A. Safri, M. T. H. Sultan, N. Yidris, and F. Mustapha, "Low Velocity and High Velocity Impact Test on Composite Materials – A review," pp. 50–60, 2014.

[31] D. Zhou, R. Li, J. Wang, and C. Guo, "Study on Impact Behavior and Impact Force of Bridge Pier Subjected to Vehicle Collision," *Shock Vib.*, vol. 2017, pp. 1–12, 2017.

[32] X. C. Zhu, H. Zhu, and H. R. Li, "Drop-weight impact test on U-shape concrete specimens with statistical and regression analyses," *Materials (Basel).*, vol. 8, no. 9, pp. 5877–5890, 2015.

[33] ACI, "Measurement of Properties of Fiber Reinforced Concrete," *Am. Concr. Inst. Mater. J.*, vol. 85, pp. 583–593, 1988.

[34] K. Fujikake, B. Li, and S. Soeun, "Impact Response of Reinforced Concrete Beam and Its Analytical Evaluation," *J. Struct. Eng.*, vol. 135, no. 8, pp. 938–950, 2009.

[35] S. Saatci and V. . . .J, "Effect of Shear Mechanisms on Impact Behaviour of reinforced Concrete Beams," *ACI Struct. J.*, vol. 106, no. 1, 2009.

[36] O. J, S. . A, I. . B, and S. . E, "Tensile Behaviour of concrete under high loading rates," *Int. J. Impact Eng.*, vol. 69, pp. 55–68, 2014.

[37] D. Zhou and R. Li, "Damage assessment of bridge piers subjected to vehicle collision,"

Adv. Struct. Eng., vol. 21, no. 15, pp. 2270–2281, 2018.

[38] D. Zhou, R. Li, J. Wang, and C. Guo, "Study on Impact Behavior and Impact Force of Bridge Pier Subjected to Vehicle Collision," *Hindawi-Shock Vib.*, vol. 2017, 2017.

[39] N. L. Gomez and A. Alipour, "Study of Circular Reinforced Concrete Bridge Piers Subjected to Vehicular Collisions," in *Structures Congress*, 2014, no. 2003, pp. 577–587.

[40] L. Chen and Y. Xiao, "[Chen] Finite Element Analysis of Vehicle Collisions with Bridge Piers," in *Seventh National Seismic Conference on Bridges & Highways*, 2016, no. August.

[41] R. G. Sargent, "Advanced Tutorials: Verification and Validation of Simulation Models," in *Proceedings of the 2011 Winter Simulation Conference*, 2011, pp. 183–198.

[42] C. A. Chung, *Simulation Modelling Hand book- Apractical Approach*. CRC Press LLC, 2004.

[43] B. Z and C. L, *Non-Linear Finite Elements for Continua & Structures*. West Sussex: John Willey & Sons Inc, 2014.

[44] G. R. Liu and S.S.Quek, *The Finite Element Method- A Practical Course*. Burlington: Butterworth Heinemann, 2003.

[45] I. Subashini, G. Smitha, and R. Aahrthy, "Low velocity impact response and failure assessment of textile reinforced concrete slabs," *Comput. Mater. Contin.*, vol. 53, no. 4, pp. 291–306, 2017.

[46] M. Munther and J. Runebrant, "Structural Response of Concrete Beams Subjected to Drop Weight Impact A parametric study using numerical modelling," 2018.

[47] D. L. Logan *et al.*, *A First Course in the Finite Element Method Fourth Edition*, Fourth. 2007.

[48] T. P. Valayil and J. C. Issac, "Crash simulation in ANSYS LS-DYNA to explore the crash performance of composite and metallic materials," *International Journal of Scientific & Engineering Research*, vol. 4, no. 8. 2013.

[49] B. S and D. J, "Livermore Software Technology Corporation," 2004. [Online]. Available: https://awy.lstc.com/tiki/tiki. [Accessed: 10-Jan-2019].

[50] D. V. Hutton, *Fundamentals of Finite Element Analysis*. The McGraw-Hill Companies, 2004.

[51] B. Minasny and A. B. M. Bratney, "A conditioned Latin Hypercube Method for sampling in the presence of Ancillary Information," *Comput. Geosci.*, vol. 32, no. 1378–1388, 2006.

[52] S. M. Ross, *Introduction to Probability and Statistics for engineers and Scientists*, Third., vol. 67, no. 6. New York: Elsevier Academic Press, 2004.

[53] D. C. Montgomery, *Applied Statistics and Probability for Engineers Third Edition*, vol. 37, no. 4. 2003.

[54] L.-C. Zhang, "On Some Common Practices of Systematic Sampling," *J. Off. Stat.*, vol. 24, no. 4, pp. 557–569, 2008.

[55] A. Olson, G. Sandberg, and O. Dahlbiom, "On Latin Hypercube Sampling for Structural Reliability Analysis," *Struct. Saf.*, vol. 25, pp. 47–68, 2003.

[56] P. Bhattacharjee, K. R. Kumar, and T. A. J. Reddy, "Structural Safety Evaluation using Modified Latin Hypercube Sampling Technique," *Int. J. Performability Eng.*, vol. 9, no. 5, pp. 512–522, 2013.

[57] L. Chu, E. S. Decursi, A. El Hami, and M. Eid, "Application of Latin Hypercube Sampling Based Kriging Surrogate Models in Reliability Assessment," *Sci. J. Appl. Math. Stat.*, vol. 6, no. 3, pp. 263–274, 2015.

[58] D. Novak, M.Vofechovsky, R. Pukl, and V. Cervenka, "Statistical Nonlinear Analysis-Size Effect of Concrete Beams," *Fract. Mech. Concr. Struct.*, vol. 09, pp. 823–830, 2001.

[59] G. W. D and K. H. Jorgensen, *A User's Guide to LHS*. Sandia Group, 1998.

[60] M. D. Mckay, R. J. Beckman, and W. J. Conover, "A Comparison of Three Methods for Selecting Values of Input Variables in the Analysis of Output from a Computer Code.," *Technometrics*, vol. 42, no. 1, pp. 55–61, 2010.

[61] M. D. Shield, K. Teferra, A. Hapij, and R. P. Daddazio, "Refined Stratified Sampling for efficient Monte Carlo Based Uncertainity Quantification," *Reliab. Eng. Syst. Saf.*, vol. 142, pp. 310–325, 2015.

[62] V. E.Larson, J.-C. Golaz, H. Jiang, and W. R. Cotton, "Supplying Local Microphysics Parameterizations with Information about Subgrid Variability: Latin Hypercube Sampling," *J. Atmos. Sci.*, vol. 62, pp. 4010–4026, 2005.

[63] A. Florian, "An Efficient Sampling Scheme: Updated Hypercube Sampling," *Probabilistic Eng. Mech.*, vol. 7, pp. 123–130, 1992.

[64] A. Saltelli, "Sensitivity analysis of model output An investigation of new techniques," *Comput. North-holl. Stat. Data Anal.*, vol. 15, pp. 211–238, 1993.

[65] C. B. Storlie and J. C. Helton, "Multiple predictor smoothing methods for sensitivity analysis : Description of techniques," *Reliab. Eng. Syst. Saf.*, vol. 93, pp. 28–54, 2008.

[66] J. C. Helton and F. J. Davis, "Illustration of Sampling-Based Methods for Uncertainty and Sensitivity Analysis," *Risk Anal.*, vol. 22, no. 3, pp. 591–622, 2002.

[67] A. Hoare, D. G. Regan, and D. P. Wilson, "Regression Sampling and Sensitivity analyses tools (SaSAT) for Computational modelling," *Int. J. BioMed Comput.*, vol. 23, pp. 97–112, 2010.

[68] G. Manache and C. S. Melching, "Sensitivity of Latin Hypercube Sampling to Sample Size and Distributional Assumptions-Uncertainty and Sensitivity Analysis," 2015.

[69] New York State Department of Transportation, "Collision Vulnerability Manual." NYSDT, New York, pp. 2.10-2.12, 1996.

[70] B. Tutorials, "University of Alberta - ANSYS Tutorials." University of Alberta, Alberta, 2001.

[71] D. N. Moulika *et al.*, "Modelling and Analysis of Reinforced Concrete Beam under Flexure using ANSYS," *Int. J. Civ. Eng. Technol.*, vol. 8, no. 3, pp. 1103–1111, 2017.

[72] R. W, "Numerical Assessment for Impact Strength," *IJIE*, vol. 36, 2009.

[73] AASHTO, "AASHTO LRFD Bridge Design Specifications," 2010.

[74] E. T. Gebremedhin, "EVALUATION OF EFFECTIVENESS OF TRAFFIC CALMING AT ROUNDABOUTS WITHIN NIFAS SILK LAFTO SUB CITY," Addis Ababa, 2015.

[75] B. T. Beyene, "Addis Ababa Institute of Technology School of Civil and Environmental Engineering Implications of axle load limitation in Ethiopia (The case study on axle load management at Holeta and Modjo weighbridge stations)," Addis Ababa, 2015.

[76] R. M.Barker and J. A. Pucket, *Design of Highway Bridges- An LRFD Approach*, 2nd ed. John Wiley & Sons, Inc, 2007.

[77] AREMA, "Manual for Railway Engineering," 2010.

[78] W. Panichkitkosolkul, "Confidence Intervals for the Coefficient of Variation in a Normal Distribution with a Known Population Mean," *J. Probab. Stat.*, vol. 2013, pp. 1–11, 2013.

[79] A. Standards, "Design of Concrete Structures- AS3600-2001 Australian Standards," 2001.

APPENDIX A

This appendix provides details about the photographic evidence of field survey for the capture of a pier susceptible to overhead impact, posted speeds along the AALRT route (these speeds were adopted for ranking of pier vulnerability) evidence of damage to the Piers and extent of protection to the piers.

Field-based Photos: These simply show some of the evidence that is entailed in Table 7-1

Table 7-1, Shows the Pier Vulnerability ranking, the Final score being 0.9 X Summation for each individual Pier.

Figure 7-1 Clearly shows the flow path taken for every individual Pier in Table A-1 to finally come up with the ranks.

Field-Based Photos



Susceptible to Overhead Collision

Posted Speed Limits

Impact with Barriers

Unprotected Bridge Piers

Table 7-1 Pier Vulnerabiltity Ranking

Pier Designation		Nature of Section	Pier Type		Protective Barrier		Pedestrian Bridge		Structural Redundancy		Characteristics of Traffic (Under ADTT)		Horizontal Clearance (Edge of Roadway to face of Pier)		Weight of Superstructure		Posted Speed Limit (Km/hr)		Evidence of Previous Impact Damage		Orientation of Piers with the direction of Traffic Under the Bridge		Final Score	Vulnerability CLASS
LINE	Pier No		Type	Score	Type	Score	YES	Score	SPE	Score	Type	Score	Type	Score	Type	Score	Type	Score	Type	Score	Type	Score		
ATIKILTERA - GOJAM BERENDA																								
NS	1	TANG	SP	0	SBR	10	NO	0	SPE	4	> 5000	15	B	4	LGT	8	Y	2	DNE	0	PAR	0	38.7	M
NS	2	TANG	SP	0	SBR	10	NO	0	SPE	4	> 5000	15	B	4	LGT	8	Y	2	DNE	0	PAR	0	38.7	M
NS	3	TANG	SP	0	SBR	10	NO	0	SPE	4	> 5000	15	B	4	LGT	8	Y	2	EWR	5	PAR	0	43.2	M
NS	4	TANG	SP	0	SBR	10	NO	0	SPE	4	> 5000	15	B	4	LGT	8	Y	2	DNE	0	PAR	0	38.7	M
NS	5	TANG	SP	0	SBR	10	NO	0	SPE	4	> 5000	15	B	4	LGT	8	Y	2	DNE	0	PAR	0	38.7	M
NS	6	TANG	SP	0	SBR	10	NO	0	SPE	4	> 5000	15	B	4	LGT	8	Y	2	DNE	0	PAR	0	38.7	M
NS	7	TANG	SP	0	SBR	10	NO	0	SPE	4	> 5000	15	B	4	LGT	8	Y	2	DNE	0	PAR	0	38.7	M
NS	8	TANG	SP	0	SBR	10	NO	0	SPE	4	> 5000	15	B	4	LGT	8	Y	2	DNE	0	PAR	0	38.7	M
NS	9	TANG	SP	0	SBR	10	NO	0	SPE	4	> 5000	15	B	4	LGT	8	Y	2	DNE	0	PAR	0	38.7	M
NS	10	TANG	SP	0	SBR	10	NO	0	SPE	4	> 5000	15	B	4	LGT	8	Y	2	DNE	0	PAR	0	38.7	M
NS	11	TANG	SP	0	SBR	10	NO	0	SPE	4	> 5000	15	B	4	LGT	8	Y	2	DNE	0	PAR	0	38.7	M
NS	12	TANG	SP	0	SBR	10	NO	0	SPE	4	> 5000	15	B	4	LGT	8	Y	2	DNE	0	PAR	0	38.7	M
NS	13	TANG	SP	0	SBR	10	NO	0	SPE	4	> 5000	15	B	4	LGT	8	Y	2	DNE	0	PAR	0	38.7	M
NS	14	TANG	SP	0	SBR	10	NO	0	SPE	4	> 5000	15	B	4	LGT	8	Y	2	DNE	0	PAR	0	38.7	M
NS	15	TANG	SP	0	SBR	10	NO	0	SPE	4	> 5000	15	B	4	LGT	8	Y	2	DNE	0	PAR	0	38.7	M
NS	16	TANG	SP	0	SBR	10	NO	0	SPE	4	> 5000	15	B	4	LGT	8	Y	2	DNE	0	PAR	0	38.7	M
NS	17	TANG	SP	0	SBR	10	NO	0	SPE	4	> 5000	15	B	4	LGT	8	Y	2	DNE	0	PAR	0	38.7	M
NS	18	TANG	SP	0	SBR	10	NO	0	SPE	4	> 5000	15	B	4	LGT	8	Y	2	DNE	0	PAR	0	38.7	M
NS	19	TANG	SP	0	SBR	10	NO	0	SPE	4	> 5000	15	B	4	LGT	8	Y	2	DNE	0	PAR	0	38.7	M
NS	20	TANG	SP	0	SBR	10	NO	0	SPE	4	> 5000	15	B	4	LGT	8	Y	2	DNE	0	PAR	0	38.7	M
GOJAM BERENDA TO AUTOBUS TERA																								
NS	21	CURVED	SP	0	SBR	10	NO	0	SPE	4	> 5000	15	B	4	LGT	8	Y	2	EWR	5	SKE	4	46.8	M
NS	22	CURVED	SP	0	SBR	10	NO	0	SPE	4	> 5000	15	B	4	LGT	8	Y	2	EWR	5	SKE	4	46.8	M
NS	23	CURVED	SP	0	SBR	10	NO	0	SPE	4	> 5000	15	B	4	LGT	8	Y	2	EWR	5	SKE	4	46.8	M
NS	24	CURVED	SP	0	SBR	10	NO	0	SPE	4	> 5000	15	B	4	LGT	8	Y	2	EWR	5	SKE	4	46.8	M
NS	25	CURVED	SP	0	SBR	10	NO	0	SPE	4	> 5000	15	B	4	LGT	8	Y	2	EWR	5	SKE	4	46.8	M
NS	26	CURVED	SP	0	SBR	10	YES	5	SPE	4	> 5000	15	B	4	MDT	4	Y	2	EWR	5	SKE	4	47.7	M
NS	27	CURVED	SP	0	SBR	10	YES	5	SPE	4	> 5000	15	B	4	MDT	4	Y	2	EWR	5	SKE	4	47.7	M
NS	28	CURVED	SP	0	SBR	10	YES	5	SPE	4	> 5000	15	B	4	MDT	4	Y	2	EWR	5	SKE	4	47.7	M
NS	29	CURVED	SP	0	SBR	10	YES	5	SPE	4	> 5000	15	B	4	MDT	4	Y	2	EWR	5	SKE	4	47.7	M
NS	30	CURVED	SP	0	SBR	10	YES	5	SPE	4	> 5000	15	B	4	MDT	4	Y	2	EWR	5	SKE	4	47.7	M

Pier Designation		Nature of Section	Pier Type		Protective Barrier		Pedestrian Bridge		Structural Redundancy		Characteristics of Traffic (Under ADTT)		Horizontal Clearance (Edge of Roadway to face of Pier)		Weight of Superstructure		Posted Speed Limit (Km/hr.)		Evidence of Previous Impact Damage		Orientation of Piers with the direction of Traffic Under the Bridge		Final Score	Vulnerability CLASS
LINE	Pier No		Type	Sco	Type	Score	YES	Score	SPE	Score	Type	Score	Type	Score	Type	Score	Type	Score	Type	Score	Type	Score		
Autobus Tera to Sebatagna																								
NS	31	CURVED	SP	0	SBR	10	NO	0	SPE	4	> 5000	15	A	8	LGT	8	Y	2	DNE	0	SKE	4	45.9	M
NS	32	CURVED	SP	0	SBR	10	NO	0	CTS	0	> 5000	15	A	8	MDT	4	Y	2	DNE	0	SKE	4	38.7	M
NS	33	CURVED	SP	0	SBR	10	NO	0	SPE	4	> 5000	15	B	4	LGT	8	Y	2	DNE	0	PAR	0	38.7	M
NS	34	CURVED	SP	0	SBR	10	NO	0	SPE	4	> 5000	15	B	4	LGT	8	Y	2	DNE	0	SKE	4	42.3	M
NS	35	CURVED	SP	0	SBR	10	NO	0	SPE	4	> 5000	15	B	4	LGT	8	Y	2	DNE	0	SKE	4	42.3	M
NS	36	CURVED	SP	0	SBR	10	NO	0	SPE	4	> 5000	15	B	4	LGT	8	Y	2	DNE	0	SKE	4	42.3	M
NS	37	CURVED	SP	0	SBR	10	NO	0	SPE	4	> 5000	15	B	4	LGT	8	Y	2	DNE	0	SKE	4	42.3	M
NS	38	CURVED	SP	0	SBR	10	NO	0	SPE	4	> 5000	15	B	4	LGT	8	Y	2	DNE	0	SKE	4	42.3	M
NS	39	CURVED	SP	0	SBR	10	NO	0	SPE	4	> 5000	15	B	4	LGT	8	Y	2	DNE	0	SKE	4	42.3	M
NS	40	CURVED	SP	0	SBR	10	NO	0	SPE	4	> 5000	15	B	4	LGT	8	Y	2	DNE	0	SKE	4	42.3	M
NS	41	CURVED	SP	0	SBR	10	NO	0	SPE	4	> 5000	15	B	4	LGT	8	Y	2	DNE	0	SKE	4	42.3	M
NS	42	CURVED	SP	0	SBR	10	NO	0	SPE	4	> 5000	15	B	4	LGT	8	Y	2	DNE	0	SKE	4	42.3	M
NS	43	CURVED	SP	0	SBR	10	NO	0	SPE	4	> 5000	15	B	4	LGT	8	Y	2	DNE	0	SKE	4	42.3	M
NS	44	CURVED	SP	0	SBR	10	NO	0	SPE	4	> 5000	15	B	4	LGT	8	Y	2	DNE	0	SKE	4	42.3	M
NS	45	CURVED	SP	0	SBR	10	NO	0	SPE	4	> 5000	15	B	4	LGT	8	Y	2	DNE	0	SKE	4	42.3	M
NS	46	CURVED	SP	0	SBR	10	NO	0	SPE	4	> 5000	15	B	4	LGT	8	Y	2	DNE	0	SKE	4	42.3	M
Abnet Station																								
NS	47	CURVED	SP	0	SBR	10	YES	5	SPE	4	> 5000	15	B	4	MDT	4	Y	2	EWP	15	SKE	4	56.7	H
NS	48	TANG	SP	0	SBR	10	YES	5	SPE	4	> 5000	15	B	4	MDT	4	Y	2	EWR	5	PAR	0	44.1	M
NS	49	TANG	SP	0	SBR	10	YES	5	SPE	4	> 5000	15	B	4	MDT	4	Y	2	EWR	5	PAR	0	44.1	M
NS	50	TANG	SP	0	SBR	10	YES	5	SPE	4	> 5000	15	B	4	MDT	4	Y	2	EWR	5	PAR	0	44.1	M
Abnet to Darmar																								
NS	51	CD-RA	SP	0	SBR	10	NO	0	SPE	4	> 5000	15	B	4	LGT	8	Y	2	DNE	0	PAR	0	38.7	M
NS	52	CD-RA	SP	0	SBR	10	NO	0	SPE	4	> 5000	15	B	4	LGT	8	Y	2	DNE	0	PAR	0	38.7	M
NS	53	CD-RA	SP	0	SBR	10	NO	0	SPE	4	> 5000	15	C	0	LGT	8	Y	2	DNE	0	SKE	4	38.7	M
NS	54	CD-RA	SP	0	SBR	10	NO	0	SPE	4	> 5000	15	C	0	LGT	8	Y	2	DNE	0	SKE	4	38.7	M
NS	55	CD-RA	SP	0	SBR	10	NO	0	CTS	0	> 5000	15	B	4	MDT	4	Y	2	DNE	0	SKE	4	35.1	M
NS	56	CURVED	SP	0	SBR	10	NO	0	SPE	4	> 5000	15	B	4	LGT	8	Y	2	DNE	0	SKE	4	42.3	M
NS	57	CURVED	SP	0	SBR	10	NO	0	CTS	0	> 5000	15	B	4	MDT	4	Y	2	DNE	0	SKE	4	35.1	M
NS	58	CURVED	SP	0	SBR	10	NO	0	SPE	4	> 5000	15	B	4	LGT	8	Y	2	DNE	0	PAR	0	38.7	M
NS	59	CURVED	SP	0	SBR	10	NO	0	SPE	4	> 5000	15	B	4	LGT	8	Y	2	DNE	0	PAR	0	38.7	M
NS	60	CURVED	SP	0	SBR	10	NO	0	SPE	4	> 5000	15	B	4	LGT	8	Y	2	DNE	0	PAR	0	38.7	M
NS	61	CURVED	SP	0	SBR	10	NO	0	SPE	4	> 5000	15	B	4	LGT	8	Y	2	DNE	0	PAR	0	38.7	M

Pier Designation		Nature of Section	Pier Type		Protective Barrier		Pedestrian Bridge		Structural Redundancy		Characteristics of Traffic (Under ADTT)		Horizontal Clearance (Edge of Roadway to face of Pier)		Weight of Superstructure		Posted Speed Limit (Km/hr)		Evidence of Previous Impact Damage		Orientation of Piers with the direction of Traffic Under the Bridge		Final Score	Vulnerability CLASS
LINE	Pier No		Type	Sco	Type	Score	YES	Score	SPE	Score	Type	Score	Type	Score	Type	Score	Type	Score	Type	Score	Type	Score		
NS	62	CURVED	SP	0	SBR	10	NO	0	CTS	0	> 5000	15	B	4	LGT	8	Y	2	DNE	0	PAR	0	35.1	M
NS	63	CURVED	SP	0	SBR	10	NO	0	CTS	0	> 5000	15	B	4	LGT	8	Y	2	DNE	0	PAR	0	35.1	M
NS	64	CURVED	SP	0	SBR	10	NO	0	SPE	4	> 5000	15	B	4	LGT	8	Y	2	DNE	0	PAR	0	38.7	M
NS	65	CURVED	SP	0	SBR	10	NO	0	CTS	0	> 5000	15	B	4	LGT	8	Y	2	DNE	0	PAR	0	35.1	M
NS	66	CURVED	SP	0	SBR	10	NO	0	SPE	4	> 5000	15	B	4	LGT	8	Y	2	DNE	0	PAR	0	38.7	M
NS	67	CURVED	SP	0	SBR	10	NO	0	SPE	4	> 5000	15	B	4	LGT	8	Y	2	DNE	0	PAR	0	38.7	M
NS	68	CURVED	SP	0	SBR	10	NO	0	SPE	4	> 5000	15	B	4	LGT	8	Y	2	DNE	0	PAR	0	38.7	M
NS	69	CURVED	SP	0	SBR	10	NO	0	SPE	4	> 5000	15	B	4	LGT	8	Y	2	DNE	0	PAR	0	38.7	M
NS	70	CURVED	SP	0	SBR	10	NO	0	SPE	4	> 5000	15	B	4	LGT	8	Y	2	DNE	0	PAR	0	38.7	M
NS	71	CURVED	SP	0	SBR	10	NO	0	SPE	4	> 5000	15	B	4	LGT	8	Y	2	DNE	0	PAR	0	38.7	M
NS	72	CURVED	SP	0	SBR	10	NO	0	SPE	4	> 5000	15	B	4	LGT	8	Y	2	DNE	0	PAR	0	38.7	M
NS	73	TANG	SP	0	SBR	10	NO	0	SPE	4	> 5000	15	B	4	LGT	8	Y	2	DNE	0	PAR	0	38.7	M
NS	74	TANG	SP	0	SBR	10	NO	0	SPE	4	> 5000	15	B	4	LGT	8	Y	2	DNE	0	PAR	0	38.7	M
NS	75	TANG	SP	0	SBR	10	NO	0	SPE	4	> 5000	15	B	4	LGT	8	Y	2	DNE	0	PAR	0	38.7	M
NS	76	TANG	SP	0	SBR	10	NO	0	SPE	4	> 5000	15	B	4	LGT	8	Y	2	DNE	0	PAR	0	38.7	M
NS	77	TANG	SP	0	SBR	10	NO	0	SPE	4	> 5000	15	B	4	LGT	8	Y	2	DNE	0	PAR	0	38.7	M
NS	78	TANG	SP	0	SBR	10	NO	0	SPE	4	> 5000	15	B	4	LGT	8	Y	2	DNE	0	PAR	0	38.7	M
NS	79	TANG	SP	0	SBR	10	NO	0	SPE	4	> 5000	15	B	4	LGT	8	Y	2	DNE	0	PAR	0	38.7	M
NS	80	TANG	SP	0	SBR	10	NO	0	SPE	4	> 5000	15	B	4	LGT	8	Z	0	DNE	0	PAR	0	36.9	M
NS	81	TANG	SP	0	SBR	10	NO	0	SPE	4	> 5000	15	B	4	LGT	8	Z	0	DNE	0	PAR	0	36.9	M
NS	82	TANG	SP	0	SBR	10	NO	0	SPE	4	> 5000	15	B	4	LGT	8	Z	0	DNE	0	PAR	0	36.9	M
NS	83	TANG	SP	0	SBR	10	NO	0	SPE	4	> 5000	15	B	4	LGT	8	Z	0	DNE	0	PAR	0	36.9	M
NS	84	TANG	SP	0	SBR	10	NO	0	SPE	4	> 5000	15	B	4	LGT	8	Z	0	DNE	0	PAR	0	36.9	M
NS	85	TANG	SP	0	SBR	10	NO	0	SPE	4	> 5000	15	B	4	LGT	8	Z	0	DNE	0	PAR	0	36.9	M
NS	86	TANG	SP	0	SBR	10	NO	0	SPE	4	> 5000	15	B	4	LGT	8	Z	0	DNE	0	PAR	0	36.9	M
NS	87	TANG	SP	0	SBR	10	NO	0	SPE	4	> 5000	15	B	4	LGT	8	Y	2	DNE	0	PAR	0	38.7	M
NS	88	TANG	SP	0	SBR	10	NO	0	SPE	4	> 5000	15	B	4	LGT	8	Y	2	DNE	0	PAR	0	38.7	M
NS	89	TANG	SP	0	SBR	10	NO	0	SPE	4	> 5000	15	B	4	LGT	8	Y	2	DNE	0	PAR	0	38.7	M
NS	90	TANG	SP	0	SBR	10	NO	0	SPE	4	> 5000	15	B	4	LGT	8	Y	2	DNE	0	PAR	0	38.7	M
NS	91	TANG	SP	0	SBR	10	NO	0	SPE	4	> 5000	15	B	4	LGT	8	Y	2	DNE	0	PAR	0	38.7	M
NS	92	CURVED	SP	0	SBR	10	NO	0	CTS	0	> 5000	15	B	4	LGT	8	Y	2	DNE	0	PAR	0	35.1	M
NS	93	CURVED	SP	0	SBR	10	NO	0	CTS	0	> 5000	15	B	4	LGT	8	Y	2	DNE	0	PAR	0	35.1	M

		Nature of Section	Pier Type		Protective Barrier		Pedestrian Bridge		Structural Redundancy		Characteristics of Traffic (Under ADTT)		Horizontal Clearance(Edge of Roadway to face of Pier)		Weight of Super structure		Posted Speed Limit (Km/hr)		Evidence of Previous Impact Damage		Orientation of Piers with direction of Traffic Under the Bridge		Final Score	Vulnerability CLASS
LINE	Pier No		Type	Sco	Type	Score	YES	Score	SPE	Score	Type	Score	Type	Score	Type	Score	Type	Score	Type	Score	Type	Score		
Common - Section																								
Darmar to St Lideta																								
NS-EW	94	CURVED	SP	0	NN	20		0	SPE	0	> 5000	15	A	8	LGT	8	Z	0	EWB		SKE	4	49.5	M
NS-EW	95	CURVED	SP	0	NN	20	NO	0	SPE	4	> 5000	15	A	8	LGT	8	Z	0	DNE	0	PAR	0	49.5	M
NS-EW	96	TANG	SP	0	NN	20		5		4	> 5000	15	A	8	LGT	8	Y	2	DNE	0	PAR	0	55.8	H
NS-EW	97	TANG	SP	0	NN	20		5		4	> 5000	15	A	8	LGT	8	Y	2	DNE	0	PAR	0	55.8	H
NS-EW	98	TANG	SP	0	NN	20		5		4	> 5000	15	A	8	LGT	8	Y	2	DNE	0	PAR	0	55.8	H
NS-EW	99	CURVED	SP	0	SBR	10	YES	5	SPE	4	> 5000	15	B	4	MDT	4	Z	0	DNE	0	SKE	4	41.4	M
NS-EW	100	CURVED	SP	0	SBR	10	YES	5	SPE	4	> 5000	15	B	4	MDT	4	Z	0	DNE	0	SKE	4	41.4	M
NS-EW	101	CURVED	SP	0	SBR	10	YES	5	SPE	4	> 5000	15	B	4	MDT	4	Z	0	DNE	0	SKE	4	41.4	M
St-Lideta to Tegbared																								
NS-EW	102	CURVED	SP	0	SBR	10	YES	5	SPE	4	> 5000	15		4	MDT	4	Z	0	DNE	0	SKE	4	41.4	M
NS-EW	103	TANG	SP	0	NN	20	YES	5	SPE	4	> 5000	15	A	8	LGT	8	Y	2	DNE	0	PAR	0	55.8	H
NS-EW	104	TANG	SP	0	NN	20	YES	5	SPE	4	> 5000	15	A	8	LGT	8	Y	2	DNE	0	PAR	0	55.8	H
NS-EW	105	TANG	SP	0	SDD	0	NO	0	SPE	4	> 5000	15	B	4	LGT	8	Y	2	DNE	0	PAR	0	29.7	L
NS-EW	106	TANG	SP	0	NN	20	NO	0	SPE	4	> 5000	15	A	8	LGT	8	Y	2	DNE	0	PAR	0	51.3	M
NS-EW	107	TANG	SP	0	NN	20	NO	0	SPE	4	> 5000	15	A	8	LGT	8	Y	2	DNE	0	PAR	0	51.3	M
NS-EW	108	TANG	SP	0	NN	20	NO	0	SPE	4	> 5000	15	A	8	LGT	8	Y	2	DNE	0	PAR	0	51.3	M
NS-EW	109	TANG	SP	0	SBR	10	NO	0	SPE	4	> 5000	15	B	4	LGT	8	Y	2	DNE	0	PAR	0	38.7	M
NS-EW	110	TANG	SP	0	SBR	10	NO	0	SPE	4	> 5000	15	B	4	LGT	8	Y	2	DNE	0	PAR	0	38.7	M
NS-EW	111	TANG	SP	0	SBR	10	NO	0	SPE	4	> 5000	15	B	4	LGT	8	Y	2	DNE	0	PAR	0	38.7	M
NS-EW	112	TANG	SP	0	SBR	10	NO	0	SPE	4	> 5000	15	B	4	LGT	8	Y	2	DNE	0	PAR	0	38.7	M
NS-EW	113	TANG	SP	0	SBR	10	NO	0	SPE	4	> 5000	15	B	4	LGT	8	Y	2	DNE	0	PAR	0	38.7	M
NS-EW	114	TANG	SP	0	SBR	10	NO	0	SPE	4	> 5000	15	B	4	LGT	8	Y	2	DNE	0	PAR	0	38.7	M
NS-EW	115	TANG	SP	0	SBR	10	NO	0	SPE	4	> 5000	15	B	4	LGT	8	Y	2	DNE	0	PAR	0	38.7	M
NS-EW	116	TANG	SP	0	SBR	10	NO	0	SPE	4	> 5000	15	B	4	LGT	8	Y	2	DNE	0	PAR	0	38.7	M
NS-EW	117	TANG	SP	0	SBR	10	NO	0	SPE	4	> 5000	15	B	4	LGT	8	Y	2	DNE	0	PAR	0	38.7	M
NS-EW	118	TANG	SP	0	SBR	10	NO	0	SPE	4	> 5000	15	B	4	LGT	8	Y	2	DNE	0	PAR	0	38.7	M
NS-EW	119	TANG	SP	0	SBR	10	NO	0	SPE	4	> 5000	15	B	4	LGT	8	Y	2	DNE	0	PAR	0	38.7	M
NS-EW	120	TANG	SP	0	SBR	10	NO	0	SPE	4	> 5000	15	B	4	LGT	8	Y	2	EWR	5	SKE	4	46.8	M
NS-EW	121	TANG	SP	0	SBR	10	NO	0	SPE	4	> 5000	15	B	4	LGT	8	Y	2	DNE	0	PAR	0	38.7	M
NS-EW	122	TANG	SP	0	SBR	10	NO	0	SPE	4	> 5000	15	B	4	LGT	8	Y	2	DNE	0	PAR	0	38.7	M
NS-EW	123	TANG	SP	0	SBR	10	NO	0	SPE	4	> 5000	15	B	4	LGT	8	Y	2	DNE	0	PAR	0	38.7	M
NS-EW	124	TANG	SP	0	SBR	10	NO	0	SPE	4	> 5000	15	B	4	LGT	8	Y	2	DNE	0	PAR	0	38.7	M
NS-EW	125	TANG	SP	0	SBR	10	NO	0	SPE	4	> 5000	15	B	4	LGT	8	Y	2	DNE	0	PAR	0	38.7	M
NS-EW	126	TANG	SP	0	SBR	10	NO	0	SPE	4	> 5000	15	B	4	LGT	8	Y	2	DNE	0	PAR	0	38.7	M
NS-EW	127	TANG	SP	0	SBR	10	NO	0	SPE	4	> 5000	15	B	4	LGT	8	Y	2	DNE	0	PAR	0	38.7	M
NS-EW	128	TANG	SP	0	SBR	10	NO	0	SPE	4	> 5000	15	B	4	LGT	8	Y	2	DNE	0	PAR	0	38.7	M

		Nature of Section	Pier Type		Protective Barrier		Pedestrian Bridge		Structural Redundancy		Characteristics of Traffic (Under ADTT)		Horizontal Clearance(Edge of Roadway to face of Pier)		Weight of Super structure		Posted Speed Limit (Km/hr)		Evidence of Previous Impact Damage		Orientation of Piers with direction of Traffic Under the Bridge		Final Score	Vulnerability CLASS
LINE	Pier No		Type	Sco	Type	Score	YES	Score	SPE	Score	Type	Score	Type	Score	Type	Score	Type	Score	Type	Score	Type	Score		
TEGBARED to Mexico																								
NS-EW	129	TANG	SP	0	NN	20	YES	5	SPE	4	> 5000	15	A	8	MDT	4	Y	2	DNE	0	PAR	0	52.2	M
NS-EW	130	TANG	SP	0	NN	20	YES	5	SPE	4	> 5000	15	A	8	MDT	4	Y	2	DNE	0	PAR	0	52.2	M
NS-EW	131	TANG	SP	0	NN	20	YES	5	SPE	4	> 5000	15	A	8	MDT	4	Y	2	DNE	0	PAR	0	52.2	M
NS-EW	132	TANG	SP	0	NN	20	YES	5	SPE	4	> 5000	15	A	8	MDT	4	Y	2	DNE	0	PAR	0	52.2	M
NS-EW	133	CURVED	SP	0	SBR	10	NO	0	SPE	4	> 5000	15	B	4	LGT	8	Y	2	DNE	0	PAR	0	38.7	M
NS-EW	134	CURVED	SP	0	SBR	10	NO	0	SPE	4	> 5000	15	B	4	LGT	8	Y	2	DNE	0	PAR	0	38.7	M
NS-EW	135	CURVED	SP	0	SBR	10	NO	0	SPE	4	> 5000	15	B	4	LGT	8	Y	2	DNE	0	PAR	0	38.7	M
NS-EW	136	CURVED	SP	0	SBR	10	NO	0	SPE	4	> 5000	15	B	4	LGT	8	Y	2	DNE	0	PAR	0	38.7	M
NS-EW	137	CURVED	SP	0	SDD	0	NO	0	SPE	4	> 5000	15	B	4	LGT	8	Y	2	DNE	0	SKE	4	33.3	M
NS-EW	138	CD-RA	SP	0	SDD	0	NO	0	SPE	4	> 5000	15	B	4	LGT	8	Y	2	DNE	0	SKE	4	33.3	M
NS-EW	139	CD-RA	SP	0	SBR	10	NO	0	SPE	4	> 5000	15	B	4	LGT	8	Y	2	DNE	0	SKE	4	42.3	M
NS-EW	140	CD-RA	SP	0	SBR	10	NO	0	SPE	4	> 5000	15	B	4	LGT	8	Y	2	DNE	0	SKE	4	42.3	M
NS-EW	141	CD-RA	SP	0	SDD	0	NO	0	SPE	4	> 5000	15	B	4	LGT	8	Y	2	DNE	0	SKE	4	33.3	M
NS-EW	142	CURVED	SP	0	SBR	10	NO	0	SPE	4	> 5000	15	B	4	LGT	8	Y	2	DNE	0	SKE	4	42.3	M
NS-EW	143	TANG	SP	0	SBR	10	NO	0	SPE	4	> 5000	15	B	4	LGT	8	Y	2	DNE	0	PAR	0	38.7	M
NS-EW	144	TANG	SP	0	SBR	10	NO	0	SPE	4	> 5000	15	B	4	LGT	8	Y	2	DNE	0	PAR	0	38.7	M
NS-EW	145	TANG	SP	0	SBR	10	NO	0	SPE	4	> 5000	15	B	4	LGT	8	Y	2	DNE	0	PAR	0	38.7	M
NS-EW	146	TANG	SP	0	SBR	10	NO	0	SPE	4	> 5000	15	B	4	LGT	8	Y	2	DNE	0	PAR	0	38.7	M
NS-EW	147	TA-INT	SP	0	SBR	10	NO	0	SPE	4	> 5000	15	B	4	LGT	8	Y	2	EWB	5	PAR	0	43.2	M
NS-EW	148	TA-INT	SP	0	SBR	10	NO	0	SPE	4	> 5000	15	B	4	LGT	8	Y	2	EWB	5	PAR	0	43.2	M
NS-EW	149	TANG	SP	0	SBR	10	NO	0	SPE	4	> 5000	15	B	4	LGT	8	Y	2	DNE	0	PAR	0	38.7	M
NS-EW	150	TANG	SP	0	SBR	10	NO	0	SPE	4	> 5000	15	B	4	LGT	8	Y	2	DNE	0	PAR	0	38.7	M
NS-EW	151	TANG	SP	0	SBR	10	NO	0	SPE	4	> 5000	15	B	4	LGT	8	Y	2	DNE	0	PAR	0	38.7	M
NS-EW	152	TANG	SP	0	SBR	10	NO	0	SPE	4	> 5000	15	B	4	LGT	8	Y	2	DNE	0	PAR	0	38.7	M
NS-EW	153	TANG	SP	0	SBR	10	NO	0	SPE	4	> 5000	15	B	4	LGT	8	Y	2	DNE	0	PAR	0	38.7	M
NS-EW	154	TANG	SP	0	SBR	10	NO	0	SPE	4	> 5000	15	B	4	LGT	8	Y	2	DNE	0	PAR	0	38.7	M
NS-EW	155	CURVED	SP	0	SBR	10	NO	0	SPE	4	> 5000	15	B	4	LGT	8	Y	2	DNE	0	PAR	0	38.7	M
NS-EW	156	CURVED	SP	0	SBR	10	NO	0	SPE	4	> 5000	15	B	4	LGT	8	Y	2	DNE	0	PAR	0	38.7	M
NS-EW	157	CURVED	SP	0	SBR	10	NO	0	SPE	4	> 5000	15	B	4	LGT	8	Y	2	DNE	0	PAR	0	38.7	M
Mexico to Leghar																								
NS-EW	158	TANG	SP	0	SBR	10	NO	0	SPE	4	> 5000	15	B	4	MDT	4	Y	2	DNE	0	PAR	0	35.1	M
NS-EW	159	TANG	SP	0	SBR	10	NO	0	SPE	4	> 5000	15	B	4	MDT	4	Y	2	DNE	0	PAR	0	35.1	M
NS-EW	160	TANG	SP	0	SBR	10	YES	5	SPE	4	> 5000	15	B	4	MDT	4	Y	2	DNE	0	PAR	0	39.6	M
NS-EW	161	TANG	SP	0	SBR	10	NO	0	SPE	4	> 5000	15	B	4	MDT	4	Y	2	DNE	0	PAR	0	35.1	M
NS-EW	162	CURVED	SP	0	SBR	10	NO	0	SPE	4	> 5000	15	B	4	LGT	8	Y	2	DNE	0	SKE	4	42.3	M
NS-EW	163	CURVED	SP	0	SBR	10	NO	0	SPE	4	> 5000	15	B	4	LGT	8	Y	2	DNE	0	SKE	4	42.3	M
NS-EW	164	CURVED	SP	0	SBR	10	NO	0	SPE	4	> 5000	15	B	4	LGT	8	Y	2	DNE	0	SKE	4	42.3	M

		Nature of Section	**Pier Type**		**Protective Barrier**		**Pedestrian Bridge**		**Structural Redundancy**		**Characteristics of Traffic (Under ADTT)**		**Horizontal Clearance(Edge of Roadway to face of Pier)**		**Weight of Super structure**		**Posted Speed Limit (Km/hr)**		**Evidence of Previous Impact Damage**		**Orientation of Piers with direction of Traffic Under the Bridge**		**Final Score**	Vulnerability CLASS
LINE	Pier No		Type	Sco	Type	Score	YES	Score	SPE	Score	Type	Score	Type	Score	Type	Score	Type	Score	Type	Score	Type	Score		
NS-EW	165	CURVED	SP	0	SBR	10	NO	0	SPE	4	> 5000	15	B	4	LGT	8	Y	2	DNE	0	SKE	4	42.3	M
NS-EW	166	CURVED	SP	0	SBR	10	NO	0	SPE	4	> 5000	15	B	4	LGT	8	Y	2	DNE	0	SKE	4	42.3	M
NS-EW	167	CURVED	SP	0	SBR	10	NO	0	SPE	4	> 5000	15	B	4	LGT	8	Y	2	DNE	0	SKE	4	42.3	M
NS-EW	168	TANG	SP	0	SBR	10	NO	0	SPE	4	> 5000	15	B	4	LGT	8	Y	2	DNE	0	PAR	0	38.7	M
NS-EW	169	TANG	SP	0	SBR	10	NO	0	SPE	4	> 5000	15	B	4	LGT	8	Y	2	DNE	0	PAR	0	38.7	M
NS-EW	170	TANG	SP	0	SBR	10	NO	0	SPE	4	> 5000	15	B	4	LGT	8	Y	2	DNE	0	PAR	0	38.7	M
NS-EW	171	TANG	SP	0	SBR	10	NO	0	SPE	4	> 5000	15	B	4	LGT	8	Y	2	DNE	0	PAR	0	38.7	M
NS-EW	172	TANG	SP	0	SBR	10	NO	0	SPE	4	> 5000	15	B	4	LGT	8	Y	2	DNE	0	PAR	0	38.7	M
NS-EW	173	TANG	SP	0	SBR	10	NO	0	SPE	4	> 5000	15	B	4	LGT	8	Y	2	DNE	0	PAR	0	38.7	M
NS-EW	174	TANG	SP	0	SBR	10	NO	0	SPE	4	> 5000	15	B	4	LGT	8	Y	2	DNE	0	PAR	0	38.7	M
NS-EW	175	CURVED	SP	0	NN	20	NO	0	SPE	4	> 5000	15	B	4	LGT	8	Y	2	DNE	0	SKE	4	51.3	M
NS-EW	176	CURVED	SP	0	NN	20	NO	0	SPE	4	> 5000	15	B	4	LGT	8	Y	2	DNE	0	SKE	4	51.3	M
NS-EW	177	CURVED	SP	0	NN	20	NO	0	SPE	4	> 5000	15	B	4	LGT	8	Y	2	DNE	0	SKE	4	51.3	M
NS-EW	178	CURVED	SP	0	NN	20	NO	0	SPE	4	> 5000	15	B	4	LGT	8	Y	2	DNE	0	SKE	4	51.3	M
NS-EW	179	CURVED	SP	0	NN	20	NO	0	SPE	4	> 5000	15	B	4	LGT	8	Y	2	DNE	0	SKE	4	51.3	M
Leghar to Stadium																								
NS-EW	180	TA-INT	SP	0	SDD	0	NO	0	SPE	4	> 5000	15	B	4	LGT	8	Y	2	EWB	5	SKE	4	37.8	M
NS-EW	181	TANG	SP	0	SBR	10	NO	0	SPE	4	> 5000	15	B	4	MDT	4	Y	2	DNE	0	PAR	0	35.1	M
NS-EW	182	TANG	SP	0	SBR	10	NO	0	SPE	4	> 5000	15	B	4	MDT	4	Y	2	DNE	0	PAR	0	35.1	M
NS-EW	183	TANG	SP	0	SBR	10	NO	0	SPE	4	> 5000	15	B	4	MDT	4	Y	2	DNE	0	PAR	0	35.1	M
NS-EW	184	TANG	SP	0	SBR	10	NO	0	SPE	4	> 5000	15	B	4	MDT	4	Y	2	DNE	0	PAR	0	35.1	M
NS-EW	185	TANG	SP	0	SBR	10	NO	0	SPE	4	> 5000	15	B	4	LGT	8	Y	2	DNE	0	PAR	0	38.7	M
NS-EW	186	TANG	SP	0	SBR	10	NO	0	SPE	4	> 5000	15	B	4	LGT	8	Y	2	DNE	0	PAR	0	38.7	M
NS-EW	187	TANG	SP	0	SBR	10	NO	0	SPE	4	> 5000	15	B	4	LGT	8	Y	2	DNE	0	PAR	0	38.7	M
NS-EW	188	TANG	SP	0	SBR	10	NO	0	SPE	4	> 5000	15	B	4	LGT	8	Y	2	DNE	0	PAR	0	38.7	M
NS-EW	189	TANG	SP	0	SBR	10	NO	0	SPE	4	> 5000	15	B	4	LGT	8	Y	2	DNE	0	PAR	0	38.7	M
NS-EW	190	CURVED	SP	0	NN	20	NO	0	SPE	4	> 5000	15	A	8	LGT	8	Y	2	DNE	0	SKE	4	54.9	M
NS-EW	191	CURVED	SP	0	NN	20	NO	0	SPE	4	> 5000	15	A	8	LGT	8	Y	2	DNE	0	SKE	4	54.9	M
NS-EW	192	CURVED	SP	0	NN	20	NO	0	SPE	4	> 5000	15	A	8	LGT	8	Y	2	DNE	0	SKE	4	54.9	M
NS-EW	193	CURVED	SP	0	NN	20	NO	0	SPE	4	> 5000	15	A	8	LGT	8	Y	2	DNE	0	SKE	4	54.9	M
NS-EW	194	CURVED	SP	0	SBR	10	NO	0	SPE	4	> 5000	15	B	4	LGT	8	Y	2	DNE	0	SKE	4	42.3	M
NS-EW	195	CURVED	SP	0	SBR	10	NO	0	SPE	4	> 5000	15	B	4	LGT	8	Y	2	DNE	0	SKE	4	42.3	M
NS-EW	196	CURVED	SP	0	SBR	10	NO	0	SPE	4	> 5000	15	B	4	LGT	8	Y	2	DNE	0	SKE	4	42.3	M
NS-EW	197	CURVED	SP	0	SBR	10	NO	0	SPE	4	> 5000	15	B	4	LGT	8	Y	2	DNE	0	SKE	4	42.3	M
NS-EW	198	CURVED	SP	0	SBR	10	NO	0	SPE	4	> 5000	15	B	4	LGT	8	Y	2	DNE	0	SKE	4	42.3	M
NS-EW	199	TANG	SP	0	SBR	10	YES	5	SPE	4	> 5000	15	B	4	LGT	8	Y	2	DNE	0	PAR	0	43.2	M
NS-EW	200	TANG	SP	0	SBR	10	NO	0	SPE	4	> 5000	15	B	4	MDT	4	Y	2	DNE	0	PAR	0	35.1	M
NS-EW	201	TANG	SP	0	SBR	10	NO	0	SPE	4	> 5000	15	B	4	MDT	4	Y	2	DNE	0	PAR	0	35.1	M
NS-EW	202	TANG	SP	0	SBR	10	YES	5	SPE	4	> 5000	15	B	4	MDT	4	Y	2	DNE	0	PAR	0	39.6	M

		Nature of Section	**Pier Type**		**Protective Barrier**		**Pedestrian Bridge**		**Structural Redundancy**		**Characteristics of Traffic (Under ADTT)**		**Horizontal Clearance(Edge of Roadway to face of Pier)**		**Weight of Super structure**		**Posted Speed Limit (Km/hr)**		**Evidence of Previous Impact Damage**		**Orientation of Piers with direction of Traffic Under the Bridge**		**Final Score**	Vulnerability CLASS
LINE	Pier No		Type	Sco	Type	Score	YES	Score	SPE	Score	Type	Score	Type	Score	Type	Score	Type	Score	Type	Score	Type	Score		
NS-EW	203	TANG	SP	0	SBR	10	NO	0	SPE	4	> 5000	15	B	4	HVY	0	Y	2	DNE	0	PAR	0	31.5	M
NS-EW	204	TANG	SP	0	SBR	10	NO	0	SPE	4	> 5000	15	B	4	HVY	0	Y	2	DNE	0	PAR	0	31.5	M
NS-EW	205	TANG	SP	0	SBR	10	NO	0	SPE	4	> 5000	15	B	4	HVY	0	Y	2	DNE	0	PAR	0	31.5	M
NS-EW	206	TANG	SP	0	SBR	10	NO	0	SPE	4	> 5000	15	B	4	HVY	0	Y	2	DNE	0	PAR	0	31.5	M
Stadium- Meshwelkya							NO																	
NS	207	CURVED	SP	0	SDD	0	NO	0	CTS	0	> 5000	15	B	4	MDT	4	Y	2	EWB	5	SKE	4	30.6	M
NS	208	CURVED	SP	0	SBR	10	YES	5	SPE	4	> 5000	15	B	4	LGT	8	Y	2	DNE	0	SKE	4	46.8	M
NS	209	TANG	SP	0	NN	20	NO	0	SPE	4	> 5000	15	A	8	LGT	8	Y	2	DNE	0	PAR	0	51.3	M
NS	210	TANG	SP	0	NN	20	NO	0	SPE	4	> 5000	15	A	8	LGT	8	Y	2	DNE	0	PAR	0	51.3	M
NS	211	TANG	SP	0	NN	20	NO	0	SPE	4	> 5000	15	A	8	LGT	8	Y	2	DNE	0	PAR	0	51.3	M
NS	212	TANG	SP	0	NN	20	NO	0	SPE	4	> 5000	15	A	8	LGT	8	Y	2	DNE	0	PAR	0	51.3	M
Lancha to Nefas Silk2																								
NS	213	TANG	SP	0	NN	20	NO	0	SPE	4	> 5000	15	A	8	LGT	8	Y	2	DNE	0	PAR	0	51.3	M
NS	214	TANG	SP	0	NN	20	NO	0	SPE	4	> 5000	15	A	8	LGT	8	Y	2	DNE	0	PAR	0	51.3	M
NS	215	TANG	SP	0	NN	20	NO	0	SPE	4	> 5000	15	A	8	LGT	8	Y	2	DNE	0	PAR	0	51.3	M
NS	216	TANG	SP	0	NN	20	NO	0	SPE	4	> 5000	15	A	8	LGT	8	Y	2	DNE	0	PAR	0	51.3	M
NS	217	TANG	SP	0	NN	20	NO	0	SPE	4	> 5000	15	A	8	LGT	8	Y	2	DNE	0	PAR	0	51.3	M
NS	218	TANG	SP	0	NN	20	NO	0	SPE	4	> 5000	15	A	8	LGT	8	Y	2	DNE	0	PAR	0	51.3	M
NS	219	TANG	SP	0	NN	20	NO	0	SPE	4	> 5000	15	A	8	LGT	8	Y	2	DNE	0	PAR	0	51.3	M
NS	220	TA-INT	SP	0	NN	20	NO	0	SPE	4	> 5000	15	A	8	LGT	8	Y	2	DNE	0	SKE	4	54.9	M
NS	221	TA-INT	SP	0	NN	20	NO	0	SPE	4	> 5000	15	A	8	LGT	8	Y	2	DNE	0	SKE	4	54.9	M
NS	222	CURVED	SP	0	NN	20	NO	0	SPE	4	> 5000	15	A	8	LGT	8	Y	2	DNE	0	SKE	4	54.9	M
NS	223	CURVED	SP	0	NN	20	NO	0	SPE	4	> 5000	15	A	8	LGT	8	Y	2	DNE	0	SKE	4	54.9	M
NS	224	CURVED	SP	0	NN	20	NO	0	SPE	4	> 5000	15	A	8	LGT	8	Y	2	DNE	0	SKE	4	54.9	M
NS	225	CURVED	SP	0	NN	20	NO	0	SPE	4	> 5000	15	A	8	LGT	8	Y	2	DNE	0	SKE	4	54.9	M
NS	226	CURVED	SP	0	NN	20	NO	0	SPE	4	> 5000	15	A	8	LGT	8	Y	2	DNE	0	SKE	4	54.9	M
NS	227	CURVED	SP	0	NN	20	NO	0	SPE	4	> 5000	15	A	8	LGT	8	Y	2	DNE	0	SKE	4	54.9	M
NS	228	CURVED	SP	0	NN	20	NO	0	SPE	4	> 5000	15	C	0	LGT	8	X	4	DNE	0	SKE	4	49.5	M
NS	229	CURVED	SP	0	NN	20	NO	0	SPE	4	> 5000	15	C	0	LGT	8	X	4	DNE	0	SKE	4	49.5	M
NS	230	CURVED	SP	0	NN	20	NO	0	SPE	4	> 5000	15	C	0	LGT	8	X	4	DNE	0	SKE	4	49.5	M
NS	231	CURVED	SP	0	NN	20	NO	0	SPE	4	> 5000	15	C	0	LGT	8	X	4	DNE	0	SKE	4	49.5	M
NS	232	CURVED	SP	0	SBR	10	NO	0	SPE	4	> 5000	15	B	4	LGT	8	X	4	DNE	0	SKE	4	44.1	M
NS	233	CURVED	SP	0	SBR	10	NO	0	SPE	4	> 5000	15	B	4	LGT	8	X	4	DNE	0	SKE	4	44.1	M
NS	234	CURVED	SP	0	SBR	10	NO	0	SPE	4	> 5000	15	B	4	LGT	8	X	4	DNE	0	SKE	4	44.1	M
CocaCola to St Lideta																								
EW	235	TANG	SP	0	SDD	0	YES	5	SPE	4	> 5000	15	B	4	LGT	8	X	4	DNE	0	PAR	0	36.0	M
EW	236	TANG	SP	0	NN	20	NO	0	SPE	4	> 5000	15	A	8	LGT	8	Y	2	DNE	0	PAR	0	51.3	M
EW	237	CD-RA	SP	0	SBR	10	NO	0	SPE	4	> 5000	15	B	4	LGT	8	X	4	DNE	0	PAR	0	40.5	M
EW	238	CD-RA	SP	0	SBR	10	NO	0	SPE	4	> 5000	15	B	4	HVY		Z	0	DNE	0	SKE	4	33.3	M

		Nature of Section	**Pier Type**		**Protective Barrier**		**Pedestrian Bridge**		**Structural Redundancy**		**Characteristics of Traffic (Under ADTT)**		**Horizontal Clearance(Edge of Roadway to face of Pier)**		**Weight of Super structure**		**Posted Speed Limit (Km/hr)**		**Evidence of Previous Impact Damage**		**Orientation of Piers with direction of Traffic Under the Bridge**		**Final Score**	Vulnerability CLASS
LINE	Pier No		Type	Sco	Type	Score	YES	Score	SPE	Score	Type	Score	Type	Score	Type	Score	Type	Score	Type	Score	Type	Score		
EW	239	CD-RA	SP	0	SBR	10	NO	0	SPE	4	> 5000	15	B	4	HVY		Z	0	DNE	0	SKE	4	33.3	M
EW	240	CD-RA	SP	0	SBR	10	NO	0	SPE	4	> 5000	15	B	4	HVY		Z	0	EWB	5	SKE	4	37.8	M
Stadium to St - Estifanos																								
EW	241	TA-INT	SP	0	SBR	10	NO	0	SPE	4	> 5000	15		4	HVY		Y	2	EWR	5	SKE	4	39.6	M
EW	242	TA-INT	SP	0	NN	20	NO	0	SPE	4	> 5000	15	A	8	MDT	4	Y	2	DNE	0	SKE	4	51.3	M
EW	243	TANG	SP	0	SBR	10	NO	0	SPE	4	> 5000	15	B	4	LGT	8	Y	2	DNE	0	PAR	0	38.7	M
EW	244	TANG	SP	0	SBR	10	NO	0	SPE	4	> 5000	15	B	4	LGT	8	Y	2	DNE	0	PAR	0	38.7	M
EW	245	TANG	SP	0	SBR	10	NO	0	SPE	4	> 5000	15	B	4	LGT	8	Y	2	DNE	0	PAR	0	38.7	M
EW	246	TANG	SP	0	SBR	10	NO	0	SPE	4	> 5000	15	B	4	LGT	8	Y	2	DNE	0	PAR	0	38.7	M
EW	247	TANG	SP	0	SBR	10	NO	0	SPE	4	> 5000	15	B	4	LGT	8	Y	2	DNE	0	PAR	0	38.7	M
EW	248	TANG	SP	0	SBR	10	NO	0	SPE	4	> 5000	15	B	4	LGT	8	Y	2	DNE	0	PAR	0	38.7	M
EW	249	TANG	SP	0	SBR	10	NO	0	SPE	4	> 5000	15	B	4	LGT	8	Y	2	DNE	0	PAR	0	38.7	M
EW	250	TANG	SP	0	SBR	10	NO	0	SPE	4	> 5000	15	B	4	LGT	8	Y	2	DNE	0	PAR	0	38.7	M
EW	251	TANG	SP	0	SBR	10	NO	0	SPE	4	> 5000	15	B	4	LGT	8	Y	2	DNE	0	PAR	0	38.7	M
EW	252	TANG	SP	0	SBR	10	NO	0	SPE	4	> 5000	15	B	4	LGT	8	Y	2	DNE	0	PAR	0	38.7	M
EW	253	TANG	SP	0	SBR	10	NO	0	SPE	4	> 5000	15	B	4	LGT	8	Y	2	DNE	0	PAR	0	38.7	M
EW	254	TANG	SP	0	SBR	10	NO	0	SPE	4	> 5000	15	B	4	LGT	8	Y	2	DNE	0	PAR	0	38.7	M
EW	255	TA-INT	SP	0	SBR	10	NO	0	SPE	4	> 5000	15	B	4	LGT	8	Y	2	DNE	0	PAR	0	38.7	M
EW	256	TA-INT	SP	0	SBR	10	NO	0	SPE	4	> 5000	15	B	4	LGT	8	Y	2	DNE	0	SKE	4	42.3	M
EW	257	TA-INT	SP	0	SDD	0	NO	0	SPE	4	> 5000	15	A	8	LGT	8	Y	2	EWB	5	SKE	4	41.4	M
EW	258	TA-INT	SP	0	SBR	10	NO	0	SPE	4	> 5000	15	B	4	LGT	8	Y	2	DNE	0	SKE	4	42.3	M
EW	259	TANG	SP	0	NN	20	NO	0	SPE	4	> 5000	15	A	8	MDT	4	Y	2	DNE	0	SKE	4	51.3	M
EW	260	TANG	SP	0	NN	20	NO	0	SPE	4	> 5000	15	A	8	LGT	8	Y	2	DNE	0	PAR	0	51.3	M
EW	261	TANG	SP	0	NN	20	NO	0	SPE	4	> 5000	15	A	8	LGT	8	Y	2	DNE	0	PAR	0	51.3	M
EW	262	TANG	SP	0	NN	20	NO	0	SPE	4	> 5000	15	A	8	LGT	8	Y	2	DNE	0	PAR	0	51.3	M
EW	263	TANG	SP	0	SBR	10	NO	0	SPE	4	> 5000	15	B	4	LGT	8	Y	2	DNE	0	PAR	0	38.7	M
EW	264	TANG	SP	0	SBR	10	NO	0	SPE	4	> 5000	15	B	4	LGT	8	Y	2	DNE	0	PAR	0	38.7	M
EW	265	TANG	SP	0	SBR	10	NO	0	SPE	4	> 5000	15	B	4	LGT	8	Y	2	DNE	0	PAR	0	38.7	M
EW	266	TANG	SP	0	SBR	10	NO	0	SPE	4	> 5000	15	B	4	LGT	8	Y	2	DNE	0	PAR	0	38.7	M
EW	267	TANG	SP	0	SBR	10	NO	0	SPE	4	> 5000	15	B	4	MDT	4	Y	2	DNE	0	PAR	0	35.1	M
EW	268	TANG	SP	0	SBR	10	NO	0	SPE	4	> 5000	15	B	4	MDT	4	Y	2	DNE	0	PAR	0	35.1	M
EW	269	TANG	SP	0	SBR	10	NO	0	SPE	4	> 5000	15	B	4	MDT	4	Y	2	DNE	0	PAR	0	35.1	M
EW	270	TANG	SP	0	SBR	10	NO	0	SPE	4	> 5000	15	B	4	MDT	4	Y	2	DNE	0	PAR	0	35.1	M
St-Estiphanos to Bambis																								
EW	271	TANG	SP	0	SBR	10	NO	0	SPE	4	> 5000	15	B	4	LGT	8	Y	2	DNE	0	PAR	0	38.7	M
EW	272	TANG	SP	0	SBR	10	NO	0	SPE	4	> 5000	15	B	4	LGT	8	Y	2	DNE	0	PAR	0	38.7	M
EW	273	TANG	SP	0	SBR	10	NO	0	SPE	4	> 5000	15	B	4	LGT	8	Y	2	DNE	0	PAR	0	38.7	M
EW	274	TANG	SP	0	SBR	10	NO	0	SPE	4	> 5000	15	B	4	LGT	8	Y	2	DNE	0	PAR	0	38.7	M
EW	275	TANG	SP	0	SBR	10	NO	0	SPE	4	> 5000	15	B	4	LGT	8	Y	2	DNE	0	PAR	0	38.7	M
EW	276	TANG	SP	0	SBR	10	NO	0	SPE	4	> 5000	15	B	4	LGT	8	Y	2	DNE	0	PAR	0	38.7	M

KEY & SCALE	
NATURE OF SECTION	
TANG	TANGENT
CA-RA	ROUNDABOUT
TA-INT	INTERSECTION
PIER TYPE	
SP	Solid Pier
MC	Multi Column
OTC	One or Two Column
Protective Barrier	
NN	None
SBR	Substandard Barrier/Railings
SDD	Standard
Structural Redundancy	
CTS	CONTINOUS
SPE	SIMPLE
Horizontal Clearance (Edge of Roadway to face of Pier)	
A	-< 9.144 m without Barrier & Mound
B	- < 9.144 with Barrier or Mound
C	- > 9.144 m
Weight of Superstructure	
LGT	- LIGHT
MDT	- MODERATE
HVY	-HEAVY
Posted Speed Limit (Km/hr.)	
W	88.5 to 104.61
X	64.4 to 80
Y	48.3 to 56.3
Z	< 48.3
Evidence of Previous Impact Damage	
EWP	Damage Exists with Pier
EWB	Damage Exists with Barrier
EWR	Damage Exists with Railings
DNE	Damage Does not exist
Orientation of Piers with the direction of Traffic Under the Bridge	
SKE	- Skewed
PAR	- Parallel
VULNERABILITY SCALE	
< 30	LOW EXPOSURE -L
30<=55	MODERATE EXPOSURE- M
>55	HIGH EXPOSURE -H

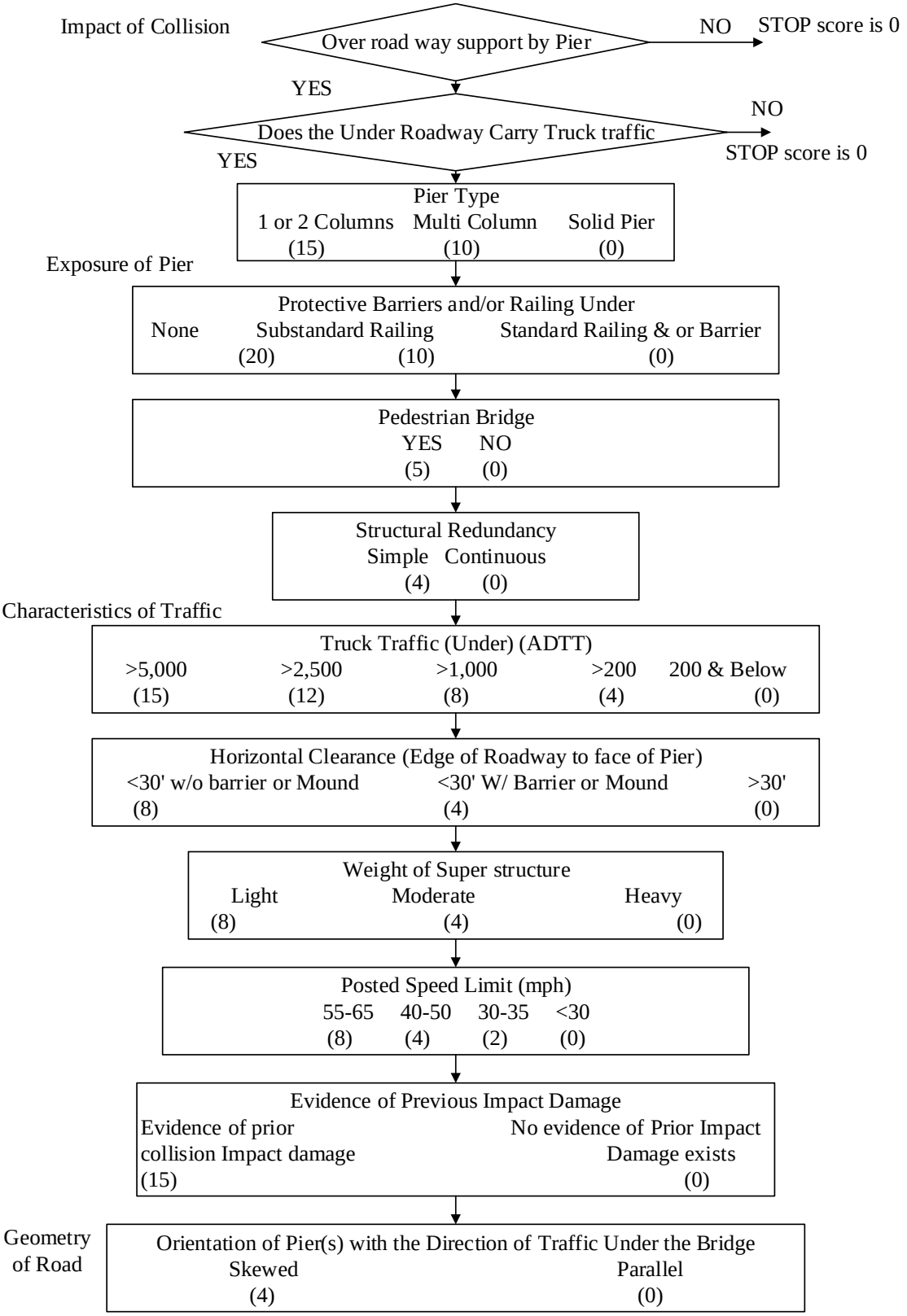

Figure 7-1-Pier Ranking Flow Chart - NYSDT [46]

APPENDIX B

This section seeks to illustrate the different parameters that were used in assessing the performance of AALRT identified vulnerable piers when subjected to vehicular impact loads.

Area of rebars in column 6 was referenced based on the Ethiopia -Djibouti lines due to lack of detailed drawings at the time of the study.

During the study of the piers, the effect of spirals and ties were neglected, though this could have a significant effect on the outcome of the pier in terms of its resistance to damage.

The nominal stirrup spacing for the links was 150 mm but due to variations that usually take place during construction two more spacings that is 145 mm and 155 mm were also considered for simulation purposes.

Table 7-2 – SIMULATION DETAILS OF AALRT

Pier-Super structure Connection	Vehicle Speed Km/hr	Vehicle Mass (Kg)	Concrete Compressive Strength (Mpa)	12 mm Stirrup Spacing (mm)	Area of Rebars	Pier Cross Sectional Area (mm^2)	Equivalent Longitudinal Steel Area	Area of 1 Bar (200mms) No of Bars	No Of Bars	Deformation (mm)	Damage Ratio
PIER 1 1400 X 1200											
SIMPLE	70	70633	30.98	141	0.0157	1680000	26376.9979	804.2477194	32	3.87530	0.080
			36.00	151						3.84500	0.078
			41.02	173						4.30680	0.083
SIMPLE	120	70633	30.98	141	0.0157	1680000	26376.9979	804.2477194	32	76.18600	1.000
			36.00	151						76.72700	1.000
			41.02	173						81.48300	1.000
PIER 2 2000 X 1500											
SIMPLE	70	70633	30.98	141	0.0157	3000000	47101.782	804.2477194	58	0.00000	0.000
			36.00	151						0.00000	0.000
			41.02	173						0.00000	0.000
SIMPLE	120	70633	30.98	141	0.0157	3000000	47101.782	804.2477194	58	0.00000	0.000
			36.00	151						0.00000	0.000
			41.02	173						0.00000	0.000
PIER 3 1700 X 1300											
SIMPLE	70	70633	30.98	141	0.0157	2210000	34698.3127	804.2477194	44	4.67450	0.092
			36.00	151						4.14740	0.075
			41.02	173						4.11250	0.048

Pier-Super structure Connection	Vehicle Speed Km/hr	Vehicle Mass (Kg)	Concrete Compressive Strength (Mpa)	12 mm Stirrup Spacing (mm)	Area of Rebars	Pier Cross Sectional Area (mm^2)	Equivalent Longitudinal Steel Area	Area of 1 Bar (200mms) No of Bars	No Of Bars	Deformation (mm)	Damage Ratio
SIMPLE	120	70633	30.98	141	0.0157	2210000	34698.3127	804.2477194	44	78.38800	1.000
			36.00	151						77.95000	1.000
			41.02	173						83.42600	1.000
PIER 4 2800 X 1800 (WITH 1200 X 1800 2N0 COMBINED PIERS)											
SIMPLE	70	70633	30.98	141	0.0157	2160000	33913.283	804.2477194	42	2.58540	0.057
			36.00	151						2.58540	0.057
			41.02	173						2.82880	0.058
SIMPLE	120	70633	30.98	141	0.0157	2160000	33913.283	804.2477194	42	41.85093	0.337
			36.00	151						41.86860	0.355
			41.02	173						46.38090	0.466
PIER 5 1800 X 1500											
SIMPLE	70	70633	30.98	141	0.0157	2700000	42391.6038	804.2477194	52	5.72910	0.098
			36.00	151						5.73310	0.098
			41.02	173						5.77350	0.099
SIMPLE	120	70633	30.98	141	0.0157	2700000	42391.6038	804.2477194	52	72.32331	1.000
			36.00	151						77.73700	1.000
			41.02	173						80.89120	1.000
PIER 5 1800 X 1500											
CONTINOUS	70	70633	30.98	141	0.0157	2700000	42391.6038	804.2477194	52	5.10617	0.054
			36.00	151						5.43210	0.054
			41.02	173						5.64938	0.054

Pier-Super structure Connection	Vehicle Speed Km/hr	Vehicle Mass (Kg)	Concrete Compressive Strength (Mpa)	12 mm Stirrup Spacing (mm)	Area of Rebars	Pier Cross Sectional Area (mm^2)	Equivalent Longitudinal Steel Area	Area of 1 Bar (200mms) No of Bars	No Of Bars	Deformation (mm)	Damage Ratio
CONTINOUS	120	70633	30.98	141	0.0157	2700000	42391.6038	804.2477194	52	77.39866	1.000
			36.00	151						82.33900	1.000
			41.02	173						85.63256	1.000
PIER 6 2400 X 2200											
CONTINOUS	70	70633	30.98	141	0.0157	5280000	82899.1363	804.2477194	104	0.68875	0.000
			36.00	151						0.63370	0.000
			41.02	173						0.48223	0.000
	120	70633	30.98	141	0.0157	5280000	82899.1363	804.2477194	104	18.31140	0.401
			36.00	151						18.78042	0.410
			41.02	173						22.39600	0.451
PIER 7 1800 X 1500											
SIMPLE	70	70633	30.98	141	0.0157	2700000	42391.6038	804.2477194	52	5.39958	0.120
			36.00	151						5.45783	0.123
			41.02	173						6.38814	0.138
SIMPLE	120	70633	30.98	141	0.0157	2700000	42391.6038	804.2477194	52.71	70.43308	1.000
			36.00	151						73.56912	1.000
			41.02	173						86.09931	1.000
PIER 8 2100 X 1600											
SIMPLE	70	70633	30.98	141	0.0157	3360000	52753.9958	804.2477194	65.59	4.12226	0.092
			36.00	151						4.41271	0.099
			41.02	173						5.28473	0.118

APPENDIX C

This shows the data that was adopted for the calculation of mean and standard deviation values for speed and axle loads. It also gives the table from which the coefficient of variation was adopted for the calculation of standard deviation given the mean value.

Table 7-3 Vehicle Masses [75]

	REC- COMESA COUNTRY	PERMISSIBLE MAXIMUM COMBINATION (MASS-KG)	M-MEAN	VALUE	
1	ANGOLA	38000	-18342	336434204.6	
2	MALAWI	56000	-342	117061.7347	
3	NAMIBIA	56000	-342	117061.7347	
4	SWAZILAND	50200	-6142	37725918.88	
5	ZAMBIA	56000	-342	117061.7347	
6	ZIMBABWE	56000	-342	117061.7347	
7	ETHIOPIA	58000	1658	2748490.306	
8		61380	5038	25380004.59	
9		57800	1458	2125347.449	
10		64240	7898	62376147.45	
11		62780	6438	41446004.59	
12		60540	4198	17622004.59	
13		63860	7518	56518176.02	
14		58080	1738	3020147.449	
15		60860	4518	20411033.16	
16		62080	5738	32923004.59	
17		58900	2558	6542633.163	
18		58260	1918	3678176.02	
19		62980	6638	44061147.45	
20		57420	1078	1161776.02	
21		60180	3838	14729147.45	
22		62180	5838	34080576.02	
23		58840	2498	6239290.306	
24	ERITREA	46000	-10342	106959918.9	
25	DJIBOUTI	46000	-10342	106959918.9	
26	KENYA	53000	-3342	11169918.88	
27	SUDAN	46000	-10342	106959918.9	
28	UGANDA	46000	-10342	106959918.9	
		1577580		1188701071	
	MEAN	56342		44025965.61	6635.207
	SD				6635.207

Table 7-4 Probabilities and COV [78]

n	κ_0	Coverage probabilities						Expected lengths					
		Miller	McKay	Vangel	Approx.	Shortest	Equal-tailed	Miller	McKay	Vangel	Approx.	Shortest	Equal-tailed
5	0.05	0.8829	0.9533	0.9440	0.9538	0.9504	0.9511	0.0661	0.0785	0.0762	0.1058	0.0758	0.0870
	0.10	0.8827	0.9537	0.9457	0.9549	0.9501	0.9506	0.1333	0.1608	0.1544	0.2113	0.1513	0.1737
	0.20	0.8847	0.9578	0.9508	0.9548	0.9500	0.9507	0.2756	0.3630	0.3282	0.4226	0.3026	0.3475
	0.33	0.8904	0.9647	0.9599	0.9542	0.9501	0.9501	0.4880	0.8954	0.6498	0.6986	0.5001	0.5743
	0.50	0.8934	0.9711	0.9656	0.9537	0.9487	0.9491	0.8276	1.3796	1.4333	1.0561	0.7561	0.8683
	0.67	0.9042	0.9795	0.9721	0.9548	0.9495	0.9502	1.2550	1.5758	1.9791	1.4140	1.0124	1.1625
10	0.05	0.9115	0.9522	0.9440	0.9511	0.9502	0.9495	0.0451	0.0490	0.0478	0.0551	0.0480	0.0515
	0.10	0.9125	0.9539	0.9460	0.9529	0.9510	0.9505	0.0912	0.0997	0.0968	0.1105	0.0962	0.1031
	0.20	0.9156	0.9588	0.9522	0.9521	0.9506	0.9498	0.1881	0.2113	0.2023	0.2209	0.1924	0.2062
	0.33	0.9201	0.9663	0.9620	0.9507	0.9499	0.9489	0.3311	0.4052	0.3718	0.3645	0.3174	0.3401
	0.50	0.9281	0.9788	0.9751	0.9510	0.9492	0.9500	0.5606	0.9797	0.7415	0.5528	0.4814	0.5159
	0.67	0.9372	0.9856	0.9812	0.9504	0.9500	0.9492	0.8470	1.7544	1.5776	0.7398	0.6442	0.6904
15	0.05	0.9244	0.9517	0.9443	0.9507	0.9506	0.9499	0.0366	0.0386	0.0377	0.0415	0.0380	0.0398
	0.10	0.9250	0.9523	0.9446	0.9494	0.9501	0.9475	0.0737	0.0781	0.0761	0.0830	0.0760	0.0796
	0.20	0.9294	0.9592	0.9537	0.9516	0.9509	0.9507	0.1520	0.1637	0.1584	0.1660	0.1521	0.1593
	0.33	0.9324	0.9681	0.9634	0.9502	0.9493	0.9489	0.2669	0.3016	0.2861	0.2737	0.2508	0.2626
	0.50	0.9418	0.9811	0.9783	0.9501	0.9490	0.9497	0.4495	0.5917	0.5267	0.4141	0.3794	0.3973
	0.67	0.9528	0.9894	0.9862	0.9496	0.9510	0.9493	0.6819	1.3361	1.0306	0.5564	0.5097	0.5338
25	0.05	0.9356	0.9513	0.9458	0.9504	0.9500	0.9505	0.0281	0.0290	0.0284	0.0302	0.0287	0.0295
	0.10	0.9338	0.9509	0.9452	0.9491	0.9481	0.9484	0.0566	0.0586	0.0573	0.0604	0.0574	0.0590
	0.20	0.9383	0.9580	0.9527	0.9497	0.9495	0.9491	0.1167	0.1219	0.1188	0.1209	0.1149	0.1181
	0.33	0.9453	0.9701	0.9664	0.9510	0.9497	0.9505	0.2043	0.2192	0.2118	0.1990	0.1892	0.1945
	0.50	0.9575	0.9839	0.9816	0.9520	0.9516	0.9512	0.3456	0.4004	0.3783	0.3024	0.2875	0.2956
	0.67	0.9651	0.9920	0.9899	0.9512	0.9503	0.9505	0.5205	0.7126	0.6382	0.4045	0.3845	0.3953
50	0.05	0.9400	0.9504	0.9458	0.9504	0.9488	0.9499	0.0198	0.0201	0.0197	0.0204	0.0199	0.0202
	0.10	0.9431	0.9520	0.9473	0.9493	0.9491	0.9492	0.0398	0.0405	0.0398	0.0409	0.0399	0.0405
	0.20	0.9479	0.9581	0.9534	0.9496	0.9491	0.9491	0.0819	0.0837	0.0821	0.0817	0.0797	0.0808
	0.33	0.9581	0.9695	0.9669	0.9506	0.9510	0.9502	0.1437	0.1490	0.1457	0.1349	0.1316	0.1334
	0.50	0.9686	0.9853	0.9834	0.9518	0.9512	0.9514	0.2420	0.2615	0.2538	0.2044	0.1994	0.2022
	0.67	0.9776	0.9940	0.9927	0.9507	0.9506	0.9510	0.3652	0.4272	0.4089	0.2740	0.2673	0.2710
100	0.05	0.9454	0.9502	0.9463	0.9496	0.9496	0.9492	0.0139	0.0140	0.0138	0.0141	0.0140	0.0141
	0.10	0.9479	0.9528	0.9494	0.9511	0.9502	0.9507	0.0281	0.0283	0.0279	0.0283	0.0280	0.0282
	0.20	0.9545	0.9590	0.9554	0.9500	0.9501	0.9501	0.0578	0.0584	0.0576	0.0566	0.0559	0.0563
	0.33	0.9621	0.9697	0.9675	0.9493	0.9489	0.9491	0.1013	0.1034	0.1018	0.0934	0.0923	0.0929
	0.50	0.9758	0.9844	0.9834	0.9489	0.9486	0.9488	0.1705	0.1789	0.1757	0.1416	0.1399	0.1408
	0.67	0.9849	0.9946	0.9939	0.9495	0.9489	0.9492	0.2570	0.2840	0.2775	0.1896	0.1873	0.1886

Table 7-5 Field based Travel time Speeds

Stretch 1	0.82 km			Strecth 2	0.96 km	
	Veh. No	Time (Seconds)	Ave. Speed	Veh. No	Time (Seconds)	Ave. Speed
	1	65.6	45	1	115.2	30
	2	55.7	53	2	98.7	35
	3	84.4	35	3	123.5	28
	4	48	62	4	62.9	55
	5	72	41	5	86.4	40
	6	82	36	6	69.2	50
	7	98.4	30	7	138.3	25
	8	72	41	8	98.8	35
	9	61.5	48	9	88.7	39
	10	70.3	42	10	50.9	68
	11	55.7	53	11	104.8	33
	12	46.9	63	12	82.3	42
	13	42.3	70	13	76.8	45
	14	46.2	64	14	73.6	47
	15	105.5	28	15	98.8	35
	16	77.7	38	16	104.7	33
	17	67.1	44	17	49.4	70
	18	49.2	60	18	57.6	60
	19	42.8	69	19	84.3	41
	20	118.8	25	20	91	38
	21	45	66	21	98.8	35
	22	47.4	62	22	115.2	30
	23	54.7	54	23	78.6	44

	24	55.8	53		24	84.3	41
	25	55.4	53		25	86.4	40
	26	52.7	56		26	65.2	53
	27	59.1	50		27	93.4	37
	28	67.1	44		28	84.3	41
	29	45.5	65		29	46.1	75
	30	54.7	54		30	55	63
	31	73.8	40		31	86.4	40
	32	65.6	45		32	69.2	50
	33	59.1	50		33	62.9	55
	34	63.6	46		34	96	36
	35	57.9	51		35	76.8	45
	36	86.9	34		36	53.2	65
	37	61.5	48		37	58.6	59
	38	65.6	45		38	98.8	35
	39	84.4	35		39	86.4	40
	40	77.7	38		40	72	48
			1935	3715	46.43908337		1780

Table 7-6 Vehicle Spot Speeds [74]

Speed Class Km/hr(x)	Frequency (f)-1	Frequency (f)-1	Frequency (f)-1	Frequency (f)	F (x)	X^2	FX^2
35	1	0	1	2	70	1225	2450
38	6	1	3	10	380	1444	14440
41	7	3	6	16	656	1681	26896
44	4	4	5	13	572	1936	25168
47	3	5	7	15	705	2209	33135
50	4	3	2	9	450	2500	22500
53	2	2	2	6	318	2809	16854
56	1	4	2	7	392	3136	21952
59	0	2	2	4	236	3481	13924
62	1	1	1	3	186	3844	11532
65	0	2	1	3	195	4225	12675
68	2	3	0	5	340	4624	23120
71	1	1	0	2	142	5041	10082
74	0	1	0	1	74	5476	5476
	32	32	32	96	4716		240204

Table 7-7 LHS Input and Output Data

```
                                                        output
*****************************************************************
Program for Latin Hypercube Sampling
*****************************************************************
randon table for latin hypercube sampling
LHS table and values (32 intervals)
imax=   32
jmax=    5

it(i,j) (initial values)
   32    5
    1    2    3    4    5
    2    3    4    5    6
    3    4    5    6    7
    4    5    6    7    8
    5    6    7    8    9
    6    7    8    9   10
    7    8    9   10   11
    8    9   10   11   12
    9   10   11   12   13
   10   11   12   13   14
   11   12   13   14   15
   12   13   14   15   16
   13   14   15   16   17
   14   15   16   17   18
   15   16   17   18   19
   16   17   18   19   20
   17   18   19   20   21
   18   19   20   21   22
   19   20   21   22   23
   20   21   22   23   24
   21   22   23   24   25
   22   23   24   25   26
   23   24   25   26   27
   24   25   26   27   28
   25   26   27   28   29
   26   27   28   29   30
   27   28   29   30   31
   28   29   30   31   32
   29   30   31   32    1
   30   31   32    1    2
   31   32    1    2    3
   32    1    2    3    4

it(i,j) (final values)
   32    5
   26    8    5    4   14
    7   24    3   19   29
    6   27    2   30   26
```

output

19	29	27	7	22
5	6	13	8	5
24	16	8	18	4
18	5	23	27	11
4	14	21	24	12
9	19	17	25	13
25	32	15	11	2
12	7	1	3	15
15	13	14	9	8
16	31	31	29	32
32	15	30	2	30
1	28	11	15	31
21	10	18	5	18
28	20	4	16	21
8	17	10	17	9
2	3	7	22	23
11	25	22	32	24
20	21	25	1	16
22	9	6	23	19
13	18	26	21	20
17	22	19	10	7
3	2	29	12	28
14	12	28	6	17
27	23	12	28	10
29	26	24	20	3
30	4	16	26	1
31	30	32	13	27
23	11	9	31	6
10	1	20	14	25

average and standard deviation of variables x(i)

i	ave(i)	std(i)
1	4.9125000E+01	9.4759998E+00
2	5.6342145E+04	6.6350000E+03
3	3.6000000E+01	2.3299999E+00
4	1.5239999E+02	9.5249996E+00
5	1.5699999E-02	8.9999998E-04

output of values of variables xval(i,j)

32 5

5.6994923E+01	5.1534992E+04	3.3489391E+01	1.4068559E+02	1.5522610E-02
4.1255077E+01	6.0496313E+04	3.2696533E+01	1.5427736E+02	1.6806873E-02
4.0153301E+01	6.2624039E+04	3.2095058E+01	1.6590451E+02	1.6447460E-02
5.0992714E+01	6.4502258E+04	3.8206001E+01	1.4448938E+02	1.6100587E-02
3.8914467E+01	5.0060250E+04	3.5352982E+01	1.4549899E+02	1.4730236E-02
5.5057915E+01	5.6082211E+04	3.4311882E+01	1.5352174E+02	1.4593126E-02
5.0240986E+01	4.9192832E+04	3.7242844E+01	1.6141809E+02	1.5299412E-02
3.7470856E+01	5.5034395E+04	3.6839104E+01	1.5836359E+02	1.5375882E-02

output

4.3192089E+01	5.7649898E+04	3.6091278E+01	1.5930099E+02	1.5450078E-02
5.5990498E+01	7.0633133E+04	3.5725594E+01	1.4816045E+02	1.4191654E-02
4.5712410E+01	5.0831703E+04	3.0981474E+01	1.3889548E+02	1.5594007E-02
4.8009010E+01	5.4499668E+04	3.5540760E+01	1.4643640E+02	1.5047937E-02
4.8753769E+01	6.7462008E+04	3.9904942E+01	1.6411440E+02	1.7638490E-02
6.9535156E+01	5.5560738E+04	3.9303467E+01	1.3643666E+02	1.6976018E-02
2.8714891E+01	6.3491465E+04	3.4962925E+01	1.5127823E+02	1.7208345E-02
5.2537590E+01	5.2802973E+04	3.6274403E+01	1.4213666E+02	1.5805991E-02
5.9335541E+01	5.8184621E+04	3.3134430E+01	1.5202684E+02	1.6024116E-02
4.2259502E+01	5.6602074E+04	3.4757156E+01	1.5277315E+02	1.5136510E-02
3.3243793E+01	4.6935063E+04	3.4064911E+01	1.5663954E+02	1.6180068E-02
4.4907265E+01	6.1149297E+04	3.7037075E+01	1.7291570E+02	1.6263489E-02
5.1756393E+01	5.8731605E+04	3.7688118E+01	1.3188434E+02	1.5664741E-02
5.3342735E+01	5.2187980E+04	3.3793999E+01	1.5748073E+02	1.5877388E-02
4.6493607E+01	5.7123547E+04	3.7935089E+01	1.5583023E+02	1.5949922E-02
4.9496227E+01	5.9295363E+04	3.6459240E+01	1.4731926E+02	1.4952539E-02
3.5689957E+01	4.5222281E+04	3.8865570E+01	1.4896976E+02	1.6669763E-02
4.7257290E+01	5.3952684E+04	3.8510612E+01	1.4338190E+02	1.5735257E-02
5.8096703E+01	5.9881320E+04	3.5160896E+01	1.6266333E+02	1.5219931E-02
6.0779144E+01	6.1852586E+04	3.7458813E+01	1.5504500E+02	1.4423982E-02
6.2560043E+01	4.8182031E+04	3.5908718E+01	1.6031061E+02	1.3761513E-02
6.5006210E+01	6.5749227E+04	4.1018539E+01	1.4975499E+02	1.6552104E-02
5.4179592E+01	5.3388930E+04	3.4541191E+01	1.6836333E+02	1.4847896E-02
4.4070408E+01	4.2051191E+04	3.6647018E+01	1.5052263E+02	1.6352063E-02

APPENDIX D

This appendix gives the details of the different stages of multiple regression analyses that were conducted based on the ANSYS simulations for the generation of deformation, as shown for the different number of parameters that were considered as shown in Table 7.2

The adjusted R Square values and P-Values were obtained from the different stages of multiple regression analyses.

Table 7-8 Regression Analysis and ANOVA results

SUMMARY OUTPUT

Regression Statistics	
Multiple R	0.999098081
R Square	0.998196975
Adjusted R Square	0.997850239
Standard Error	0.063845236
Observations	32

ANOVA

	df	*SS*	*MS*	*F*	*Significance F*
Regression	5	58.6738872	11.7347774	2878.842182	8.58717E-35
Residual	26	0.10598157	0.00407621		
Total	31	58.7798688			

	Coefficients	*Standard Error*	*t Stat*	*P-value*	*Lower 95%*	*Upper 95%*	*Lower 95.0%*	*Upper 95.0%*
Intercept	-8.322218284	0.3363843	-24.74021	1.34881E-19	-9.01366612	-7.63077044	-9.0136661	-7.63077
Vehicle Speed Km/hr	0.14186516	0.00140718	100.81543	3.01523E-35	0.138972666	0.14475765	0.13897267	0.1447577
Vehicle Mass (Kg)	1.42117E-06	1.8484E-06	0.76885374	0.448908374	-2.3783E-06	5.2207E-06	-2.378E-06	5.221E-06
Concrete Compressive Strength (Mpa)	-0.003416033	0.00541202	-0.6311939	0.533423941	-0.01454059	0.00770853	-0.0145406	0.0077085
10 mm Stirrup Spacing (mm)	0.058624075	0.00124945	46.9200373	1.16331E-26	0.056055801	0.06119235	0.0560558	0.0611923
Longitudinal Steel Ratio	-38.11216896	14.450659	-2.6374001	0.013915248	-67.815924	-8.40841392	-67.815924	-8.408414